Tailoring Polymer Micro-extraction Phases to Enhance the Sensitivity and Selectivity of Raman Spectroscopy

Ikechukwu Nwaneshiudu

A dissertation submitted in partial fulfillment of the requirements for the degree of

Doctor of Philosophy

University of Washington

2013

Reading Committee:

Daniel Schwartz, Chair

Danilo Pozzo

Qiuming Yu

Barry Lutz

Program Authorized to Offer Degree:
Department of Chemical Engineering

University of Washington

Abstract

Tailoring Polymer Micro-extraction Phases to Enhance the Sensitivity and Selectivity of

Raman Spectroscopy

Ikechukwu C. Nwaneshiudu

Chair of the Supervisory Committee:

Professor Daniel Schwartz

Chemical Engineering

Raman Spectroscopy (RS) systems are evolving toward portable, affordable, and highly versatile analytical chemistry platforms, though sensitivity, selectivity, and fluorescence in many complex multi-component real-world samples remains challenging. We investigated the combination of solid phase micro-extraction (SPME) with Raman spectroscopy as a strategy to address some of these limitations. SPME is best known as a technique in chromatography that uses hydrophobic polymer phases like polydimethylsiloxane (PDMS) to extract and preconcentrate non-polar target analyte in headspace analysis. SPME not only enhances detection by pre-concentration of analytes, but when combined with Raman spectroscopy, offers an opportunity to reduce interference from the background by tailoring the polymer phase to specific classes of analytes in complex mixtures. Here we establish SPME/Raman as a quantitative technique that is capable of enhancing the measurement of organic contaminates in water, anesthetic compounds in serum, and inhibitory molecules in the multi-phase and multi-component broths produced by pretreatment of biomass. Flory-Huggins theory is used to describe the predicted trends in the thermodynamic partitioning of dilute analytes into polymer phases. We show experimentally and theoretically that the equilibrium partitioning, denoted by the partition coefficient K, can enhance the Raman signal by 2 orders of magnitude or more when the analyte is detected in the polymer phase rather than the solvent phase. Specifically, we find that SPME/Raman measurements of aqueous benzene and toluene partitioning into PDMS phases have log (K) values of 2.35 and 1.90, respectively, matching literature values determined with other methods. We also examine the use of SPME/Raman for enhanced detection of general anesthetics (halothane, isofluorane, propofol), quinoline, and fermentation inhibitors (furfural, HMF) into either PDMS or epoxy polymer phases. We then demonstrate the utility of Flory-Huggins theory in understanding and optimizing the selection of polymer-analyte pairs to enhance the sensitivity and selectivity of SPME/RS.

Contents

List of Figures & Tables

Acknowledgements

For the work presented in Chapter 1: this work has been supported by the Gates Millennium Scholarship program as well as the NSF IGERT program at the University of Washington. I. Nwaneshiudu would also like to acknowledge Rory E. Bieanz and Evangeline Drink for their efforts towards the work. For the work presented in Chapter 2: I. Nwaneshiudu acknowledges partial funding from the Gates Millennium Scholarship as well as contributing work by Chniwe Nwaneshiudu. Raman experiments were performed at the University of Washington NanoTech User Facility, a member of the NSF National Nanotechnology Infrastructure Network (NNIN). For the work presented in Chapter 3: this work was jointly supported by the NARA research grant and the Gates Millenium Scholarship. We thank the members of Schwartz research group, especially Sathana Kitayaporn, Carolynn Grosh, Perry Cheung and Tyler House for helpful discussions. I. Nwaneshiudu would like to thank Professors Francois Baneyx, Danilo Pozzo, Qiuming Yu, and Barry Lutz for assistance and support in all phases of the project. Finally, I'd like to thank my family for all their support.

Chapter 1
Introduction

1.1 Motivation: Raman Spectroscopy

As an analytical technique, Raman spectroscopy (RS) has undergone many developmental phases since its discovery in the late 1920s[1]. At its early stages, after Sir Chandrasekhara Venkata Raman discovered the scattering phenomena using sunlight[2, 3], the method gained little traction as a viable analytical technique due to (1) its low sensitivity and (2) the high cost of instrumental parts (light sources, detectors, and filters)[1]. The advent of lasers in the 1960s[4] and improvements to detector technologies in the 1980s brought a renewed interest in Raman spectroscopy (RS) and other optical detection techniques. More specifically, the late 80s brought about charge coupled device (CCD) technologies, first as high end detectors that subsequently dropped in price as inexpensive mass produced CCDs became ubiquitously use in digital cameras[5]. The final technological revolution that culminated in a significant broadening of the availability and popularity of RS occurred in the early 1990s with the emergence of the first commercial holographic notch filters, reducing the complexity of the spectrometer required for RS and increasing the throughput.

Figure 1.1 is a plot of number of published articles concerning *Raman Spectroscopy* versus time generated within the web of science database. As the plot shows, a noticeable increase in the number of published works on RS occurred around 1990, when the last component to the "perfect storm" of Raman instrumental technology emerged. More importantly, the interest in RS is still increasing. We see the number of Raman related publications spanning 2010-2012 almost equal the total of the entire 1990s. The continual interest in RS has given the technique more traction for further advancement towards applications in many different fields of research.

1.1.1 Development and Applications

Raman instrumentation has benefited greatly from many crucial advances of the past three decades[1]. Advances in laser, CCD, and filter technology has not only made Raman detection more practical, but has also made the technique cost effective, compact and very adaptable[1, 5]. Raman has quickly become a routine and staple detection method that can be readily implemented and used alongside a wide variety of instruments and analytical techniques[6, 7]. This grants it access into many disciplines. Raman systems are now commonly used together with Scanning Electron Microscopy (SEM) and Atomic Force Microscope (AFM) for a variety of applications ranging from nano-material fabrication to cellular imaging[8-10].

Along with its adaptability, Raman systems are also becoming increasingly portable[11]. The need for onsite, real-time chemical analysis for food/water quality[12], environmental trace analysis[13, 14], homeland security[15], and medical diagnostics[16, 17] has spurred the development of portable detection systems. Currently, portable Raman systems are being used for rapid screening of narcotics[18, 11]. Rapid and sensitive screening of chemical and biological hazards "onsite" is a real challenge that many believe portable Raman systems could tackle[19]. Compact and adaptable Raman instrumentation also offers the ability to perform long distance remote sensing, which may be applied in areas such as planetary exploration and astro-spectroscopy[20].

1.1.2 Limitations to Versatile Detection

Emerging portable Raman Spectroscopy (RS) systems are at the threshold of filling the much needed the role of a "universal" sampling platform. In light of the potential applications of Raman spectroscopy, a number of limitations must be addressed. Firstly, although the minimal sample preparation required in RS proves advantageous in almost all settings, it can be limiting when dealing with complex multicomponent real world samples, where the desired signal may

be obscured by many overlapping spectral peaks or fluorescence [21]. Therefore, development of probes, sampling platforms, and software that can provide an easy sample preconditioning towards specific classes of analytes can help address this issue, de-convoluting some of the interferents for quantitative and molecularly-specific analysis.

The second and more intrinsic limitation of Raman spectroscopy is its low sensitivity[22]. Though every sample is different, routine detection using unenhanced RS methods range from micro to milli-molar concentrations, which is inferior when compared with many other techniques (i.e. mass spectroscopy)[22]. The modest limit of detection (LOD) can largely be attributed to the modest Raman scattering cross-section, meaning the inelastic scattering events are rare,[1]. This means the rare Raman scattered light that loses (Stokes shifted) or gains energy (anti-Stokes shifted) from interactions with vibrational and rotational states of a molecule must be detected in a sea of elastically scattered light [1, 23]. The low Raman scattering cross-section in a general unenhanced RS measurement often results in modest detection limits.

1.1.3 Enhancing Detection

Many efforts continually seek to address the inherent challenges of Raman spectroscopy. Through these efforts, many kinds of Raman spectroscopic techniques have been developed; each with practical and theoretical advantages and disadvantages. Resonance Raman Spectroscopy (RRS), Coherent Anti-Stokes Raman Spectroscopy (CARS), Tip Enhanced Raman Spectroscopy (TERS) are some of these enhanced Raman techniques[23-25]. Of all these enhancement techniques, Surfaced Enhanced Raman Spectroscopy (SERS) has attracted a great deal of attention due to its potential for versatile and ultrasensitive bio/chemical analysis[26]. While the main part of this thesis does not address SERS, it is important to understand its strengths and

weaknesses vis-a-vis the approach we take. The appendix and concluding remarks do note the way our approach can be combined with SERS.

The discovery of SERS in 1974 by Martin Fleischman *et al* stimulated others to investigate the enhanced Raman signals of pyridine adsorbed on roughen silver electrodes[27]. By 1977, two groups (Van Duyne *et al*, Creighton *et al*) discovered that the pre-concentration of scattering species on the surface of roughen silver does not account for the huge enhancements (10^6) being observed. Van Duyne *et al* proposed an electromagnetic effect to explain the phenomena, while Creighton *et al* proposed a charge-transfer effect. Van Duyne proposed an increase in the amplitude of the electric field, which involves analyte molecules being in the vicinity of surface plasmons on noble metal surface[1, 28]. The amplitude of these surface plasmons are enhanced when introduced to light with a wavelength close to the plasmon's oscillation frequency[1]. Creighton's charge transfer model involves a chemical interaction that increases the polarisability of the molecule[29]. This increase occurs when a free electron on the metal surface is excited into the LUMO energy levels of the analyte molecule and then tunnels/relaxes back down to its ground state, which releases a photon as Raman scattering[29]. Today however, the electromagnetic description of the SERS phenomenon has being widely accepted and has enabled the computational modeling that drives the design of better SERS active substrates[28, 30-33].

Developments in nanotechnology within the past few decades have brought about rapid growth in SERS research[28]. Numerous nano-write/patterning, fabrication, and synthesis techniques have been developed to create a wide range SERS active nano-structures[28]. Commercially available SERS nano-particle probes are being utilized for biochemical sensing and imaging[34]. Additionally, many research efforts seek to create novel SERS nanostructures that

can maximize enhancement. Van duyne *et al* has been at the forefront these efforts, creating SERS active silver nano-structures using Nano-Sphere Lithography (NSL) and Filmed-Over Nano particles (FON) which are able to reach enhancement factors of 10^{6-13} [28]. Other groups (Kneipp *et al*.) have lead the way in using metal nano-particles in vivo live cell imaging[35, 36]. Although SERS sensor design is advancing rapidly, the nature of analytes that can be detected with SERS has some restrictions. The SERS mechanisms restricts analytes to those that chemisorb or physisorb on SERS nanostructures[28]. Several research efforts are looking towards widening the library of SERS active molecules. Although SERS restricts the universality of RS, it does enhance the detection limits by many orders of magnitude when an analyte is well suited to the method.

1.2 Solid Phase Micro-extraction (SPME)

SPME is a sampling technique that uses properties of polymer matrices to favorably partition and pre-concentrate target gas or liquid phase compounds into a solid polymer phase[37, 38]. SPME-based analytical techniques have a variety of applications including water and air quality analysis as well as assessment of bioavailability/fate of many organic pollutants (i.e. carcinogens such as benzene and toluene)[22]. The partitioning of these organics into polymer phases has been extensively characterized by techniques based on mass spectrometry[22]. Techniques such as Purge-Trap-GC/MS and MIMS have enhanced sensitivity, owing to the use of a polymer pre-concentration step, and are also capable of extracting crucial quantitative parameters that dictate analyte permeation[39, 40]. One such parameter that influences how dilute analytes interact with polymer is the equilibrium partition coefficient (K)[41]. The partition coefficient is the thermodynamic parameter that quantitatively relates the analyte preference for the polymer phase over the aqueous phase (a common solvent system with SPME). Previous work using organic

analytes in aqueous phases has shown that values for the partition coefficient are influenced by the polarity of the analyte and the hydrophobicity of the polymer[22]. Here we approximate the partition coefficient (K) between the polymer and dilute aqueous phase as:

$$K = \frac{C_s}{C_a}, \quad (1)$$

where C_s is the concentration of analyte in the solid polymer and C_a is the concentration in water. This approximation is appropriate in the limit of dilute solutions. The partition coefficient K is the cornerstone of SPME-based detection methods because a value K > 1 means the analyte enriches the polymer phase enabling enhanced detection.

1.2.1 PDMS-SPME Analytics and a connection to Microfluidics Fabrication

Poly(dimethlysiloxane) (PDMS) is a polymer which has been the cornerstone of SPME-based analytics[42]. Analytical platforms such as Membrane Inlet Mass Spectrometry (MIMS) and Headspace SPME Gas Chromatography – Mass Spectrometry (GC-MS) commonly use PDMS as the polymeric coating for sensing probes[40, 41]. These SPME methods (MIMS and GC-MS) are proven quantitative analytical methods. SPME sampling has also been used to enhance optical detection techniques such as ultraviolet-visible (UV-vis)[43, 44], Infrared[45-48], and even Raman spectroscopies. For example, Tilotta *et al* have shown qualitative SPME signal enhancement of BTEX contaminants using Raman spectroscopy[22]. Although mostly qualitative, these are some of the first attempts toward Raman signal enhancement using sampling polymer membranes.

PDMS is also the polymer of choice for simple fabrication of transparent, microfluidic device platforms[49]. These devices are often compatible with optically-based sensing technologies. Raman is one such optical sensing technique that is frequently used alongside these transparent devices platforms[49]. The merging of lab on chip platforms with Raman spectroscopy

has being the objective of many research endeavors. Lau *et al* have reported developing a Raman-activated cell sorting optofludic platform fabricated with PDMS soft lithography[50].

Recent interest in handheld Raman devices has spurred on many efforts to enhance the technique's sensitivity while keeping the system portable. Lim et al report the loss of sensitivity as Raman spectrometers become more compact[19]. This can be offset by the enhanced sensitivity of SERS. Therefore, many groups are working to integrate SERS active nano-structures into optofluidic platforms. The merging of compact, SERS-ready, optofluidic platforms with portable Raman devices has been realized[19]. However, few efforts have addressed the possibilities of coupling SPME & SERS enhancements within such a platform (being that most of the devices are fabricated with PDMS). Attributes of PDMS, welcomed in SPME analytics, are barriers in some optofluidic sensing platforms. However, Senapik *et al* have been at the forefront of emphasizing the added enhancement provided when PDMS SPME is coupled with SERS nano-structures[51-53].

Although nascent, and only touched on at the end of this thesis, the prospects of efficiently combining SPME and SERS could further enhance SERS signals, provide a selective/protective polymeric coating for SERS nano-structures, and also provide a platform for better analysis in microfluidic devices. The polymer could also possibly be a layer that anchors analyte unto SERS surfaces, which would widen the library of SERS active analytes. Understanding and tailoring SPME polymer phases toward better Raman sampling and detection will improve Raman sensing, especially in the emerging lab-on-chip experimental platforms.

1.2.2 Thermodynamic Theory: Enhanced Sensitivity

The partitioning of analytes between the two phases in SPME is based on fundamental thermodynamic principles. The properties of SPME polymers (e.g. PDMS, melting point: -50^{o}C,

glass transition temperature: -126^{o}C) means that SPME extraction obeys the rules of conventional liquid-liquid equilibrium extraction[38, 54]. Thermodynamic equilibrium of an analyte species (i) between two phases, means that the chemical potentials of the analyte in either phase are equal, which is given by[38]:

$$\mu_i^{\beta} = \mu_i^{\alpha} , \tag{2}$$

where μ is the chemical potential and β denotes polymer phase while α denotes aqueous. This can be restated in terms of activity:

$$\mu_i^{o} + RTLn(a_i^{\beta}) = \mu_i^{o} + RTLn(a_i^{\alpha}) , \tag{3}$$

where μ_i^{o} is the standard state chemical potential of the analyte (i), a_i the activity of the analyte (a measure of the "corrected concentration"), R is the gas constant, and T is the temperature. Algebraic manipulation gives:

$$\exp\left(\frac{(\mu_i^{o} - \mu_i^{o})}{RT}\right) = \frac{a_i^{\beta}}{a_i^{\alpha}} , \tag{4}$$

If at equilibrium, temperature, pressure, and bulk composition are left constant, the equation can be simply expressed as:

$$a_i^{\beta} = a_i^{\alpha} , \tag{5}$$

which means that at equilibrium (with temperature, pressure, composition constant) the activities of the species in both phases must then be equal. Activities can be expressed as a function of concentration:

$$\gamma_i^{\alpha} c_i^{\alpha} = \gamma_i^{\beta} c_i^{\beta} , \tag{6}$$

where γ_i, is the activity coefficient (a dimensionless quantity describing deviation from ideality), and c_i is analyte concentration. The partition coefficient ($K_{\beta\alpha}$) (distribution coefficient) can therefore be represented by the ratio of concentration between the two equilibrated phases[55]:

$$\frac{\gamma_i^{\alpha}}{\gamma_i^{\beta}} = \frac{c_i^{\beta}}{c_i^{\alpha}} = K_{\beta\alpha} \ , \tag{7}$$

In the dilute analyte limit, Henry's Law suggests that the activity coefficients have a constant value (independent of concentration), which reduces **Equation 7** to:

$$K_{\beta\alpha} = \frac{c_i^{\beta}}{c_i^{\alpha}}. \tag{8}$$

1.2.3 Thermodynamic Theory: Tailoring by Polymer Selection

Effective tailoring of polymer SPME phases requires an analysis of the relevant parameters that dictate how analytes interact with the aqueous and polymer phases. Experimentally, we used the expression in **Equation 1** to quantify the partitioning of analytes. To understand the factors that govern these measured parameters requires a molecularly-based theory that incorporates parameters that describe the analyte-solvent interactions and the analyte-polymer interactions. A molecular description of the analyte partition coefficient from water into an amorphous polymeric or macromolecular phase, K_{pw}, can be express as:

$$logK_{pw} = -logS_w\bar{V} - \frac{\left[\left(1-\frac{\bar{V}}{\bar{V}_p}\right)+\chi\right]}{2.303} - \ \log(\frac{\gamma_w}{\gamma_w^*}), \tag{9}$$

where S_w is the solubility of the analyte in water, $\bar{V}$ is the molar volume of the analyte, $\bar{V}_p$ is the molar volume of the polymer, and χ is the Flory-Huggins interaction parameter which takes into account the energy required to homogeneously disperse the analyte into the polymer. Flory-Huggins theory takes into account the molecular size differences between the analyte and the polymer subunits.

The last term $\log(\frac{\gamma_w}{\gamma_w^*})$ is a *solubility enhancement factor* (SEF) which accounts for any effects the polymer has on the analyte's water solubility. In a PDMS/water system, the SEF is assumed to be negligible because, unlike other well know solvent system (octanol-water), there is little or no solvent interactions (PDMS dissolving in water) occurs. Since the macromolecular polymer is much bigger than analytes we will evaluate, we further assume that $\frac{\bar{V}}{\bar{V}_p} \approx 0$, which simplifies the expression to:

$$logK_{pw} = -logS_w\bar{V} - \frac{[1+\chi]}{2.303}. \quad (10)$$

Equation (10) indicates that the two main parameters that dictate how an analyte partitions from water into a polymer is its water solubility (S_w), a measure of water-analyte interactions, and the Flory-Huggins parameter (χ).

1.3 Research Objectives

Our proposed research seeks to understand and provide guidelines towards the tailoring of SPME micro-extraction phases for better selectivity and sensitivity of quantitative Raman spectroscopy. These guidelines, based on established polymer/solvent mixing theory can be applied to various other systems that are also adaptable to SPME.

1.3.1 Objective 1: Evaluate SPME/Raman as a quantitative analytical method.

We demonstrate that SPME/Raman can be quantitative. We establish a procedure to estimate the equilibrium partition coefficients for a variety of organic water contaminants in the dilute regime. The quantitative nature of the method is verified by comparing our estimates of K to literature values for toluene and benzene. We extend the technique to a compound, quinoline, with an unknown partition coefficient. Development of this method has implications for PDMS-based lab on chip experimentation and optical detection.

1.3.2 Objective 2: Apply quantitative SPME/Raman to detecting anesthetic compounds

The partitioning of general anesthetics into lipid rich biological materials has been a point of interest in a variety of research and healthcare disciplines[56, 57]. Anesthetics like halothane, enflurane, desflurane and isoflurane have been well studied because their partitioning between different physiological phases influences how much is administered and drug efficacy[58]. Partition coefficients for these compounds between critical physiological phases such as blood/brain (BB) or alveolar gas/blood are well documented[58]. We use SPME/Raman technique to quantify partitioning of these molecules into bio-compatible polymer phases as a means to enhance detection.

1.3.3 Objective 3: Polymer phases selection to enhance detection of fermentation inhibitors.

One approach to increased ethanol production is to decrease the amount of fermentation inhibitors formed during the pretreatment of plant fibers[59]. Previous research has shown that, at high enough concentrations, molecules such as furfural and (hydroxymethyl) furfural (HMF) can be toxic to culture growth[59, 60]. Weil *et al* have shown that polymeric adsorbent XAD-4 can be used to remove furfural (the most prevalent of the inhibitors) from batch solution[59]. Here we seek to use the partitioning into a hydrophobic polymer as a means to selectively remove and detect these inhibitory compounds.

1.3.4 Objective 4: Optimization of SPME using a thermodynamic approach

Using Flory-Huggins polymer theory for small molecules in large backbone polymers, we seek to develop guidelines that will inform the literature about use of such polymer phases. Understanding how different polymers interact with these systems is crucial towards desired separations and enhancements.

1.4 Figures

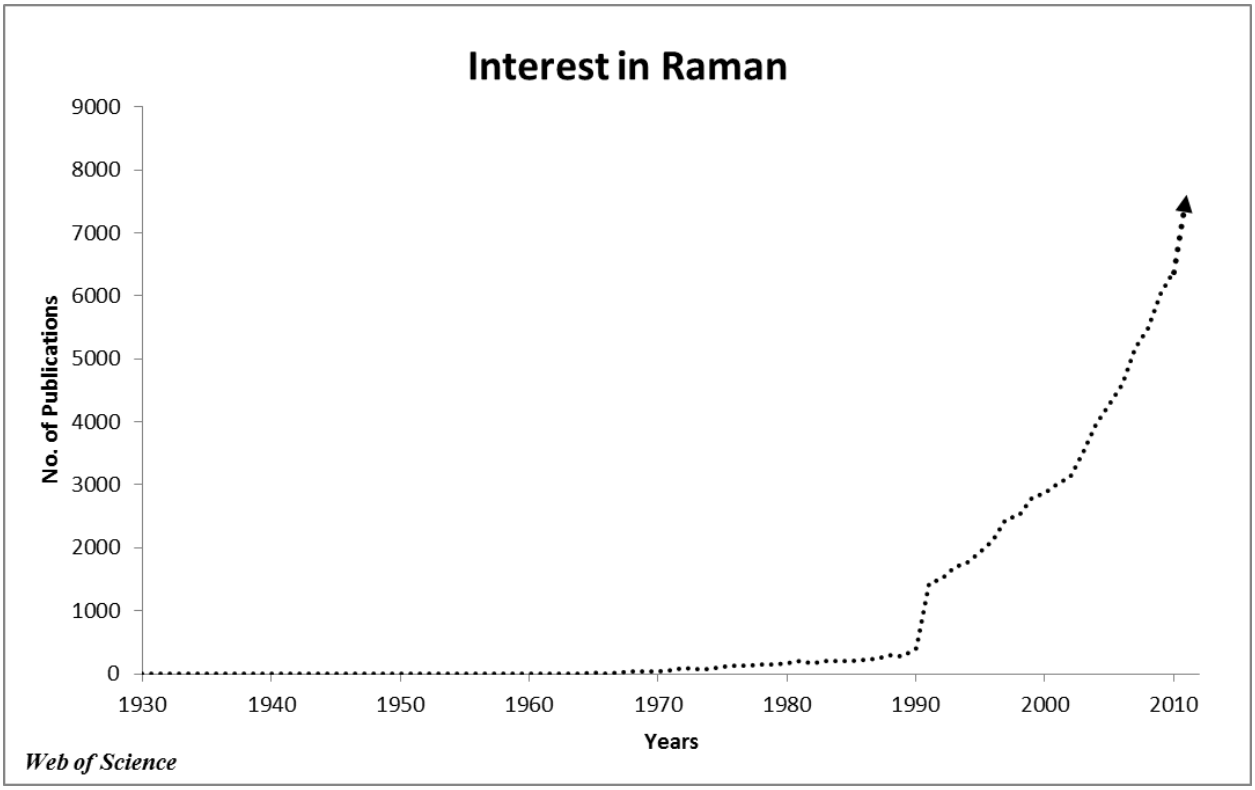

Figure 1.1: Publications concerning Raman Spectroscopy from 1930-2011.

Chapter 2

SPME/Raman as a Quantitative Analytical Method

2.1 Summary

Solid phase micro-extraction (SPME) was used along with Raman Spectroscopy to quantify the partitioning of trace organics into polydimethylsiloxane (PDMS) matrices. PDMS has previously been utilized with SPME/Raman to pre-concentrate trace BTEX (benzene, toluene, ethyl-benzene, xylene) fuel components from contaminated water, thereby enhancing detected Raman signals. Here we show that SPME can increase Raman signals more than 2 orders of magnitude for the compounds investigated. We also demonstrate the quantitative features of SPME/Raman by estimating PDMS/organic partition coefficients ($K_{PDMS/WATER}$) for benzene (log (K) = 1.90 ± 0.10) and toluene (log (K) = 2.35 ± 0.20) using linear regression fits in the dilute limit of concentrations. The K values obtained are within the range of values obtained using other quantitative SPME techniques. The method was also used to characterize quinoline, a pyridine-based organic, which yielded reasonable K values (log (K) = 1.20 ± 0.20). Combining PDMS-based SPME with a technique like Raman spectroscopy could potentially enhance optical detection methods used in microfluidic systems, where PDMS is a common material of construction.

2.2 Introduction

Poly(dimethlysiloxane) (PDMS) is a cornerstone of soft lithography-based fabrication and solid phase micro-extraction (SPME)-based analytical chemistry.[42] Current microfluidics devices use PDMS because it provides a simple route to fabricate microfluidic platforms that are compatible with bio-analysis, especially optically-based sensing technologies.[49] PDMS is also

used in various SPME procedures.[61] Analytical platforms such as Membrane Inlet Mass Spectrometry (MIMS) and Headspace SPME Gas Chromatography – Mass Spectrometry (GC-MS) commonly use PDMS as the polymeric coating for sensing probes.[40, 41] SPME utilizes the hydrophobicity of PDMS to favorably partition and pre-concentrate non-polar gas or liquid phase compounds into a solid polymer phase.[41] SPME-based analytical techniques have a variety of applications including water and air quality analysis and the assessment of bioavailability/fate of many organic pollutants.[39-42, 49, 61, 62] This is the first in a series of papers that explores how the analytical uses of PDMS can be merged with modern micro-fluidics to perform next generation micro-analysis.

Organic analytes such as toluene and benzene are well known carcinogenic contaminants in ground/surface water.[14] The partitioning of these organics into PDMS polymer has been extensively characterized by techniques based on mass spectrometry.[63, 64] Techniques such as Purge-Trap-GC/MS and MIMS have enhanced sensitivity, owing to the use of a polymer pre-concentration step, and are also capable of extracting crucial quantitative parameters that dictate analyte permeation.[64, 65] One such parameter that influences how non-polar organics interact with PDMS is the equilibrium partition coefficient (K). The partition coefficient is the thermodynamic parameter that quantitatively relates the analyte preference for the polymer phase over the polar aqueous phase. Previous work has shown that values for the partition coefficient are influenced by the polarity of the analyte and the hydrophobicity of the polymer.[22] Here we approximate the partition coefficient (K) between the polymer and aqueous phase as:

$$K = \frac{C_s}{C_a} \tag{1}$$

where C_s is the concentration of analyte in the solid polymer and C_a is the concentration in water. This approximation is appropriate in the limit of dilute solutions. The partition coefficient K is the cornerstone of SPME-based detection methods because a value K > 1 means analyte enriches the PDMS phase enabling enhanced detection.

Though most SPME techniques rely on mass spectrometry, optical methods are more compatible with microfluidic platforms.[49] PDMS microfluidic devices are transparent and readily combined with fluorescence and Raman detection techniques.[49] However, there is recent recognition among users of PDMS based microfluidic, that partitioning of non-polar analytes into PDMS channel wall can lead to significant experimental errors.[42] The frequent use of such platforms requires a thorough understanding of how the fabrication polymer (PDMS) affects experiments and optical detection in such devices.

Some literature exists for optical SPME methods, mostly based on ultraviolet and infrared (IR) absorption. Tilotta *et al* successfully coupled SPME with IR spectroscopy and extracted reasonable partition coefficient values for a variety of organic compounds.[46-48] Besides improving optical detection limits, they derived partition coefficients of several different organic/polymer combinations. Hawthorne *et al* have shown that ultraviolet (UV) spectroscopy coupled with SPME can also yield reliable partition coefficients.[43, 44] Raman scattering methods have better compatibility with modern microfluidics than transmission-based optical systems.[42] Prior SPME methods using Raman detection have demonstrated its ability to detect contaminant organics different kinds of contaminated water samples.[14, 22] However, SPME/Raman has yet to be used as a quantitative method capable of using and predicting the partitioning traits of PDMS.

We present a quantitative SPME/Raman method which can be used to estimate partition coefficients for a variety of organic water contaminants, using similar dilute concentrations as

prior work.[22] Using simple linear relationships within this dilute regime, we are able to extract partition coefficients for benzene and toluene. The quantitative nature of our method is verified by comparing our estimates of K to literature values for toluene and benzene. We extend the technique to quinoline, whose partitioning into PDMS has not been extensively characterized. Development of this method has implications for PDMS based lab on chip experimentation and optical detection.

2.3 Materials and Methods

2.3.1 PDMS and Organic/Aqueous Solution Preparation

PDMS Samples - Slygard 184 PDMS and catalyst were obtained from Dow Corning. Samples of PDMS used in the experiment were prepared as follows. Uncured PDMS was mixed using the standard 10:1 polymer to catalyst ratio in a poly(methyl-methacrylate) (PMMA) mold 1.5mm deep. This was cured at 70^{o}C overnight to make a ~1.5mm thick sheet of PDMS. Samples were punched out of the PDMS sheet using a 2mm diameter punch. The resulting PDMS plugs were sealed and kept until used.

Organic Aqueous Solutions – Toluene and benzene were purchased from EMDchemical and quinoline was purchased from Acros Organics. All were used as purchased. Experimental solutions were prepared by spiking the appropriate amount of reagent into 20 mL of deionized (DI) water. The solutions were then shaken vigorously by hand, tightly capped, and left to sit until fully dissolved in a single aqueous phase. Spiked solutions were used within 15mins of preparation to prevent evaporative loses.

2.3.2 SPME/Raman Extraction Procedure

20mL glass vials with Teflon-lined lids were used for the solid phase micro-extraction procedure. Solutions of toluene, benzene, and quinoline were prepared in separate 20mL vials.

Vials were completely filled to minimize evaporative headspace loses. Three PDMS plugs were introduced to each vial, tightly capped, and left to equilibrate undisturbed at room temperature for at least 48 hours. To first approximation, the large excess volume ratio of aqueous phase solution to PDMS plugs means the aqueous concentration in solution before and after equilibration is negligibly altered.

2.3.3 Raman Spectra Acquisition

Raman spectra were collected using a Renishaw inVia Raman micro-spectrometer attached to a Leica DM IRBE upright optical microscope. A 785 nm diode laser operated full power (nominal 180mW) was used to irradiate samples through a 50x (N.A. 0.8) objective lens. The spot area was ~50μm^2. Raman scattered light was acquired through the same objective lens and detected on a thermoelectrically cooled (-60 ^oC) CCD. All PDMS sample measurements were acquired for 10 seconds. Time acquisitions for water sample measurements ranged from 20-300sec depending on signal to noise considerations. Spectra of equilibrated PDMS and water samples were collected using a custom wet sample holder sealed with an optical coverslip. Laser stability was assured using the 520 cm^{-1} peak of Silicon (experiment to experiment variation in intensity did not exceed ±3%). The PDMS peak at 1410 cm^{-1} was acquired with all solid phase spectra and served as an internal standard that helped normalize for sample to sample variations in system focus.

2.3.4 Raman Intensity Normalization & Peak Analysis

Spectral, reported in counts per second (cps), to account for acquisition time differences, were analyzed using Wire 2.0 software. **Figure 2.1** shows the processing of a typical spectrum acquired in PDMS equilibrated with 5mM quinoline. Baselines were modeled well using second

order polynomial or cubic spline functions for PDMS and water experiments, respectively, producing flat baselines for subsequent analysis. **Figure 2.1(A)** shows preprocessed solid phase spectra with a polynomial baseline fit, while **Figure 2.1(B)** shows the post processed spectra with the flat baseline. **Figure 2.1(C)** shows the curve fits used to obtain reported integrated peak areas. The quinoline peaks at 1375 cm^{-1} and 1442 cm^{-1} are shown adjacent to the PDMS internal standard peak at 1410 cm^{-1} (denoted by the asterisk). Spectral peaks were fit to standard Vogt distribution profiles and curve fit parameters were used to calculate integrated peak areas. Integrated peak areas of the PDMS internal standard were used to normalize reported analyte peak areas.

2.4 Results and Discussion

To explore SPME/Raman we select a homologous series of increasingly polar and soluble aromatic compounds. Prior work has extensively characterized the full spectral range of PDMS as well as identifying spectral windows where prominent toluene and benzene peaks can be seen in a PDMS background.[14, 22] **Figure 2.2** shows the full Raman Spectrum of PDMS along with PDMS soak in three different organic compounds: (top to bottom) quinoline, toluene, benzene, respectively. **Figure 2.3** shows the concentration dependence of the Raman spectral peak for the toluene ring breathing mode at 1005 cm^{-1}, taken in the equilibrated PDMS and aqueous phases, respectively. The baseline subtracted spectral data points are presented along with corresponding curve fits. Scale bars show the intensity of the Raman signal in counts per second (cps). The toluene ring breathing mode is the most prominent peak that does not overlap with any PDMS or water peaks. Comparing peak intensities from equilibrated measurements in PDMS and water, we see a ~250 fold enhancement of the 1005 cm^{-1} toluene peak intensity in PDMS. The

normalization of peak intensity, using PDMS as an internal standard, means that these peak intensities should be proportional to concentration in the dilute limit we are operating in. We expect toluene to favorably partition into PDMS because it is a non-polar molecule with a low aqueous solubility (~5.1mM at 25^{o}C).[66] Its low solubility translates into a substantial thermodynamic driving force to partition into the hydrophobic polymer.

Benzene is a molecule with higher water solubility (~23mM at 25^{o}C) than toluene.[67] As a result, we expect benzene to have less favorable partitioning into PDMS than was observed for toluene. Raman signals of benzene equilibrated between PDMS and water are shown in **Figure 2.**4. Here the spectral window (965-1250 cm^{-1}) is centered on benzene's symmetric ring breathing mode at 992 cm^{-1}. Within this spectral window, we see that the partitioning of benzene into PDMS results in a ~50 fold signal increase in the polymer compared to the water. Again, because of the internal standard normalization, this should be proportional to analyte concentration.

Lastly, we examine quinoline which has the highest water solubility (~50mM) among the aromatic molecules we are evaluating. **Figure 2.5** shows Raman signals for quinoline equilibrated between PDMS and water. Within the spectral window, a quinoline peak at 1375cm^{-1} as well as a broader PDMS peak at 1410 cm^{-1}(from the PDMS) can be seen. The 1375 cm^{-1} quinoline peak corresponds to an asymmetric ring-breathing vibrational mode of the molecule. We see a ~10 fold signal increase of this peak in PDMS compared to spectra taken in water, which continues to follow our anticipated inverse relationship between PDMS partitioning enhancement and aqueous solubility.

2.5 Quantifying Partitioning

The quantitative partitioning of toluene and benzene into PDMS has been extensively studied with various SPME techniques such as SPME-GC and MIMS.[54, 68] This has yielded consistent values for equilibrium partition coefficients. Quinoline and its derivatives have been less studied in the literature, despite being a potent inhibitory compound for biological activity. Using SPME/Raman, we quantify the observed partitioning of these three molecules into PDMS**.** **Figure 2.6A** shows the normalized analyte peak areas in the PDMS phase as a function of the aqueous analyte concentration. Similarly, **Figure 2.6B** shows the normalized peak area of the analyte when measured in the water phase. Each data point in these plots represents triplicate measurements performed on two separate samples. Data points were fit using linear regression analysis. In the dilute regime we are operating in, there is negligible polymer swelling, so the normalized Raman signals obtained in PDMS and water ought to vary linearly with changing concentration, as verified in **Figure 2.6**. Previous SPME/Raman work by Wittkamp *et al* has also shown this general linearity for toluene and benzene in PDMS.[22] To assess the quantitative character of SPME/Raman in the dilute regime, we extend prior work by calculating the PDMS partition coefficient for each organic compound. The normalized peak areas in **Figure 2.6** are proportional to concentration, the Raman scattering cross-sections of each organic molecule (in each phase), and other instrument factors. If we assume the Raman cross-sections and instrument factors remain constant between phases, then the equilibrium partition coefficient K_i for each molecule i can be estimated from the data in **Figure 2.6** as:

$$K_i = \frac{(Slope)_{PDMS,i}}{(Slope)_{Water,i}}, \quad (2)$$

where $(Slope)_{PDMS,i}$ is the slope of the best fit line for each molecule i measured in the PDMS phase (**Figure 2.6A**) and $(Slope)_{Water,i}$ is the slope of the best fit measured in the aqueous phase (**Figure 2.6B**). We can assess the reasonableness of this simplistic approach by comparing our values of K_i computed using Eqn. 2 and data from **Figure 2.6** with known literature values determined using mass spectrometry and other SPME-based optical techniques. **Table 1** shows $\log(K_i)$ values obtained using our method as well as SPME-GC/MS,[54, 68, 69] MIMS,[63, 68] Attenuated Total Reflectance Fourier Transformed IR spectroscopy (ATR/FTIR),[62] and Quantitative Structure Property Relationship (QSPR) modeling in PDMS/water systems.[70] As the table shows, our measured values fall within a reasonable range of expected K_i values for toluene and benzene. Extending our technique to quinoline also gives a reasonable K_i value based on its intrinsic chemical structure and higher water solubility than toluene or benzene. The analysis used to estimate our results in **Table 1** assumes the Raman cross-section of each molecule is largely unchanged in the PDMS and water solvent environments. The fact that our K values fall within the expected ranges is evidence this assumption is largely met. Moreover, the molecular vibrations being probed in **Figures 2.3-2.5** are shifted only modestly, adding indirect evidence that the different solvent environments have not radically altered the Raman scattering.

2.6 Conclusions & Implications

We have demonstrated that SPME makes Raman Spectroscopy 1-2 orders more sensitive. We have also shown that SPME/Raman can be a reasonably quantitative method depending on how well the particular analyte conforms to the basic assumptions used in our analysis, namely, operating in the dilute limit with modest polymer swelling, and little perturbation of the scattering cross-section and instrumental factors in the different phases. The merging of PDMS-based analytics with modern microfluidics fabricated using PDMS requires a quantitative

understand of the polymer/analyte interactions using modern optics. Quantitative characterization of PDMS/analyte interactions using SPME/Raman is a first step towards this goal.

2.7 Acknowledgements

We gratefully acknowledge supporting work by Rory E. Biesanz and Evangeline Drink as well as the support of the Gates Foundation (Millennium Scholarship to IN), the National Science Foundation (DGE-0654252), and the USDA National Institute of Food and Agriculture (AFRI 2011-68005-30416).

2.8 Figures

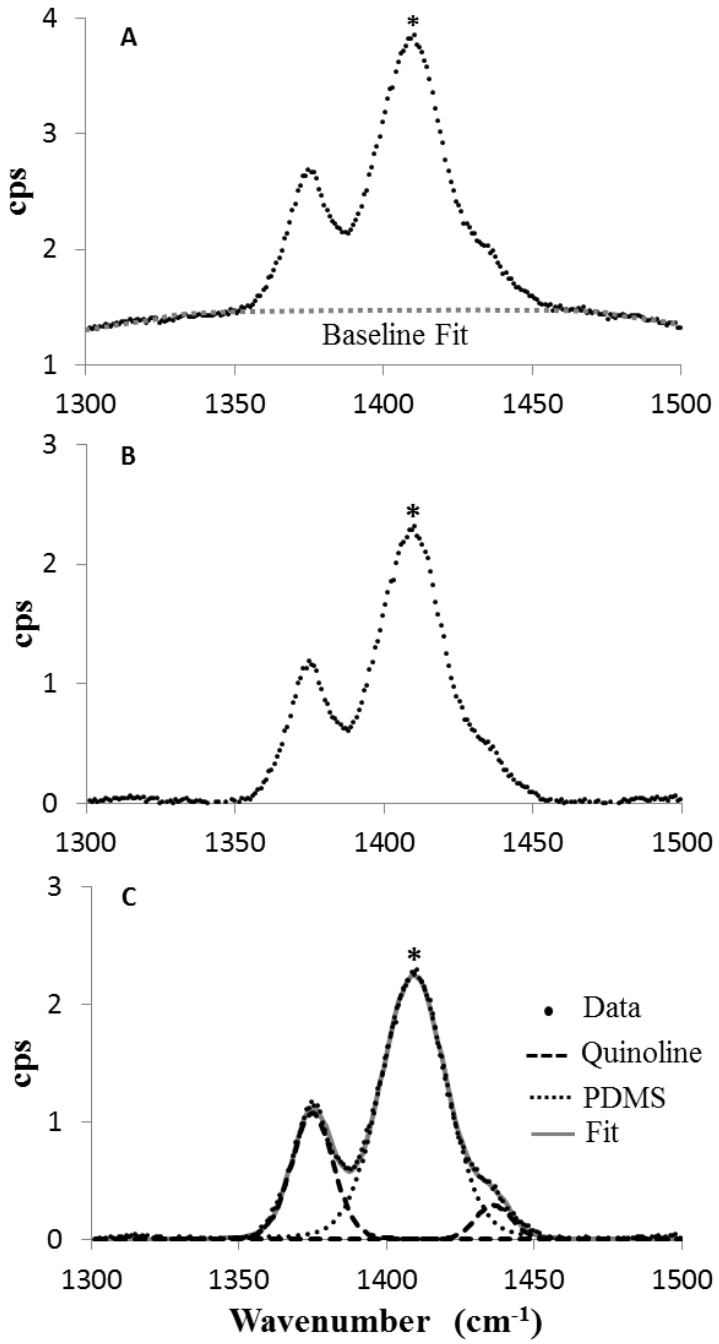

Figure 2.1: Raman spectra of 5mM quinoline in PDMS before (**A**) and after (**B**) baseline subtraction. Spectra **C** is the curve fitting of the subtracted spectra. The asterisked (*****) peak at 1410cm^{-1} is the PDMS internal standard.

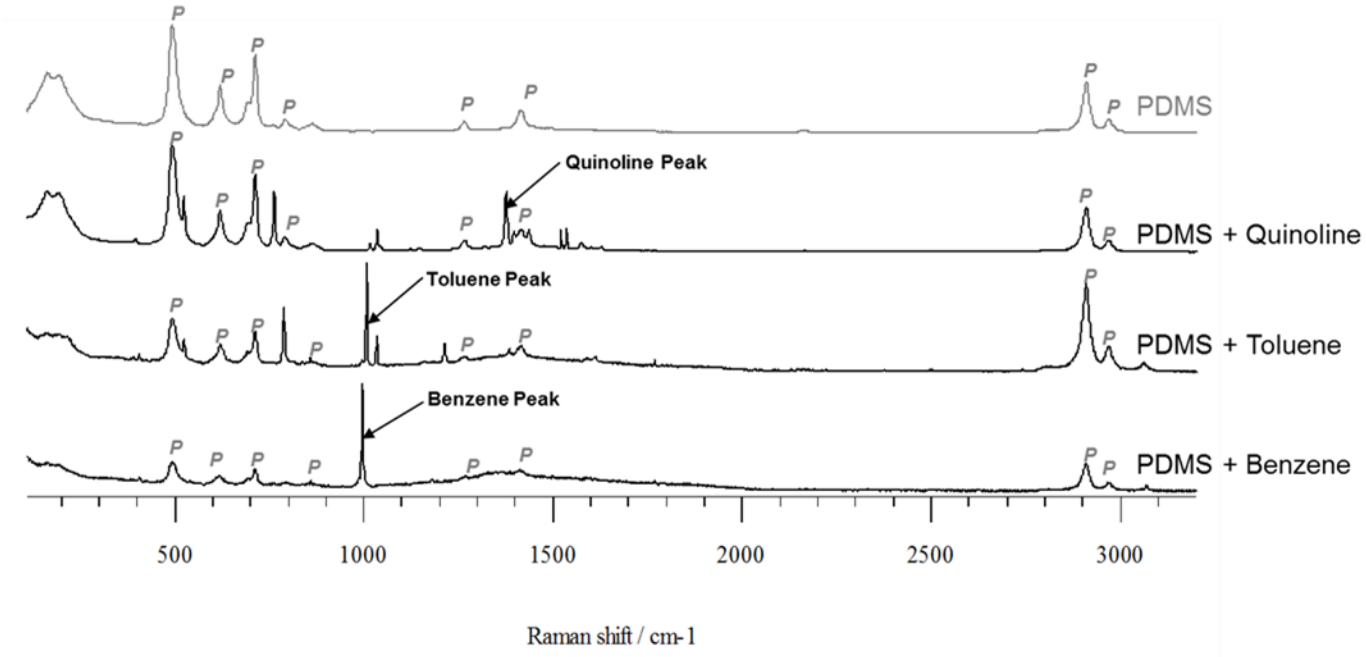

Figure 2.2: Full range spectra of PDMS as well as PDMS completely immersed and soaked in neat quinoine, toluene, and benzene (top to bottom). Analysis peaks are identified by the labeled arrows and PDMS peaks are identified by the (P).

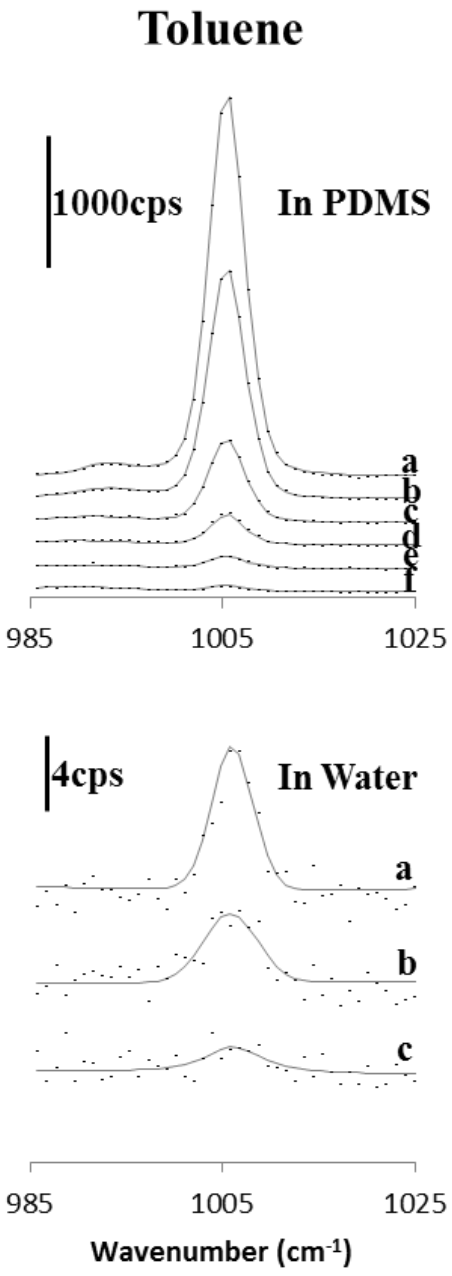

Figure 2.3: Baseline subtracted Raman spectra detected in PDMS (top) and solution phase (bottom) of toluene equilibrated between PDMS and water at different concentrations. **a, b, c, d, e, f** present concentrations **5, 3.5, 2, 1, 0.5, 0.2** mM respectively. Data points present the raw data.

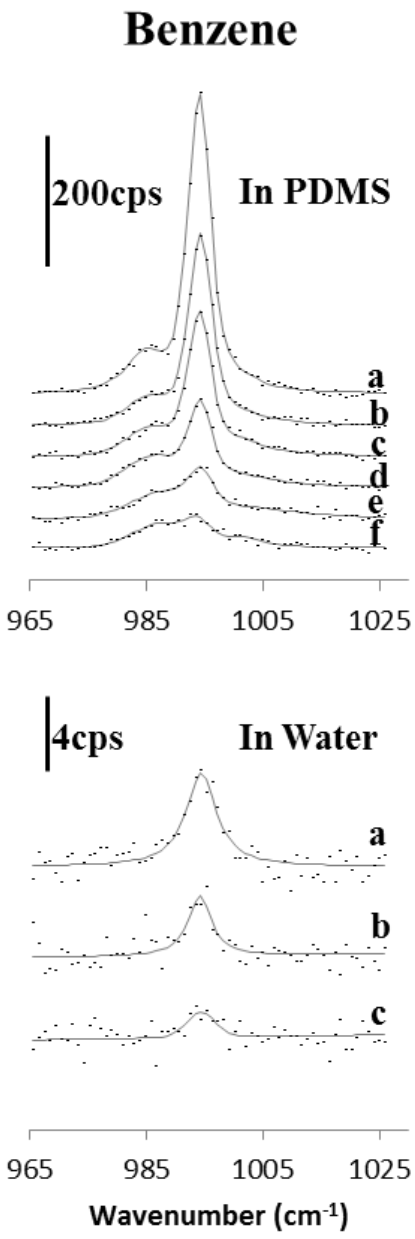

Figure 2.4: Baseline subtracted Raman spectra detected in PDMS (top) and solution phase (bottom) of benzene equilibrated between PDMS and water at different concentrations. **a, b, c, d, e, f** present concentrations **5, 3.5, 2, 1, 0.5, 0.2** mM respectively. Data points present the raw data while solid lines are the curve fits of the data.

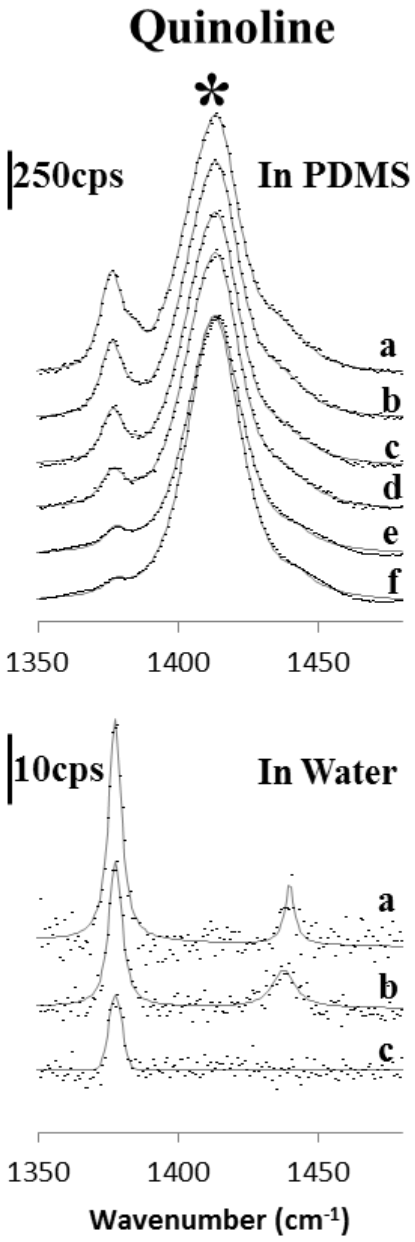

Figure 2.5: Baseline subtracted Raman spectra detected in PDMS (top) and solution phase (bottom) of quinoline equilibrated between PDMS and water at different concentrations. **a, b, c, d, e, f** present concentrations **5, 3.5, 2, 1, 0.5, 0.2** mM respectively. Data points present the raw data while solid lines are the curve fits of the data. The asterisked (*****) peak at 1410cm^{-1} is the PDMS internal standard.

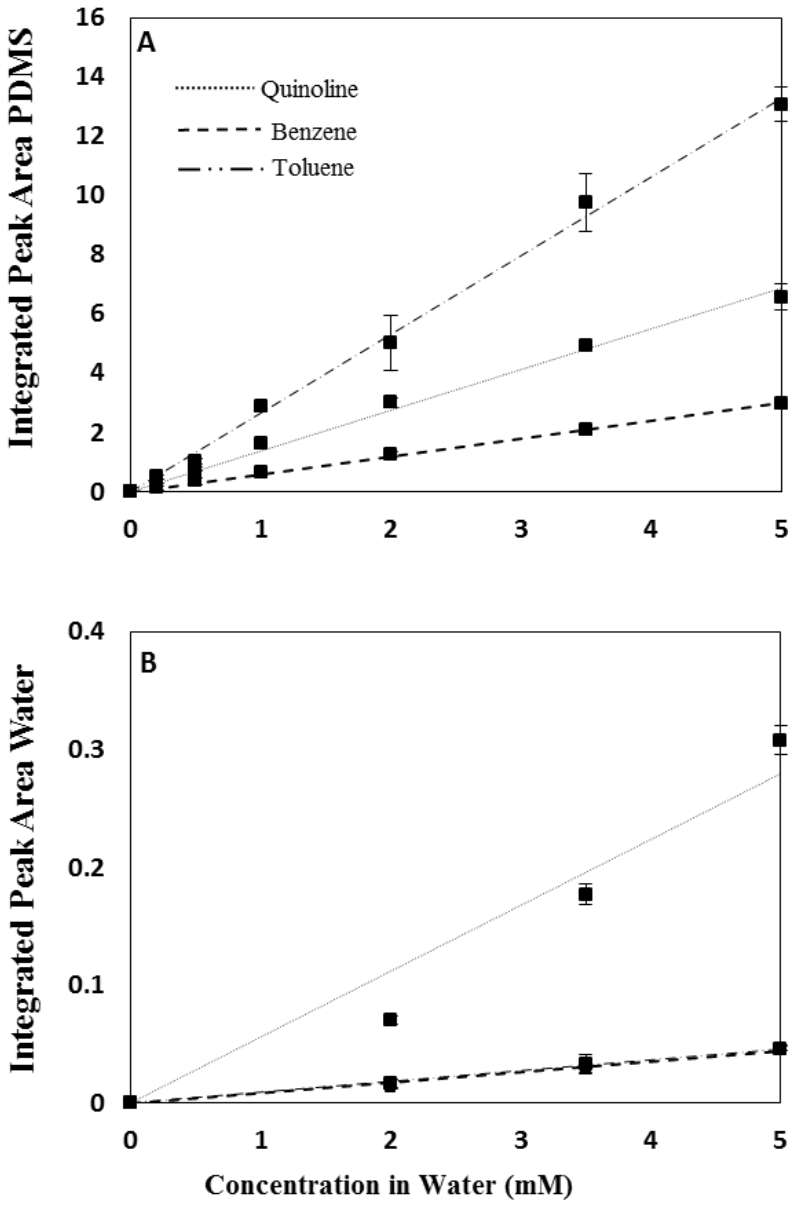

Figure 2.6: Plots are generated by averaging the normalized integrated peak areas of specified peaks of benzene, toluene, and quinoline from the PDMS (Panel A) and water (Panel B) experiments. Reported peak areas are in units of kilo-counts per second (kcps).

SPME Techniques	**log($K_{Toluene}$)**	**log($K_{Benzene}$)**	**log($K_{Quinoline}$)**
SPME/GC/MS [20, 22]	2.06-2.09	1.59-1.61	----
MIMS [9, 21]	2.3-3	----	----
QSPR Modeling [23]	2.24-2.38	2.04-2.10	----
ATR/FTIR [7]	2.25	----	----
SPME/Raman [This Data]	**2.35 ± .20**	**1.90 ± .10**	**1.20 ± .20**

Table 1: The SPME/Raman data represents the range of partition coefficients obtained from triplicate experiments using our technique. We compare our data to values from other quantitative methods.

Chapter 3

Quantitative SPME/Raman to detect Anesthetic Compounds

3.1 Summary

One challenge in anesthesiology is accounting for anesthetics compounds in the body. Although adequate estimates can be made by detecting exhaled gasses, actual concentrations in the body remain elusive due to partitioning of these compounds into lipid-like phases in blood. This ambiguity can potentially lead to surgical complications. Solid phase micro-extraction (SPME) was used along with Raman Spectroscopy to separate and enhance detection of anesthetics from aqueous and biological phases. Five anesthetic compounds were analyzed: two intravenous (halothane & propofol) and three volatile (isoflurane, enflurane, and etomidate). Linear regression analysis used to estimate the partition coefficient of halothane between PDMS and water. We estimate partition coefficients (log (K) = 1.93± 0.17) for halothane using our quantitative method as well as qualitatively demonstrating the ability of SPME to enhance Raman detection toward clinically relevant concentrations of both compounds (halothane 200µM, propofol 6.5µM). Additionally, we explore the potential for separation of these two compounds from human pooled serum. We also show the improved detection of isoflurane, enflurane, and etomidate using SPME/Raman. SPME is a pre-concentration technique that does not rely on a particular detection system, making it a versatile approach for complimenting several different analytical platforms.

3.2 Introduction

Anesthesiology as a clinical practice has made significant progress towards safe and effective use of analgesic compounds[71]. Transitioning from compounds like halothane and enflurane

towards safer inhaled anesthetics such as isoflurane and servoflurane is largely responsible for the reduced analgesic-related complications during surgeries. The use of fast-acting intravenous anesthetics like propofol, ketamine, and etomidate has also improved the clinical practice.[71] However, one challenge in the field is accounting for these anesthetics in the body[72]. Although adequate estimates can be made by detection of inhaled and exhaled gas concentrations, actual internal concentrations remain elusive due to partitioning of these compounds into lipid-like phases in the body[72]. This ambiguity can lead to unnecessary surgical complications[72]. Ways to directly measure concentrations in relevant biological fluids maybe beneficial to practitioners in hospitals.

Partitioning of anesthetics between physiological phases such as blood/brain (BB) or alveolar gas/blood, and blood/lipid has been well documented[58]. The magnitude of partitioning is directly influenced by the equilibrium partition coefficient (K), the thermodynamic parameter that quantitatively relates the analyte concentration in each phase. Although physiological partitioning can complicate administration and detection of anesthetics[73], the same partitioning process can be used to enhance detection of analytes via the method known as SPME[74].

SPME is a well-known analytical technique that utilizes hydrophobic traits of polymers to extract and pre-concentrate non-polar analytes for better detection[74]. PDMS (polydimethylsiloxane), a staple, biocompatible polymer, for SPME analytics, has been well established for liquid as well as gas phase detection. Techniques that benefit from SPME pre-concentration are well documented in the literature[14, 45, 61, 64, 75]. SPME coupled to Raman Spectroscopy (SPME-RS), is emerging as a quantitative analytical method, showing 1-3 orders of magnitude improved detection over normal Raman Spectroscopy[14, 76]. Over the last decade, Raman-based devices like the RASCAL (Raman Scattering Analyzer) have become

commonplace in hospitals for monitoring exhaled gas-phase anesthetics during surgery[77]. New opportunities may exist for combining SPME-RS with anesthesiology.

Here we explore using PDMS-based SPME to enhance Raman detection directly in the relevant aqueous and serum liquid phases. Three volatile anesthetic compounds (isoflurane, enflurane, and halothane) and two intravenous anesthetics (propofol and etomidate) were examined for their enhanced detectability using SPME polymer phases. As well as signal enhancement, SPME has the potential to separate out macromolecules that may complicate detection, allowing smaller target analytes to be better seen. This sort of separation could prove very useful when dealing with detection analytes in a complex system such as blood.

3.3 Materials and Methods

3.3.1 Sample Preparation

PDMS Samples - As described in [72] but briefly: Slygard 184 PDMS and catalyst were obtained from Dow Corning. Samples of PDMS used in the experiment were prepared as follows. Uncured PDMS was mixed using the standard 10:1 polymer to catalyst ratio in a poly(methyl-methacrylate) (PMMA) mold .5mm deep. This was cured at 70^{o}C overnight to make a ~.5mm thick sheet of PDMS. Samples were punched out of the PDMS sheet using a 0.2mm diameter punch. The resulting PDMS plugs were sealed and kept until used.

Organic/Aqueous Solutions – Halothane, isoflurane and propofol were purchased from Sigma Aldrich. Pooled human serum was purchased from Biochemed Services (Winchester, VA). All were used as purchased. Experimental solutions were prepared by spiking the appropriate amount of reagent into 20 mL of deionized (DI) water. The solutions were then shaken vigorously, tightly capped, and left to fully dissolve. Spiked solutions were used within 15mins of preparation to prevent evaporative loses. Stock solutions of etomidate were prepared by

saturating 20mL of DI water with the solids and letting the solution equilibrate for 72hrs. Dissolve etomidate solutions were filtered before use.

3.3.2 SPME/Raman Extraction Procedure

Water SPME: As described in [72] but briefly: 20mL glass vials with Teflon-lined lids were used for the solid phase micro-extraction procedure. Solutions of halothane, propofol, isoflurane, enflurane, and etomidate were prepared in separate 20mL vials. PDMS plugs were introduced to each vial, capped, and left to equilibrate undisturbed at room temperature for 48 hours.

Serum SPME: Frozen 2mL serum aliquots were thawed to room temperature and centrifuge at 600rpm to separate out precipitates. Precipitate free serum was then transferred into glass vials (2mL) and spiked with halothane and propofol water solutions to reach the desired concentrations. PDMS plugs were introduced to each vial, capped, and left to equilibrate undisturbed at room temperature for at least 48 hours.

3.3.3 Raman Spectra Acquisition

Raman spectra were collected using a Renishaw inVia Raman micro-spectrometer attached to a Leica DM IRBE upright optical microscope. A 785 nm diode laser operated full power (nominal 180mW) was used to irradiate samples through a 50x (N.A. 0.8) objective lens. The spot area was ~50μm^2. Raman scattered light was acquired through the same objective lens and detected on a thermoelectrically cooled (-60 ^oC) CCD. All PDMS sample measurements were acquired for 10 seconds. Time acquisitions for water sample measurements ranged from 10-300sec depending on signal to noise concerns. Spectra of pure compounds (halothane, isoflurane, enflurane, and propofol) where collected with a 10x objective, irradiated within a capped 2mL glass vial. Spectra of equilibrated PDMS and water samples were collected using a wet sample holder sealed with an optical coverslip. Laser stability was assured using the 520 cm^{-1} peak of Silicon.

The PDMS peak at 1410 cm^{-1} was acquired with all solid phase spectra and served as an internal standard that helped normalize for sample to sample variations in system focus.

3.3.4 Raman Intensity Normalization & Peak Analysis

As described in [72], spectral, reported in counts per second (cps), to account for acquisition time differences, were analyzed using Wire 2.0 software. Spectral peaks were fit to standard Vogt distribution profiles and curve fit parameters were used to calculate integrated peak areas. Integrated peak areas of the PDMS internal standard were used to normalize reported analyte peak areas.

3.4 Results and Discussion

Figure 3.1 shows characteristic Raman spectra of all five of these anesthetic compounds (neat) within the 200-1090 cm^{-1} range. These compounds not only represent diverse anesthetics, but over this range there are unique spectral features for all the compounds which make it effective for fingerprinting. Also in this region, we see a diverse range of Raman scattering intensities. This makes halothane the easiest and etomidate the most difficult to detect using the system. To illustrate the quantitative aspect of SPME/Raman (as also detail in prior work [11]) we examine halothane, which produced the largest signals as shown in the top spectra of **Figure 3.1**. In the spectral window (285-350 cm^{-1}), which has two large peak that do not overlap with known PDMS (our SPME phase) or water (our solvent phase) peaks, we examine the C-Cl bending mode of halothane at 310cm^{-1}. **Figure 3.2** shows the Raman spectral peaks for the C-Cl bending mode of halothane at 310 cm^{-1} taken in the equilibrated PDMS (top) and aqueous (bottom) phases. The baseline subtracted spectral data points are presented along with corresponding curve fits and scale bars show the intensity of the Raman signal in counts per second (cps). Comparing detection in PDMS to that in water, we see a ~50 fold peak intensity

enhancement. **Figure 3.2** illustrates that SPME/Raman is capable of signal improvement of halothane towards concentrations that are clinical relevant (0.25-0.50mM)[78].

3.4.1 Quantifying Partitioning

Following the procedure previously described [11]; we quantify the partitioning of halothane in from water into PDMS**.** The method entails the ratio of slopes generated by plotting the integrated peak areas of the compound (in both phases) at different concentrations. **Figure 3.3** shows a plot of the 310 cm^{-1} halothane peak areas as a function of water concentration. Peaks areas were normalized to a PDMS internal standard peak at 1410 cm^{-1}, eliminating any variation base on PDMS sample preparation. This directly relates peaks to concentration of analyte in the system. Data points represent triplicate measurements performed on two separate samples and were fit using linear regression analysis. The linearity of this plot suggests we are in the dilute range where there is negligible swelling and solute-solute interactions are modest. Assuming instrument factors remain constant between phases, we can estimate the equilibrium partition coefficient K_i for each molecule i from the data in **Figure 3** as:

$$K_i = \frac{(Slope)_{PDMS,i}}{(Slope)_{Water,i}} \ , \qquad (1)$$

where $(Slope)_{PDMS,i}$ is the slope of the best fit line for each molecule i measured in the PDMS phase and $(Slope)_{Water,i}$ is the slope of the best fit measured in the aqueous phase. **Equation 1** provides a partition coefficient value for halothane ($\log K_i$). Values obtained where ranged from log (K) = 1.93± 0.17. Although there are no known value of K for PDMS/water systems, others report values of log (K) = 2-3 for halothane partitioning into lipids[56, 79]. PDMS is a hydrophobic polymer known to display lipid-like partitioning, which makes our estimated values reasonable.

3.4.2 Qualitative Detection

Next, we examine propofol, a commonly used intravenous anesthetic. Unlike halothane that has a relatively high water solubility (~20mM), propofol solubility is low (700µM). At these concentrations and using reasonable acquisition times, we could not detect the compound in the aqueous phase using Raman. However, with SPME propofol was readily at clinically relevant concentrations. Concentrations of administered propofol typically range from 1-60µM in blood[72]. **Figure 3.4A** shows spectra of the characteristic 1046 cm^{-1} aromatic peak of propofol taken in the equilibrated PDMS. All spectra were acquired with 10 sec of exposure, which highlights the potential to improve signal-to noise ratio at lower concentrations where compound peak are difficult to discern. As expected, **Figure 3.4B** shows that the partitioning of propofol behaves linearly at these dilute concentrations.

Fingerprinting with Raman spectroscopy is challenging for complex multi-component samples such as blood and urine. SPME pre-concentration has the potential to selectively separate and concentrate the desired analyte, thereby avoiding interference from other components. As a simple proof of concept, a mixture of 10mM halothane and 60µM propofol in human pool serum was examined. **Figure 3.5A** shows a Raman spectrum obtained directly in serum while **Figure 3.5B** shows a typical spectrum in PDMS after the serum mixture was equilibrated with the polymer. **Figure 3.5A** displays the broad spectrum we expect from a complex aqueous protein mixture like serum. None of the peaks from the anesthetic compounds are discernible. However, the spectrum acquired from the equilibrated PDMS phase has none of the protein peaks and therefore lets us resolve anesthetic peaks (box & inset of **Figure 3.5B**), in much the same way we saw in neat and aqueous SPME measurements presented earlier. An interesting difference between aqueous mixtures and serum is the fact that only the halothane

peaks are visible. Given the concentration of propofol used here, one expects to easily see propofol in the PDMS phase since it was clearly evident at these concentrations in water. However, it is known that propofol complexes with proteins in serum[72, 80, 81]. The protein-propofol complex competes with SPME partitioning, reducing the SPME effect. We can express this competition and its impact on PDMS-phase propofol $[Pf]_{PDMS}$ with a simple equilibrium mass-action model:

$$[Pf]_{PDMS} = \frac{K_i[Pf]_{total}}{1+ K_b+K_i}, \quad (2)$$

where K_b is the equilibrium propofol-protein complex binding constant and $[Pf]_{total}$ is the total propofol concentration (i.e., total added propofol). As expressed in **Equation 1,** K_i is the analyte partition coefficient with i being propofol in this case. Equation (2) makes it clear that the absence of propofol peaks in **Figure 3.5B** means that K_b is much greater than K_i, which results in a diminished partitioning into the polymer.

Lastly, we illustrate the improved detection using SPME of isoflurane, enflurane, and etomidate. These anesthetic compounds gave the weakest Raman signals as measured in **Figure 1**. Although the inherently weak signals from these compounds make them undetectable in water, when equilibrated with a PDMS phase distinct signature peaks can be seen. The main spectrum in **Figure 3.6** (gray) shows the large characteristic peak from PDMS which dwarf any anesthetic peaks on this scale. The spectral windows where anesthetic peaks reside are 250-450 cm^{-1} and 950-1050 cm^{-1}as shown in insets **Inset (1)** & **(2)**, respectively. The top spectra in the 250-450 cm^{-1} range (**Inset 1**) includes the characteristic 360 cm^{-1} enflurane peak and is directly followed by an isoflurane and PDMS background spectrum, respectively. Four distinct isoflurane peaks (300, 340, 370, 420 cm^{-1}) can be seen within the equilibrated PDMS/Isoflurane spectrum

and no peaks can be seen in the normal PDMS spectrum. The two spectra on the bottom (bold) are the difference spectra of the two anesthetic plots minus the PDMS. The top spectra in the 950-1050 cm^{-1} range (**Inset 2**) shows a characteristic 1005 cm^{-1}etomidate peak neighboring a PDMS background peak at 995 cm^{-1}. The middle spectra in the inset is the PDMS background in that range and the bottom spectra in bold is the difference spectrum of the etomidate minus the PDMS background. As evident, even with the poorest Raman scattering (for our 785nm laser system), we see that SPME does enhance Raman signals of these anesthetics.

3.5 Conclusions & Implications

We show that SPME improves the Raman signals of all the anesthetics examined in this study. With halothane and propofol, which displayed the strongest Raman signals, SPME lets us easily detect clinically relevant concentration (200µM and 35µM respectively) with modest acquisition times (10 sec). We quantify partitioning of halothane into PDMS and obtained a range of partition coefficients (log (K) = 1.93± 0.17) for the system. Finally, signals for isoflurane, enflurane, and etomidate could be easily discerned within a PDMS background using SPME but were undetectable in the water phase under similar conditions.

SPME is a pre-concentration technique that does not rely on a particular detection system, making it a versatile approach for complimenting several different analytical platforms. In the case of detecting anesthetics compounds, this means it can enhance many of the analytical methods used for their detection. This could also open doors for direct detection of these compounds in biological fluids using a variety of optically-based systems.

3.6 Figures

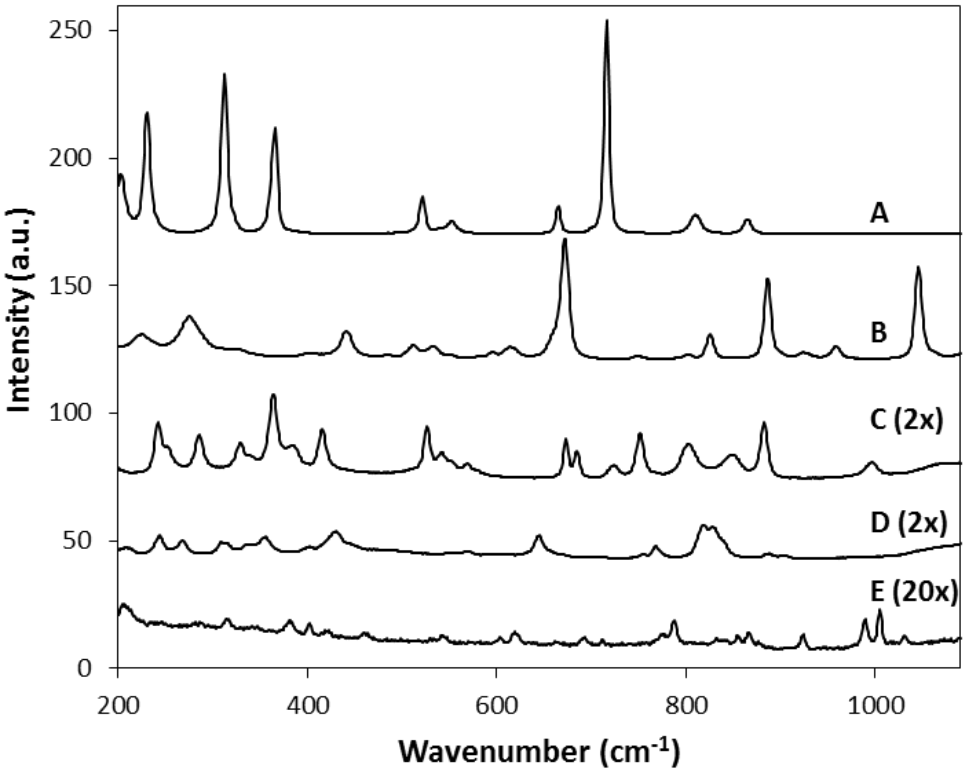

Figure 3.1: Raman spectra of neat anesthetic compounds. (A) Halothane, (B) Propofol, (C) Isoflurane, (D) Enflurane, (E) Etomidate. Multipliers next to spectra denote the magnification provided to make spectral features visible.

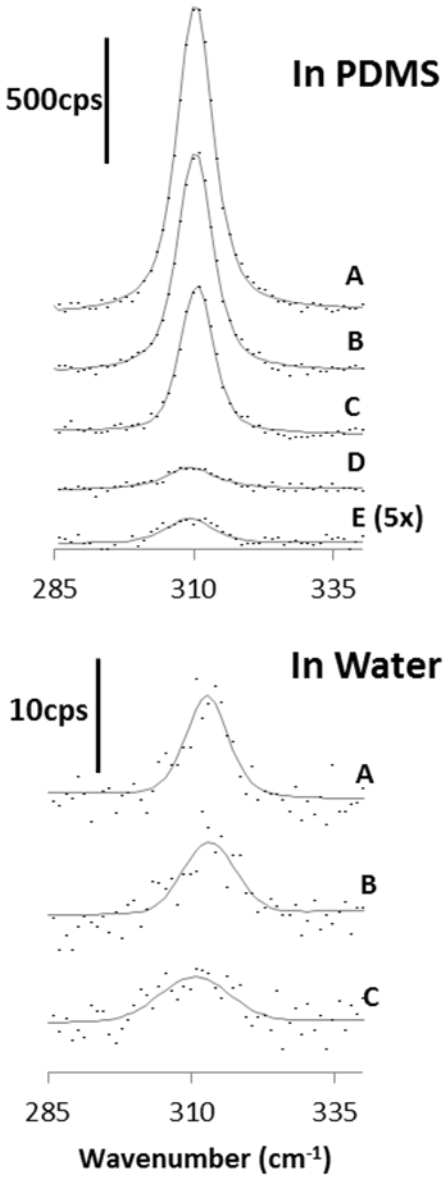

Figure 3.2: Raman spectra of the 310cm^{-1} halothane peak acquired in the PDMS (top) and water (bottom) phases. A-E are aqueous concentrations of 20, 15, 10, 2, and .2mM (respectively). Data points are raw data and lines are the Vogt curve fits.

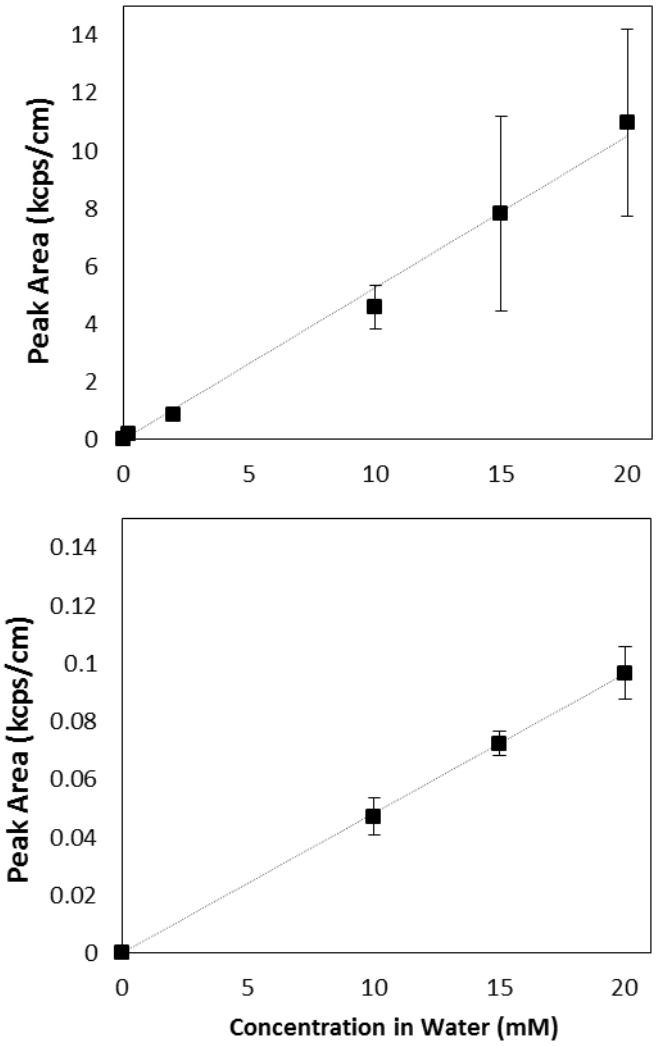

Figure 3.3: Integrated peak areas versus water concentrations of the 310cm^{-1} halothane peak acquired in the PDMS (top) and water (bottom) phases. Data points represent three different experimental trials.

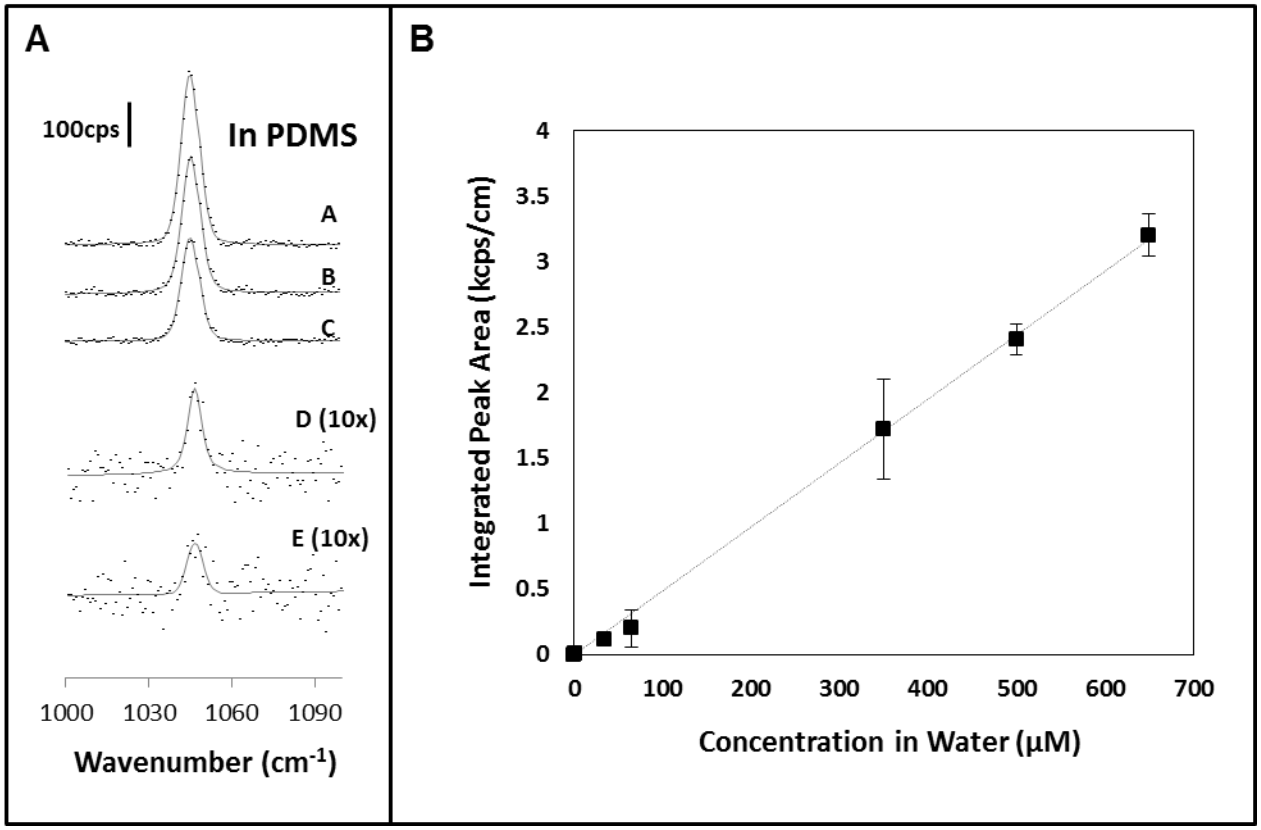

Figure 3.4: Spectra A-E in Panel A were acquired in the PDMS phase at propofol concentrations of 650, 500, 350, 65, and 35µM (respectively) in water. Panel B are the representative integrated peak areas of the spectra plotted versus water concentration. Data points represent two different experimental trials, n = 6.

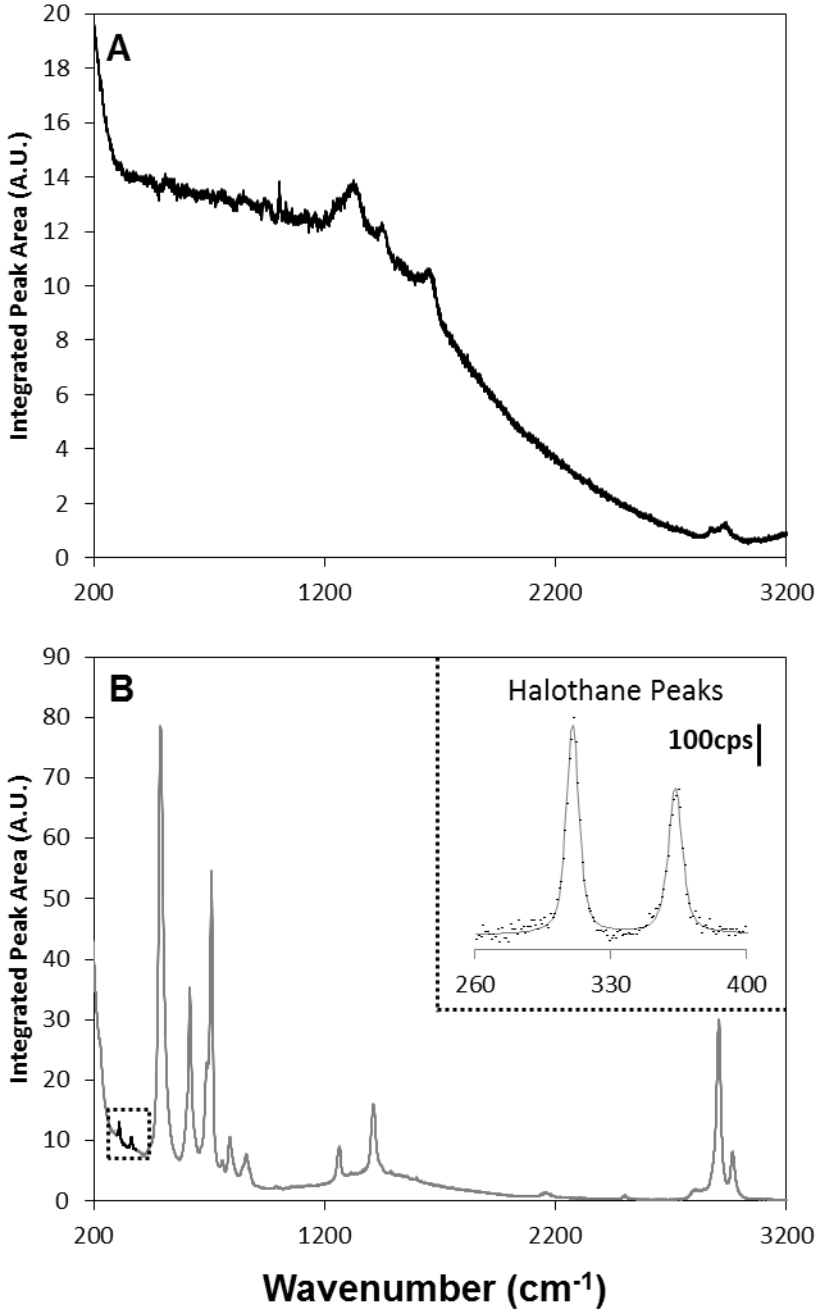

Figure 3.5: 10mM Halothane 60uM Propofol in Serum (A) and in PDMS (B). The Inset in B is the baseline subtracted region where the halothanes peak are present.

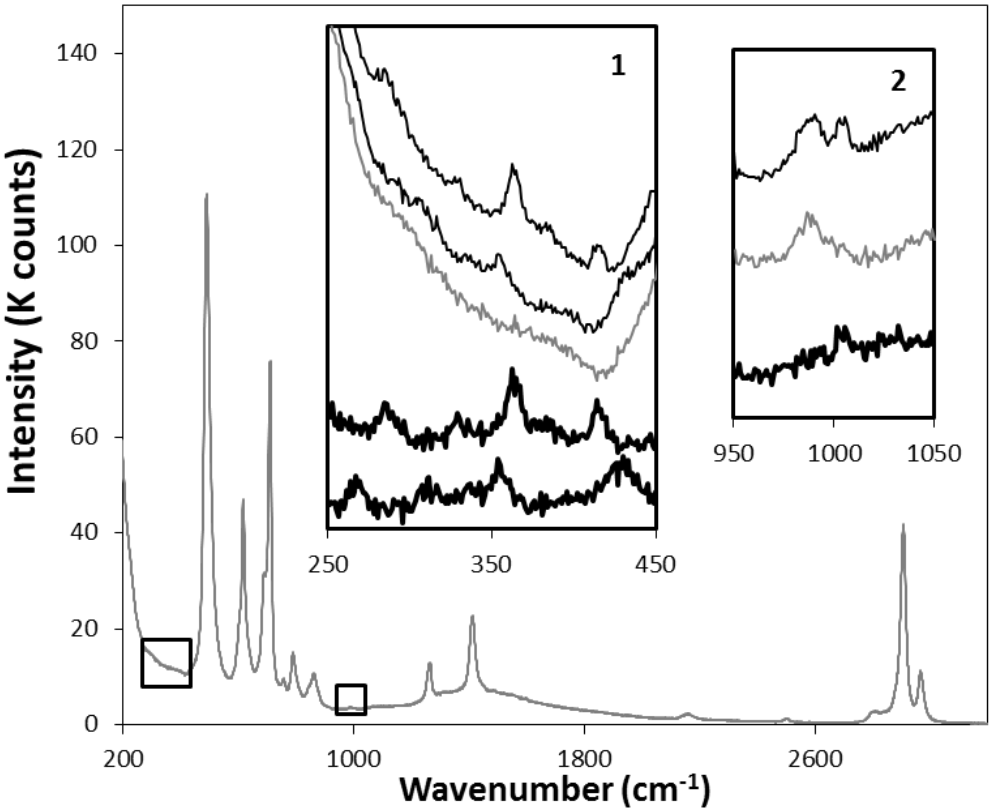

Figure 3.6: The PDMS background spectra (gray) illustrates the spectral ranges highlighted by the insets. Inset (1) shows two spectra: enflurane and isoflurane in PDMS. Inset (2) shows etomidate in PDMS. Bottom plots (bold) are the difference spectra of the equilibrated compound spectra minus the PDMS background.

Chapter 4

Selection of Polymer Phases towards Detection of Fermentation Inhibitors

ABSTRACT. Solid phase micro-extraction (SPME) was used along with Raman Spectroscopy to selectively extract and detect furfural from aqueous systems. Pretreatment methods such as steam explosion and dilute acid, used to release sugars from woody biomass, create fermentation inhibitors like furfural through side reactions. At high enough concentrations, furfural hinders downstream hydrolysis and fermentation processes. Although polymeric adsorbents are typically used to extract furfural from these batch systems, SPME phases may offer a means to detect and extract at relevant concentrations. Here, we test two polymer phases, Polydimethlysiloxane (PDMS) and Bisphenol A diglycidyl ether resin (5 Minute Epoxy) for extraction and improved detection of furfural using thermodynamic partitioning. We find the 5 minute epoxy is a better extractor of the molecule than PDMS. This is based qualitatively on the better Raman signals obtained in epoxy than in PDMS and the optical color change of the epoxy resin before and after soaking. We quantify the extent of partitioning using prior established methods and get log (K) = -0.41 for PDMS and log (K) = 0.24 for epoxy. We show that predicted values of log (K) from Flory-Huggins theory match those obtained experimentally. Lastly, we show we can use these polymers to extract and detect furfural in a simulated multi-component pretreatment mixture.

4.1 Introduction

Steam explosion and dilute acid are frequently used pretreatment techniques for the extraction of sugars from woody biomass[60, 82, 83]. However, side reactions during these pretreatment methods create fermentation inhibitors such as furfural, hydroxymethylfurfural

(HMF), and vanillin[83]. These degradation products are known to hinder downstream hydrolysis and fermentation processes in these batch systems[59, 60]. Furfural is a principal of these products that inhibit fermentation[59, 84]. This xylose degradation product at high enough concentrations (1-4g/L) is toxic to culture growth[59]. Detection furfural at these relevant concentrations is critical to will improved yields of sugar and other downstream products.

Strategies for enhanced detection of furfural can be gleaned from methods involving furfural extraction using polymers. Weil *et al* have shown that polymeric adsorbents XAD-4, XAD-7 can be used to remove furfural from batch solutions, thereby improving sugar and ethanol yields in fermentation processes [59]. Other works also used hydrophobic resins to extract furfural in solution. This extraction exploits hydrophobic properties of materials to pre-concentrate target molecules. Detection techniques that rely on pre-concentrating analytes via bulk phase partitioning may offer a way to simultaneously extract and detect furfural in batch systems.

Solid Phase Micro-extraction (SPME) is a technique which also exploits hydrophobic traits of polymers to pre-concentrate analytes for better detection [41, 45, 48, 74, 76, 85]. Techniques that benefit from SPME pre-concentration are well documented in the literature [14, 45, 61, 64, 75]. SPME coupled to Raman Spectroscopy (SPME/RS), an emerging analytical technique, is one such technique that can utilize the extractive properties of the polymers for enhanced detection of furfural in these batch systems.

As well as signal enhancement, SPME has the potential to separate out macromolecules that may complicate detection, allowing smaller target analytes to be better seen. Choice of SPME polymer also enables one to potential select one that may be better suited for targeted analyte species. Here examine two different polymer phases (PDMS and 5 Minute Epoxy) for

detection furfural in aqueous systems. Improved detection and extraction of furfural would be valuable for its removal from these batch systems.

4.2 Materials and Methods

4.2.1 Sample Preparation

PDMS Samples - Slygard 184 PDMS and catalyst were obtained from Dow Corning. Samples of PDMS used in the experiment were prepared as follows. Uncured PDMS was mixed using the standard 10:1 polymer to catalyst ratio in a poly(methyl-methacrylate) (PMMA) mold 1.5mm deep. This was cured at 70^{o}C overnight to make a ~1.5mm thick sheet of PDMS. Samples were punched out of the PDMS sheet using a 2mm diameter punch. The resulting PDMS plugs were sealed and kept until used.

Epoxy Samples –5 Minute Epoxy was obtained from ITW Devcon. Epoxy resin and hardener were poured and mixed on a sheet of paper and spread into a thin layer approximately 1-2mm thick. This was cured at room temperature for 4hrs, allowing the polymer resin to harden completely. ~2x4mm samples were cut out of the slab using a razor blade. Epoxy slabs were sealed and kept until used.

Organic/Aqueous Solutions – All reagents (furfural, vanillin, xylan, and glucose) were purchased from Sigma-Aldrich and used as purchased. Experimental solutions were prepared by adding the appropriate amount of reagent into 20 mL of deionized (DI) water. The solutions were mixed, tightly capped, and left to sit until fully dissolved. Spiked solutions were used within 15mins of preparation.

4.2.2 SPME/Raman Extraction Procedure

Solutions of furfural were prepared in 20mL glass scintillation vials. These were used for the solid phase micro-extraction procedure. Two sample plugs (PDMS) or slabs (Epoxy) were

introduced to each vial, tightly capped, and left to equilibrate undisturbed at room temperature for at least 48 hours. To first approximation, the large excess volume ratio of aqueous phase solution to PDMS plugs means the aqueous concentration in solution before and after equilibration is negligibly altered.

4.2.3 Raman Spectra Acquisition

Spectra were collected using a Renishaw inVia Raman micro-spectrometer attached to a Leica DM IRBE upright optical microscope. A 785 nm diode laser operated full power (nominal 180mW) was used to irradiate samples through a 50x (N.A. 0.8) objective lens. The spot area was ~50μm^2. Scattered light was acquired through the same objective lens and detected on a thermoelectrically cooled (-60 ^oC) CCD. All polymer and aqueous sample measurements were acquired for 10 seconds. Spectra of neat furfural acquired 1% of the nominal laser power due to the fluorescence of the molecule. All sample spectra were collected using a wet sample holder sealed with an optical coverslip. Laser stability was assured using the 520 cm^{-1} peak of Silicon. The PDMS peak at 1410 cm^{-1} and the Epoxy peak at 1610 cm^{-1} was acquired with all polymer phase spectra and served as an internal standard that helped normalize for sample to sample variations in optical focus.

4.2.4 Raman Intensity Normalization & Peak Analysis

Spectral peaks were analyzed using Wire 2.0 software. All spectra were baseline subtracted using second order polynomial or cubic spline functions, producing very flat baselines for subsequent analysis. Spectral peaks where fit to standard Vogt distribution profiles. Curve fit parameters were used to calculate the reported integrated peak areas. Peak areas are reported in counts per second (cps).

4.3 Results & Discussion

To explore the improved detection of furfural using SPME/Raman, we select two different polymers as potential SPME phases. 5 minute Epoxy (Bisphenol A diglycidyl ether resin) and PDMS are both cross-linked polymer networks. PDMS is a conventional polymer in SPME analytics and epoxy is more widely used as an adhesive. We first examine the partitioning of these two polymers using a 50mM solution of furfural in water. **Figure 4.1** visually illustrates the difference in partitioning of the two polymers. **Figure 4.1(A)** is a 2ml glass vial filled with neat furfural (dark brown due to light exposure). **Figure 4.1(B)** is two pieces of epoxy resin (one before and the other after being introduce to 50mM furfural), while **Figure 4.1(C)** is two pieces of PDMS before and after equilibration. There is a significant color change in epoxy from before (yellow) to after (brown) as compared with the two pieces of PDMS. Interestingly, we noticed that pure furfural is clear in color, which means that the brownness in the purchased neat furfural (99%) comes from the 1% percent impurity of 5-methylfurfural (brown in color). This impurity seems to partition strongly in the equilibrated epoxy sample, which makes it much more fluorescent than the PDMS sample due to the greater partitioning of the brown impurity. This will be assessed further in future works. **Figure 4.2** shows characteristic Raman spectra of furfural in four different solvent environments within the 1300-1750 cm^{-1} range. Spectrum A shows the characteristic peaks of neat furfural while spectrum B shows it dissolved in water (100mM). Spectra C & D are epoxy and PDMS polymers, respectively equilibrated in 50mM furfural in water. Dissolved furfural in the three solvent phases can be discerned by the characteristic furfural peak at 1372 cm^{-1} (highlighted by the arrow).

Qualitatively, we compare the partitioning of furfural into both polymer phases from aqueous solution. **Figure 4.3** shows furfural dissolved in water at 50, 35, 20mM (A, B, C respectively).

Figure 4.4 shows the furfural peak at 1372 cm^{-1} taken in the PDMS equilibrated in aqueous solutions of furfural at those same concentrations. The baseline subtracted spectral data points are presented along with corresponding curve fits and scale bars show the intensity of the Raman signal in counts per second (cps). **Figure 4.5** shows the furfural peak at 1372 cm^{-1} taken in the epoxy equilibrated in identical aqueous solutions of the compound. Firstly, we see the signal acquired in epoxy is slight more enhanced than in the water phase. We also see that the signal in PDMS is significant attenuated than in water (25% of water). It is evident that for extraction and detection of furfural from aqueous systems, epoxy performs better than PDMS. Although the detection of furfural is only slightly improved in epoxy than in water, the data shows the potential extractive properties of epoxy resin. This is evident in the analogous peak intensities when detecting in the water and epoxy, meaning that the concentration of furfural in both phases are similar. This also means that, within pretreatment slurry, epoxy could be used to better discern concentrations by separating furfural from other interfering components in the broth.

We quantify partitioning of furfural into both PDMS and Epoxy solid phases by estimating the partition coefficients of both polymers in aqueous systems. This method is detailed in prior work [72], but briefly, we compare the slopes generated from linear regression fits from plots of the integrated areas of the 1372 cm^{-1} furfural peak versus water concentration. **Figure 4.6** shows three data plots and fits of the furfural peak in the epoxy (•), water (◊), and PDMS (▪) phases. Data points represent 2 different experimental trials. Peaks areas were normalized to a PDMS internal standard peak at 1410 cm^{-1} PDMS plot and to Epoxy internal standard at 1610 cm^{-1}. This eliminates any variation base on solid phase sample preparation so that peaks can be directly related to concentration of furfural in the system. Data points represent two experiments where

four measurements were taken. We estimate partition coefficient K_i for each molecule i from the data in **Figure 4.6** as:

$$K_i = \frac{(Slope)_{Polymer,i}}{(Slope)_{Water,i}}, \quad (1)$$

where $(Slope)_{Polymer,i}$ is the slope of the fit for each molecule i measured in either epoxy or PDMS phase and $(Slope)_{Water,i}$ is the slope of the best fit measured in the aqueous phase. **Equation 1** provides a partition coefficient value for furfural (K_i). For the PDMS/water system, we obtained values of log (K) = -0.44 and -0.37 for the two separate experimental trials. For epoxy/water experiment we obtain log (K) = 0.61.

To assess the reasonableness of our values of log (K), we using the Flory-Huggins approximation to select polymer based on known solubility characteristic. Specifically, the polymer's solubility parameter is a quantity which can be used to discern its compatibility with other polymers or solvents[86]. Using this model, the partition coefficient is expressed as:

$$logK_{pw} = -logS_w\bar{V} - \frac{[1+\chi]}{2.303}, \quad (2)$$

where K_{pw} is the equilibrium partition coefficient between polymer (p) and water (w) phases. S_w and $\bar{V}$ are the water solubility and molar volume of furfural (respectively). χ is the interaction parameter between furfural and the different solvent phases, which is a function of both the analyte (furfural) and polymer solubility parameters. This is expressed as:

$$\chi = \frac{(\delta_1-\delta_2)^2\bar{V}}{RT}, \quad (3)$$

where δ_1 and δ_2 solubility parameters for analyte and polymer respectively. Using these two expressions, we can predict values of $logK_{pw}$ to compare with our experimental values. **Figure 4.7** shows a table of experimental and predicted values of $logK_{pw}$ of both polymers in water. We

see that our values match the predicted trend that PDMS gives a negative partition coefficient (making detection worse than in the aqueous phase), while 5 minute epoxy give a positive partition coefficient.

Next, we use SPME/Raman Spectroscopy to detect furfural within a complex aqueous pretreatment sample. The sample, obtained from the Bura group, was the product of poplar biomass pretreated with steam explosion. The concentration of furfural in the sample was 30 mM. Besides furfural, other components were 12 g/L glucose, 24.5 g/L xylose, 9.3 g/l acetic acid, and 0.5 g/L HMF. We use epoxy and PDMS to detect furfural in these complex multicomponent systems. **Figure 4.8 (A)** shows Raman spectra of steam exploded pretreatment sample. **Figure 4.8 (B)** shows epoxy equilibrated in pretreatment sample. The Raman signal was saturated signal due to fluorescence and needed to be photo bleached to see the signal. **Figure 4.8 (C)** shows PDMS equilibrated in pretreatment sample and the furfural peak is mark with the asterisk and show in the inset within a smaller spectral window. The intense fluorescence of the epoxy contrasted with the lack of fluorescence in the PDMS sample indicates that epoxy partitions more of the impurities of the multicomponent pretreatment system than PDMS. This however is a detriment to detection within the epoxy, which was evident by the saturated signal. The PDMS within this system works well because it more effectively screens components that partitions into its matrix than epoxy.

Lastly, in order to better understand partitioning of furfural into the epoxy matrices, we assess the dynamics of partitioning of furfural by SPME/Raman. To this end, we performed a time-series experiment to see how quickly furfural equilibrates into the epoxy. **Figure 4.9** shows the furfural peak at 1372 cm^{-1} taken in epoxy equilibrated in a 50mM solution of furfural at different times. The baseline subtracted spectral data points are presented along with

corresponding curve fits and scale bars show the intensity of the Raman signal in counts per second (cps). **Figure 4.10** shows a plot of integrated peak areas as a function of time. We can see that the signal levels off at about the 15hr time point.

4.4 Conclusions & Implications

We demonstrate the use of two polymers (PDMS & 5 minute epoxy) to enhance the detection of furfural in aqueous systems using SPME/Raman. We show that detection using the conventional SPME polymer PDMS actually decreases the RS signal of furfural when compared to detection in the aqueous phase. We select of 5 Minute Epoxy using Flory-Huggins approximation of the compatible solubility and show that the polymer does better than PDMS at detecting this fermentation inhibitor. We can quantify both of these partitioning systems using previously a establish methodology and show that PDMS, as expected, gives negative values for $logK_{pw}$ while epoxy gives positives values. We applied the Flory-Huggins approximation to variety this values using known values of solubility parameters for PDMS, Epoxy, and furfural. We show that our values match the predicted values. This work demonstrates the need for careful tailoring of SPME polymers towards specified solvent-analytes systems. More specifically we show that extractive polymers, that used partitioning to separate fermentation inhibitors from batch systems, could be used for enhanced detection within such systems.

4.5 Figures

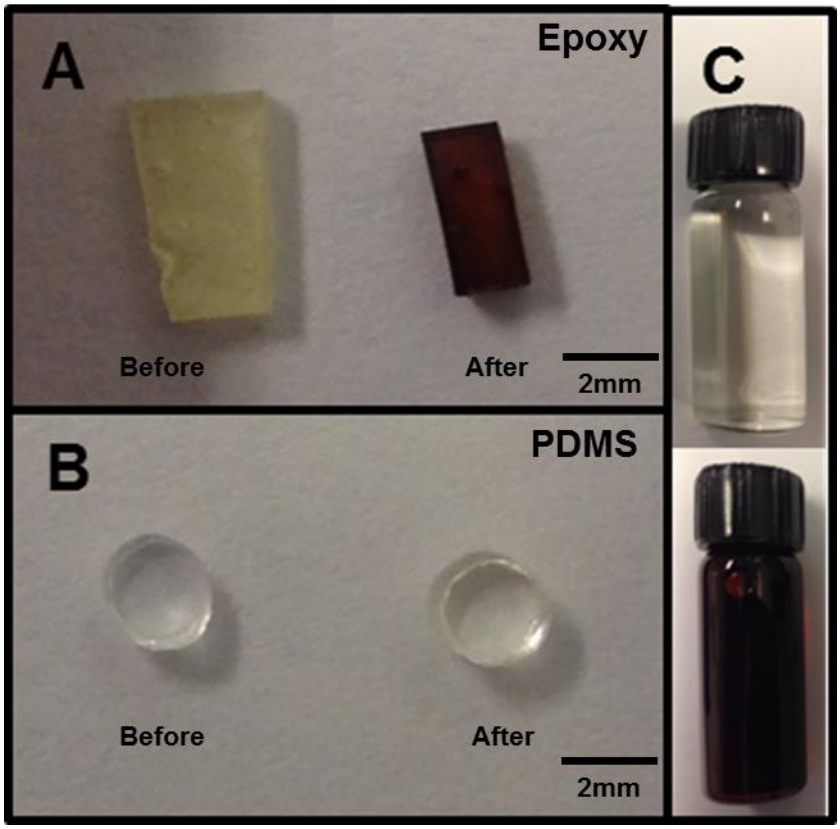

Figure 4.1: (A) Two slabs of epoxy before and after equilibration in 50mM Furfural, (B) Two plugs of PDMS before and after equilibration in 50mM Furfural, (C) Top 2ml vial is filled with 50mM furfural and the bottom is filled with neat furfural.

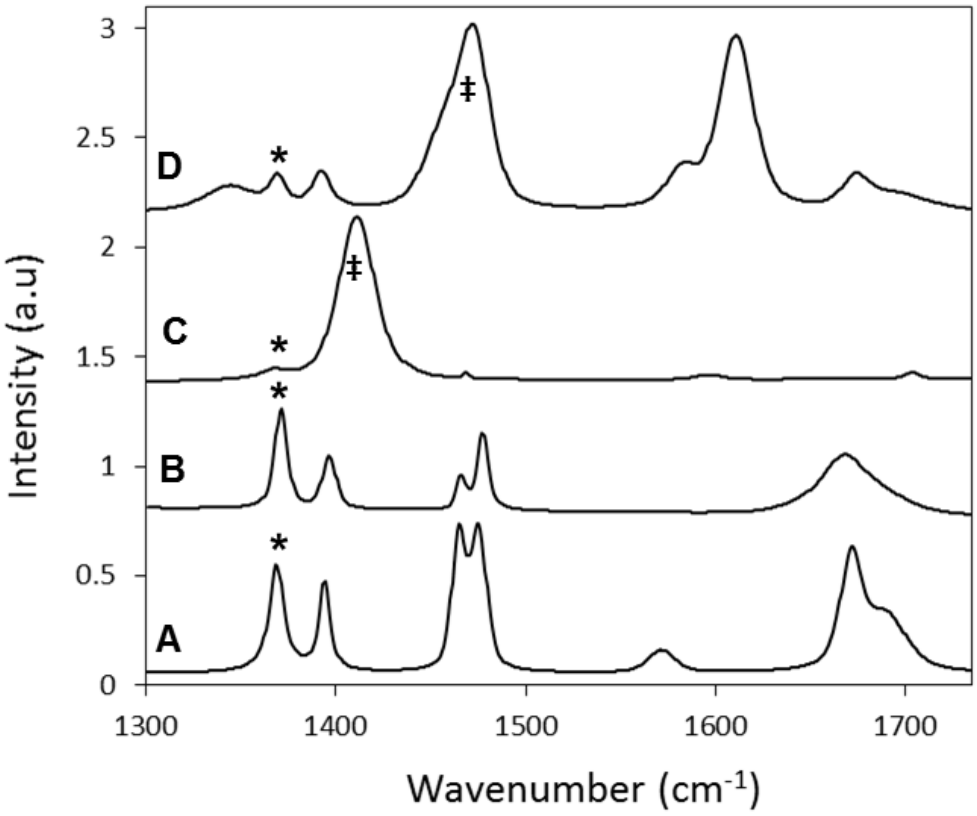

Figure 4.2: Raman spectra of furfural in different phases. (A) Furfural Neat, (B) In Water, (C) In PDMS, (D) Epoxy. Multipliers next to spectra denote the intensity multiplier needed to make spectral features visible on the same plot. Asterisks (*) indicates furfural spectral peak used for analysis. (‡) indicate internal standards.

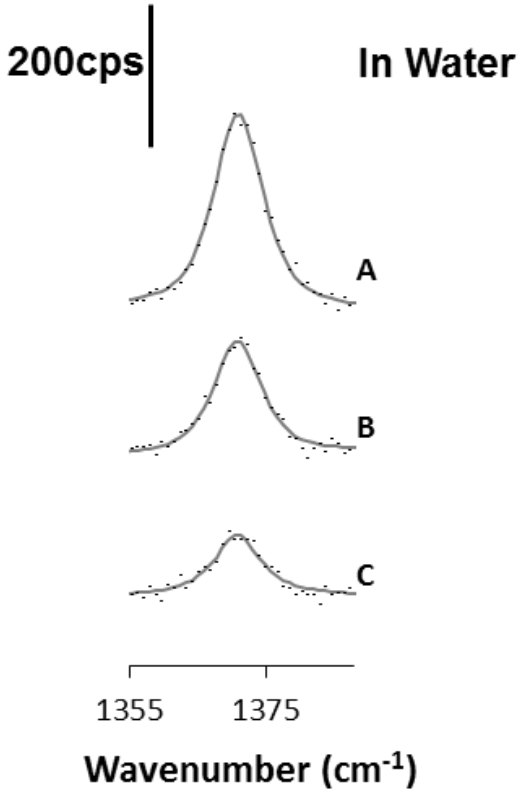

Figure 4.3: Raman spectra of the 1372cm^{-1} furfural peak acquired in water. A-C are aqueous concentrations of 50, 35, 20mM, (respectively). Data points are raw data and lines are the Vogt curve fits. The normalize signal intensity is shown as (cps).

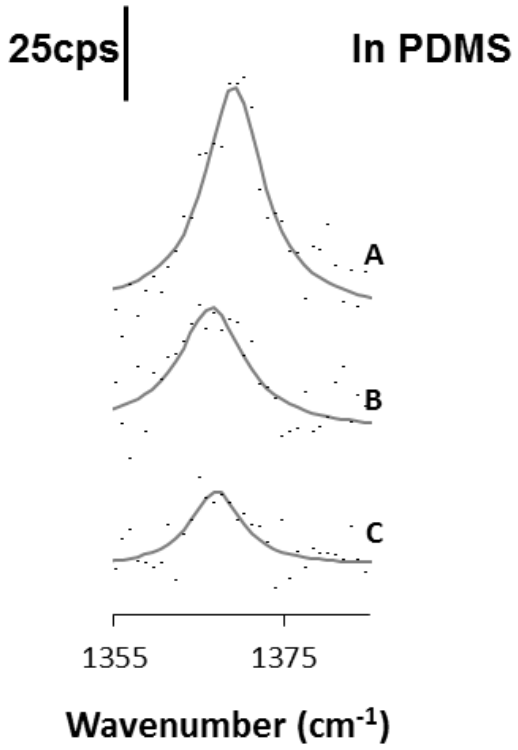

Figure 4.4: Raman spectra of the 1372cm^{-1} furfural peak acquired in PDMS. A-C are aqueous concentrations of 50, 35, 20mM, (respectively). Data points are raw data and lines are the Vogt curve fits. The normalize signal intensity is shown as (cps).

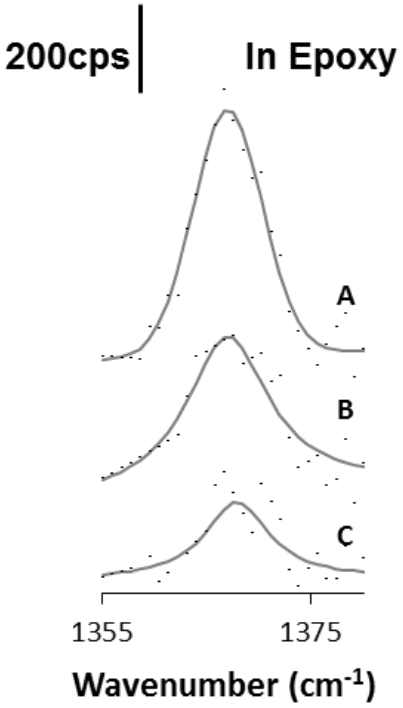

Figure 4.5: Raman spectra of the 1372cm^{-1} furfural peak acquired in epoxy. A-C are aqueous concentrations of 50, 35, 20mM, (respectively). Data points are raw data and lines are the Vogt curve fits. The normalize signal intensity is shown as (cps).

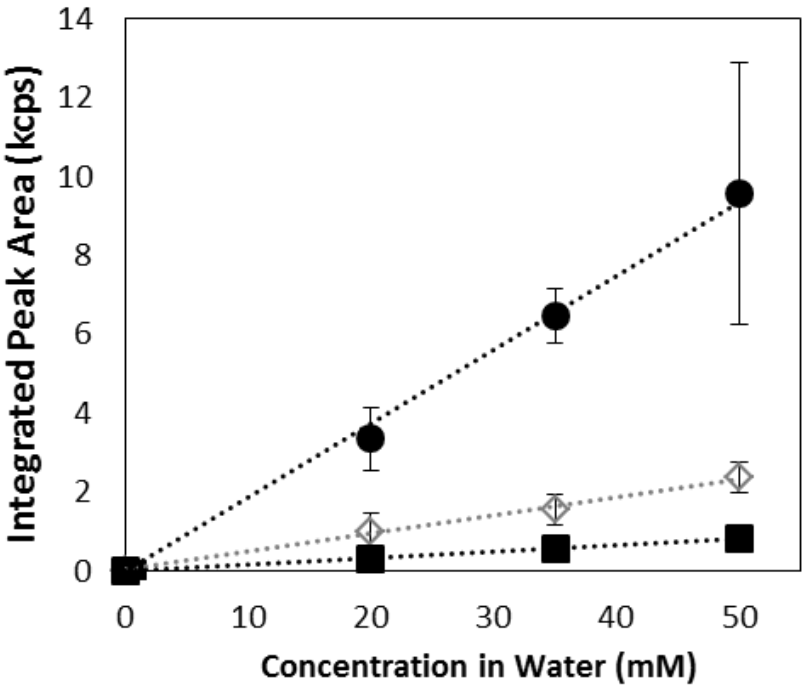

Figure 4.6: Integrated peak areas of the 1372cm^{-1} furfural peak versus water concentrations. Signal was acquired in the PDMS phase (▪) and water phase (◊) and Epoxy phase (•). Data points represent 2 different experimental trials.

SPME Polymer Phases	Average Log(K) (Measured)	Log(K) (Predicted)
PDMS	-0.41	-0.21
5 Minute Epoxy	0.61	0.70

Figure 4.7: Predicted and experimental values of log (K) of furfural within PDMS/water and epoxy/water systems. Predicted values where obtained using the Flory-Huggins Approximation.

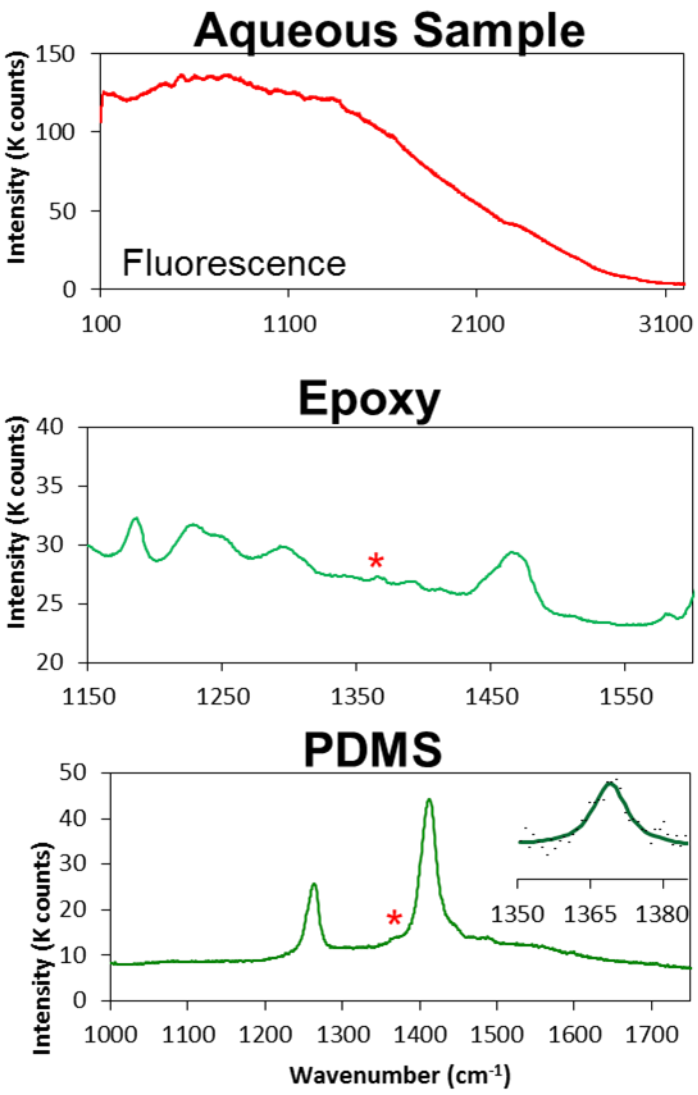

Figure 4.8: (A) Raman spectra of the steam explosion pretreatment sample. (B) Epoxy equilibrated in pretreatment sample. (C) PDMS equilibrated in pretreatment sample. Furfural peak is marked with the asterisk and shown in the inset.

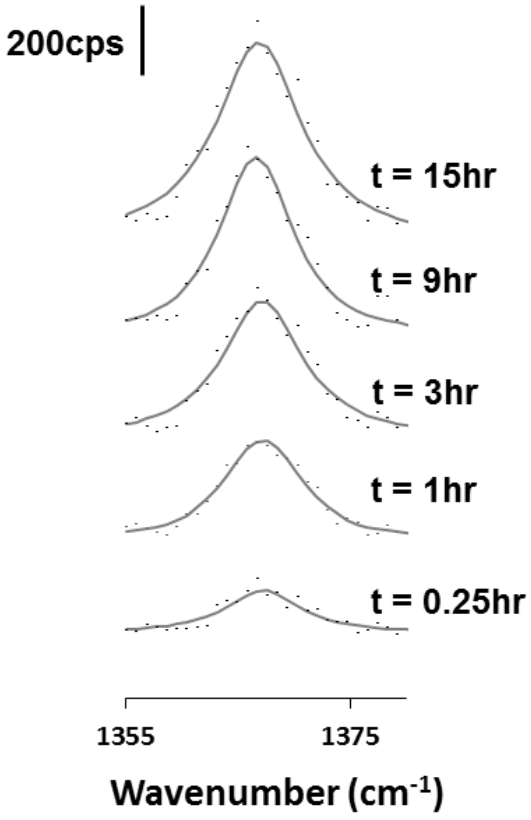

Figure 4.9: Furfural peak at 1372 cm^{-1} taken in the epoxy equilibrated in a 50mM solution of furfural at different times. The baseline subtracted spectral data points are presented along with corresponding curve fits and scale bars show the intensity of the Raman signal in counts per second (cps).

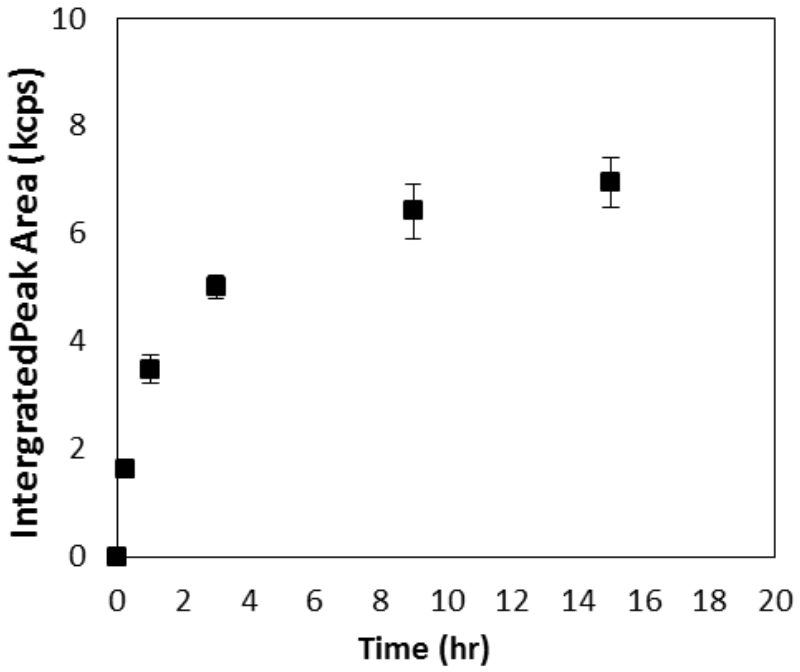

Figure 4.10: A plot of the integrated peak areas of the furfural peak at 1372 cm^{-1} as a function of time. Data points represent 2 replicates of 2 different experiments.

Chapter 5

Optimization of Solid Phase Micro-extraction (SPME): A Thermodynamic Approach

ABSTRACT. The fact that solid phase micro-extraction (SPME) is being used in many fields including; pharmacology, pharmacokinetics, food safety, and plant/environmental monitoring means it's exposed to a wide array of potential analytes. Optimization for the best polymer phase is critical to the effectiveness of the technique in the future. Using the Flory-Huggins theoretical approach, we show we can tailor SPME phases for different molecules; toluene, quinoline, and furfural. We examine three polymer/solvent phases (Polydimethylsiloxane (PDMS), Bisphenol A diglycidyl ether resin (5 Minute Epoxy), and water) which cover a wide range of solubility characteristic. We use an already establish technique (SPME/RS) to quantify partitioning as well as illustrate the potential for selectivity in multi-component systems. We find that our experimental values for log (K) reasonably match those predicted using the modified theory. Combining theoretical predictions with experiments towards tailoring polymers for target analytes could be the next steps towards SPME robustness.

5.1 Introduction

SPME is a well-known analytical technique that utilizes hydrophobic traits of polymers to partition and pre-concentrate non-polar analytes for better detection[74]. Techniques that benefit from SPME pre-concentration are well documented in the literature[14, 45, 61, 64, 75]. Mass spectrometry-based techniques such as Membrane Inlet Mass Spectrometry (MIMS) and Headspace SPME Gas Chromatography – Mass Spectrometry (GC-MS) have shown 2-3 orders

of magnitude improved detection. Additionally, optical methods like Infrared (IR) and Raman Spectroscopy (RS) have also shown improved signals quantitatively as well as qualitatively.[40, 41]

The fact that SPME is a pre-concentration technique that does not rely on a particular detection system makes it versatile for complimenting several analytical platforms[45, 62, 64]. This has translated into its use in many fields including; pharmacology, pharmacokinetics, food safety, and plant/environmental monitoring[74, 87-89]. This means the technique is exposed to a wide array of potential analytes. Currently, SPME fibers are typical made of polydimethylsiloxane (PDMS), divinyl benzene (DVB), or Carbowax[90]. However, there is a large library of polymers that could potentially be utilized for the technique. Guided selection of polymers to compliment the growing number of analytes is critical for future applications of the SPME technique.

Experimental efforts to improve SPME by polymer selection are well documented[38, 62, 87, 91]. These typically involve obtaining partition coefficients (log (K), the thermodynamic parameter that quantitatively relates the analyte concentration in each phase) for the analyte between solid polymer and liquid solvent phases. However, optimization based on theory could provide guidelines to tailor polymer phases towards targeted analytes. Several theoretical approaches for predicting of log (K) include molecular connectivity index[92], linear solvation energy relationships (LSERs)[93], and Flory–Huggins theory[68, 94, 95].

In environmental applications, including partitioning into polymer-like soil phases, the Flory-Huggins theoretical approximation has been applied because it accounts for size disparities between solute and polymer[95-97]. For dilute small analytes partitioning into large polymer chains (as is the case with most SPME), Choiu *et al* use the Flory–Huggins approximation to express log (K) as:

$$logK_{pw} = -logS_w\bar{V}_1 - \frac{[1+\chi]}{2.303}, \quad (1)$$

where K_{pw} is the equilibrium partition coefficient between polymer (p) and water (w) phases, S_w is the water solubility and $\bar{V}_1$ is the molar volume of the analyte. The Flory Huggins interaction parameter χ, can be approximated by using the analyte and polymer solubility parameters, δ_1 and δ_2, respectively:

$$\chi = \frac{(\delta_1-\delta_2)^2\bar{V}_1}{RT}, \quad (2)$$

where R is the universal gas constant and T is temperature (K). Key simplifying assumptions in Equation 1 are: 1) $\bar{V}_1/\bar{V}_p \cong 0$ (molar volume of analyte is significantly smaller than that of the polymer), and operation in the dilute regime.

Here we use the Flory-Huggins theory, laid out above, to assess its suitability for identifying optimal SPME polymers. We calculate the SPME partitioning of toluene, quinoline, and furfural into diverse polymer phase. We compare these theoretical calculations to experimental results from the literature as well as new results using SPME/Raman. These analytes are selected because they display a wide range of solubility parameters, thereby testing the utility of our approach.

5.2 Materials & Methods

5.2.1 Polymer/Aqueous Sample Preparation

PDMS Samples - Slygard 184 PDMS and catalyst were obtained from Dow Corning. Samples of PDMS were prepared as follows: PDMS was mixed using the standard 10:1 polymer to catalyst ratio and cured at 70^{o}C overnight. Samples were punched out of a PDMS ~1.5mm deep sheet using a 2mm diameter punch. The resulting PDMS plugs were sealed and kept until

used.

Epoxy Samples –5 Minute Epoxy was obtained from ITW Devcon. Epoxy resin and hardener were poured and mixed on a sheet of paper, which was spread into a thin layer ~1-2mm thick. This was cured at room temperature for 6hrs, allowing the polymer resin to harden completely. ~2x4mm samples were cut out of the slab using a razor blade. Paper was removed from the bottoms of the slabs. Epoxy slabs were sealed and kept until used.

Organic Aqueous Solutions – Furfural was purchased from Sigma-Aldrich and toluene was purchased from EMDchemical. Quinoline was purchased from Acros Organics. All chemicals were used as purchased. Solutions were prepared by adding the appropriate amount of reagent into 20 mL of deionized (DI) water. The solutions were mixed, tightly capped, and left to sit until fully dissolved. Solutions were used within 15mins of preparation to minimize evaporative loses.

5.2.2 SPME Extraction Procedure

Solutions of furfural, quinoline, and toluene were prepared in 20mL glass scintillation vials. Two sample plugs (PDMS) or slabs (Epoxy) were introduced to each vial, tightly capped, and left to equilibrate undisturbed at room temperature for at least 48 hours. To first approximation, the large excess volume ratio of aqueous phase solution to PDMS plugs means the aqueous concentration in solution before and after equilibration is negligibly altered.

5.2.3 Raman Spectral Acquisition

Spectra were collected using a Renishaw inVia Raman micro-spectrometer attached to a Leica DM IRBE upright optical microscope. A 785 nm diode laser operated full power (nominal 180mW) was used to irradiate samples through a 50x (N.A. 0.8) objective lens. The spot area was ~50μm^2. Scattered light was acquired through the same objective lens and detected on a thermoelectrically cooled (-60 ^oC) CCD. All polymer and aqueous sample measurements were

acquired for 10 seconds. Spectra of neat furfural acquired 1% of the nominal laser power due the fluorescence of the molecule. All sample spectra were collected using a wet sample holder sealed with an optical coverslip. Laser stability was assured using the 520 cm^{-1} peak of Silicon. The PDMS peak at 1410 cm^{-1} and the Epoxy peak at 1610 cm^{-1} was acquired with all polymer phase spectra and served as an internal standard that helped normalize for sample to sample variations in optical focus.

5.2.4 Normalization & Peak Analysis

Spectral peaks were analyzed using Wire 2.0 software. All spectra were baseline subtracted using second order polynomial or cubic spline functions, producing very flat baselines for subsequent analysis. Spectral peaks where fit to standard Vogt distribution profiles. Curve fit parameters were used to calculate the reported integrated peak areas. Peak areas are reported in counts per second (cps).

5.3 Results & Discussion

To explore the Flory-Huggins theoretical approximation, we examine a series of cyclic molecules of increasing polarity within different polymer phases. The three molecules furfural, quinoline, and toluene cover diverse a range of solubility parameters (δ): 11.2, 10.8, 8.9 $(cal/cm^3)^{1/2}$, respectively. Solubility parameters (δ) of PDMS and epoxy are 7.3 and 10.7 $(cal/cm^3)^{1/2}$. We start with the least polar of the set, toluene, which has of low water solubility of ~5.1mM[76]. **Figure 5.1** is a table of known solubility parameters used to plot the theoretical calculations of the partition coefficient[98]. **Figure 5.2** shows the predicted partition coefficient (log (K) of toluene as a function of solubility parameters (δ) using **Equations 1** & **2**. Experimental values obtained from our prior work (x)[76] are also plotted alongside experimental

values from other research efforts. We can see that PDMS is a commonly used polymer for these types for toluene experiments because, based on Flory-Huggins, it's a polymer that is close to the theoretical maximum log (K) for that system. Polystyrene-co-butadiene (PSB) and polyacrylonitrile-co-butadiene (PAB) have also been shown by other groups to come closer than PDMS to this maximum, having solubility parameters closer to that of toluene (PAB = 9.48, PSB = 8.84). We can also see from the figure that there is opportunity for more hydrophilic polymers to be examined.

Next, we examine quinoline, a molecule that has higher water solubility that toluene (~35mM). Knowing the value of its solubility parameter, we now look to a more hydrophilic polymer, 5 Minute Epoxy (Bisphenol A diglycidyl ether resin), as a better match for the molecule. **Figure 5.3** shows the 1375 cm^{-1}asymmetric ring-breathing vibrational mode of quinoline peak in Epoxy and water. We show quinoline detected at 3 concentrations (5, 3.5, 2mM) in both phases; equilibrated Epoxy (top) and aqueous (bottom). The baseline subtracted spectral data points are presented along with corresponding curve fits and scale bars show the intensity of the Raman signal in counts per second (cps). Comparing detection in both phases we see 10 fold enhancement of the quinoline peak intensity.

We quantify the partitioning of quinoline in from water into Epoxy by the plotting the integrated peak areas of the compound (in both phases) at their respective water concentrations. **Figure 5.4** shows a plot of the 1375 cm^{-1}peak areas as a function of water concentration. Peaks areas from the epoxide phase were normalized to an epoxy internal standard peak at 1610 cm^{-1} (as shown from prior work). Data points represent two separate measurements performed each having two samples and were fit using linear regression analysis. The linear behavior of the

system lets us express the equilibrium partition coefficient K_i for each molecule i from the data in **Figure 5.4** as:

$$K_i = \frac{(Slope)_{Epoxy,i}}{(Slope)_{Water,i}} \ , \tag{3}$$

where $(Slope)_{Epoxy,i}$ is the slope of the best fit line for each molecule i measured in the Epoxy phase and $(Slope)_{Water,i}$ is the slope of the best fit measured in the aqueous phase (as shown in the figure). **Equation 1** provides a partition coefficient K_i, which we express as logK_i (i being quinoline). Values obtained were log (K) = ~1.60 and 1.51 from two separate experiments which are compared to values obtained using the Flory-Huggins approximation. **Figure 5.5** shows these values plotted against Flory-Huggins predictions for log (K) of quinoline versus solubility parameters of known polymers. Interestingly, we see that even with very similar solubility parameters of quinoline and epoxy (10.8 & 10.7 respectively) the theoretical maximum of quinoline is lower than that of toluene, topping out at log (K) = 1.82. This shows the significant influence of water solubility on driving partitioning. Also in the figure is the averaged experimental value of log (K) from prior SPME/RS work with PDMS is also plotted. It is evident from the plot that our experimental values roughly follow the same expected trend as the predicted Flory-Huggins. Using a less hydrophobic polymer phase than PDMS, we can increase the partition coefficient as the theory predicts.

Lastly among the series of molecules, we look at the partitioning of furfural from water into PDMS and 5 Minute Epoxy. Furfural has a water solubility of 864mM making it the molecule of the set with the lowest theoretical maximum of its partition coefficients (log (K) = 0.70). We see this in **Figure 5.6** which shows the Flory-Huggins plot of log (K) of furfural versus polymer solubility parameters. Experimental values (x) are also plotted in the figure and represent the

average of two trials. Here we also see a general adherence to the predicted trend of the theory. Partitioning of furfural within a PDMS/water system gives a negative partition coefficient. However, with epoxy as the polymer, whose solubility parameter more closely matches that of furfural, we see an increased and now positive partition coefficient.

To illustrate robustness of the thermodynamic approach to SPME polymer selection, we experimentally show selectivity with the ability to enhance and attenuate various compound peaks by detecting in different phases within a multi-component polymer/aqueous system. Two separate polymer/aqueous phase experiments were carried out: 1) epoxy/aqueous 2) PDMS/aqueous. The aqueous solutions were spiked with toluene and quinoline at 5mM and 20mM, respectively. **Figure 5.7** shows the three spectra obtained within the 950-1100 cm^{-1} spectral range were 2 toluene and quinoline peaks are present. The toluene peaks are at 1041 and 1005cm^{-1} while the quinoline peaks are at 1036 and 1014cm^{-1}. Both sets of peak correspond to different ring breathing and stretching modes of the aromatic molecules. The gray lines are the Vogt curve fits and the black dots are the raw data. Scale bars are in cps (counts per second). Firstly, in the water phase, we see a preference for quinoline. Two prominent quinoline peaks and one significantly smaller toluene peak are seen. This is mainly due to quinoline more favorable water solubility (~35mM[76]) as compared to toluene's solubility at (~5.1mM). In short, the prominence of quinoline peaks is expected because quinoline can dissolved at 5x the concentration of toluene in water. In the equilibrated epoxy phase however, we see a ~50 fold increase in the signal for both toluene and quinoline. This shows an overall enhancement of both toluene and quinoline in the epoxy matrix with no significant preference for any of the two species. The top spectrum of the PDMS equilibrated in the multicomponent sample

demonstrates a preference for toluene by showing to prominent toluene peaks. Even at a concentration 5x less that quinoline, we see the high preference the PDMS has for toluene (quantified by it larger partition coefficient log (K) in **Figure 5.2**), making PDMS more selective of toluene.

Georgi *et al*, using a modified version of the Flory-Huggins concept, describe an analyte specie's preference for one organic phase over another. The expression describes the competition between two macromolecular phases for an analyte as a ratio of the analytes partition coefficient into the phases. We use this expression of selectivity (a ratio of partition coefficients) towards describing the competition of two analytes in solution for one polymer phase. We express selectivity as:

$$\text{Selectivity} = \log\left(\frac{K_i}{K_j}\right), \tag{4}$$

where *i* and *j* are the two species in question. We use the values of log (K) derived from the expression by Chiou *et al*. **Figure 5.8** plots our theoretically derived values for selectivity versus polymeric/solvent solubility parameters ($\delta_{\text{polymer/solvent}}$). The two species *i* and *j* are toluene and quinoline, respectively. As depicted in the **Figure 5.8**, the highest selectivity that toluene has over quinoline is in the PDMS phase, which has selectivity of 1.82. Qualitatively, this is evident from the more prominent toluene peaks. The selectivity of toluene over quinoline in epoxy is 0.4. This means that in epoxy, at equal concentrations, the toluene peaks should be only slightly bigger than that of quinoline. Detection of both molecules is still significantly enhanced as depicted by the inset spectrum.

We also create the same predictive plots for two other systems where; 1) toluene = *i* and furfural = *j*, 2) quinoline = *i* and furfural = *j*. **Figure 5.9** plots the selectivity of these two systems

versus solubility parameters of polymers. As can be seen from the plot of the toluene/furfural system, there is a drastic group in selectivity as the $\delta_{polymer}$ is increased. This is due to the fact that furfural is more polar than toluene. The solubility parameters for furfural and toluene are 11.7 and 8.9 $(cal/cm^3)^{1/2}$, respectively. Furfural is also much more soluble in water (864mM), which shows why its partition coefficient was negative for PDMS and slight positive for epoxy. Its polarity keeps it predominantly in the aqueous phase. Toluene is very non-polar, which means it outcompetes furfural for the PDMS and epoxy phase. But there is a decline that gets negative when water-like solubility parameters are reached. However, for the quinoline/furfural system, we see no significant changes in the selectivity. This is expected because both are polar molecules. Interestingly, there is a slight parabolic shape to the plot meaning that the maximum selectivity of this system lies somewhere in the middle of this range. In contrast, the toluene/furfural clearly has a maximum that lies outside the range of the plot.

5.4 Conclusions & Implications

We have demonstrated the potential for optimization of SPME polymer phase using the Flory-Huggins theoretical approach. We have shown that we can tailor SPME phase using this approach for different molecules; toluene, quinoline, and furfural. We examine three polymer/solvent phases (PDMS, Epoxy, and water) which cover a wide range of solubility characteristic. Similar to what is for environment and industrial applications; we combine theoretical predictions with experiments to show that tailoring polymer towards compatible solubility parameters can be a means of optimizing SPME. We use our establish technique (SPME/RS) to quantify partition and also to demonstrate the potential of selectivity in multi-component systems.

5.5 Figures

Polymers	$(\delta = (cal/cm^3)^{0.5}$
polyterafluoroethylene	6.5
PDMS	7.3
Poly (butadiene)	7.57
Poly(ethylene)	8
Poly(proylene)	8.2
Polyn buytl Methacrylate	8.7
PEMA	9.04
Polyn buytl Acrylate	9.04
PolyChloropene	9.04
Poly(styrene)	9.13
Poly(phenyl oxide)	9.15
PMMA	9.3
Acrylic	9.4
PVC	9.5
polyVinyl Acetate	9.8
PMA	10.02
PET	10.1
Epoxy	10.7
Cellulose Acetate	11.7
Nylon 6,6	13.7
PEO	14.7

Figure 5.1[98]: Solubility parameters of different polymers we use as tailoring tool. Data in figure comes from [95].

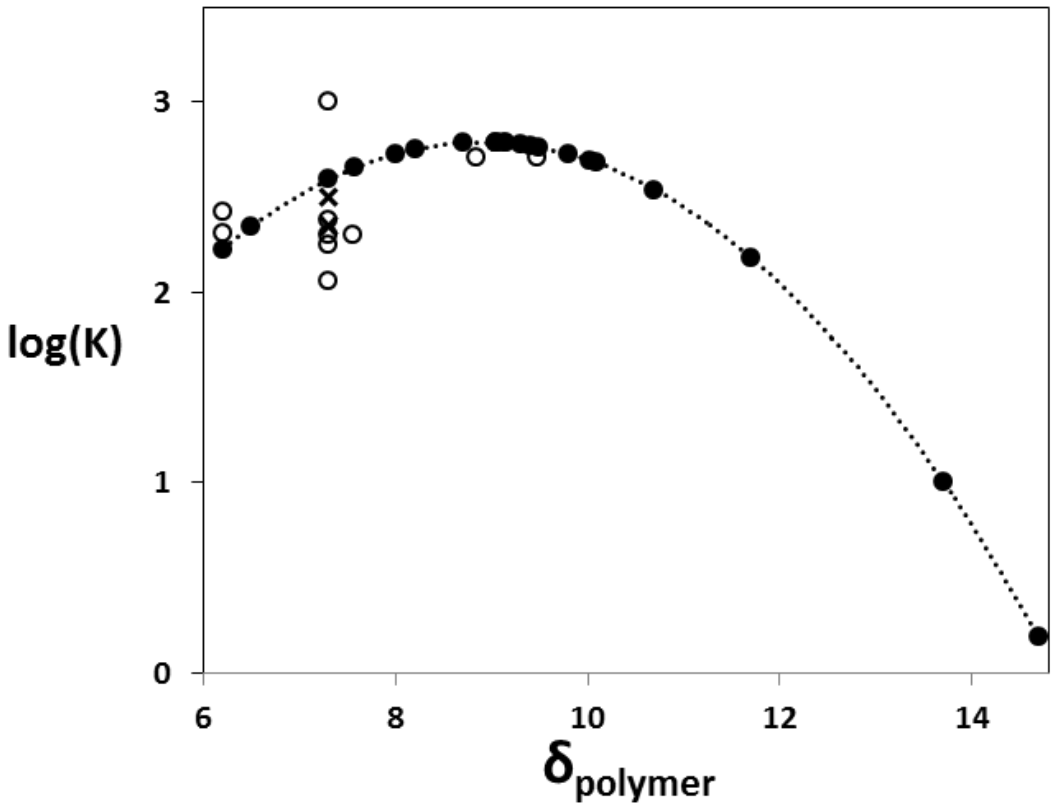

Figure 5.2: Flory-Huggins theoretical calculations of log (K) for toluene are plotted versus polymer solubility parameters of different polymers. Theoretically data is plotted with filled circles. Our experimentally obtained data are plotted as (x). Circles without fills (o) are other experimental values from the literature**.**

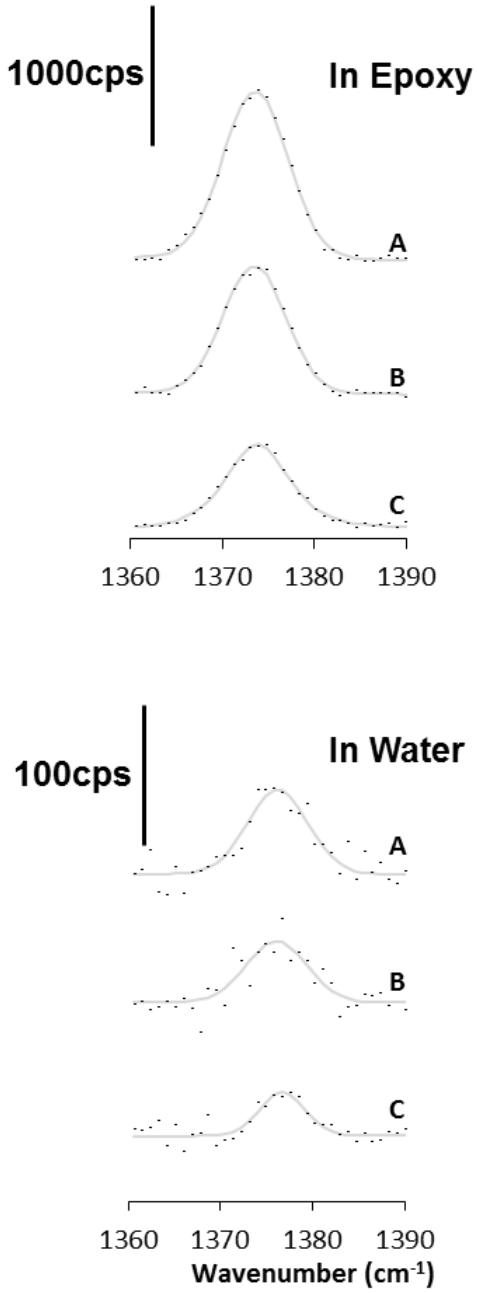

Figure 5.3: Raman spectra of the 1375cm^{-1} quinoline peak acquired in the PDMS (top) and water (bottom) phases. A-C are aqueous concentrations of 5, 3.5, and 2 (respectively). Data points are raw data and lines are the Vogt curve fits. The normalize signal intensity is shown as (cps).

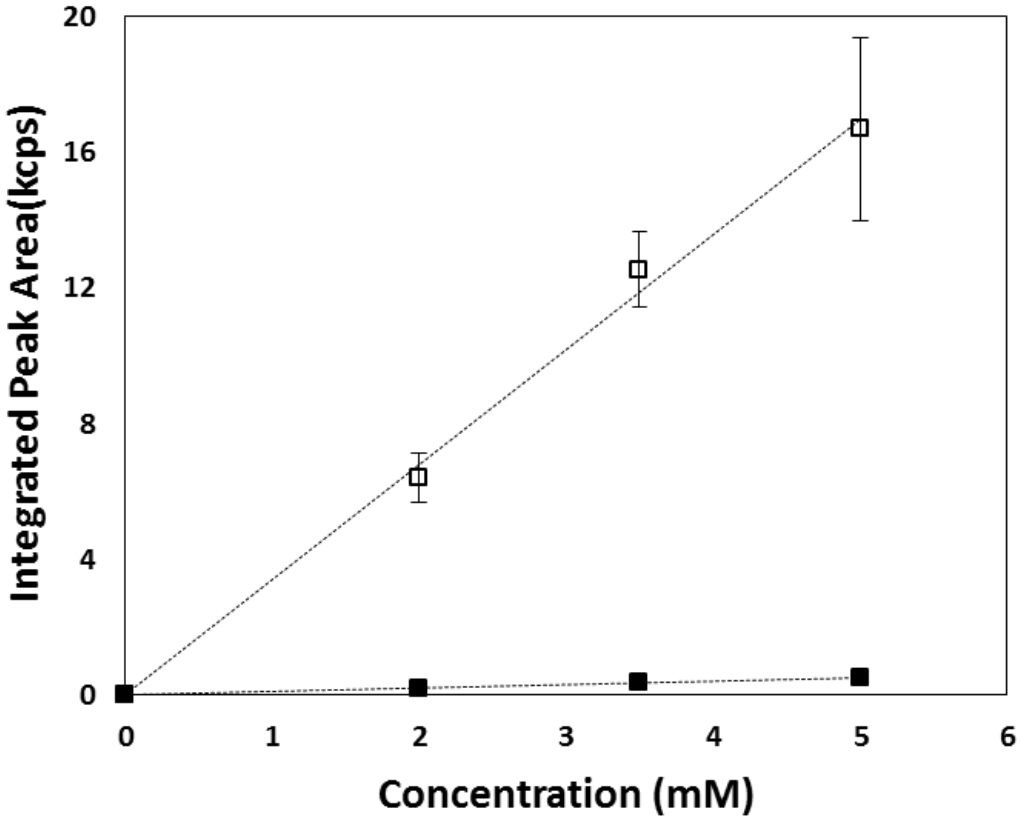

Figure 5.4: Integrated peak areas of the 1375cm^{-1} quinoline peak versus water concentrations. Signal was acquired Epoxy (■) and water phase (□). Data points represent an average of 2 different experimental trials.

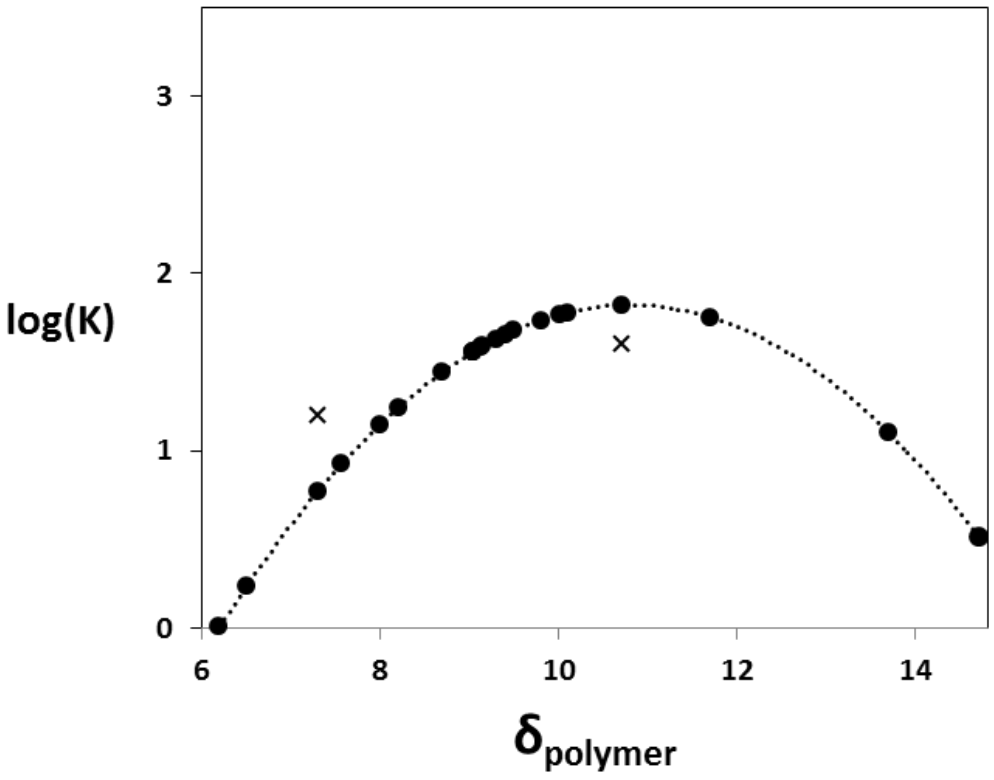

Figure 5.5: Flory-Huggins theoretical calculations of log (K) for quinoline are plotted versus polymer solubility parameters. Theoretically data is plotted with filled circles. Our SPME/Raman data are plotted as (x).

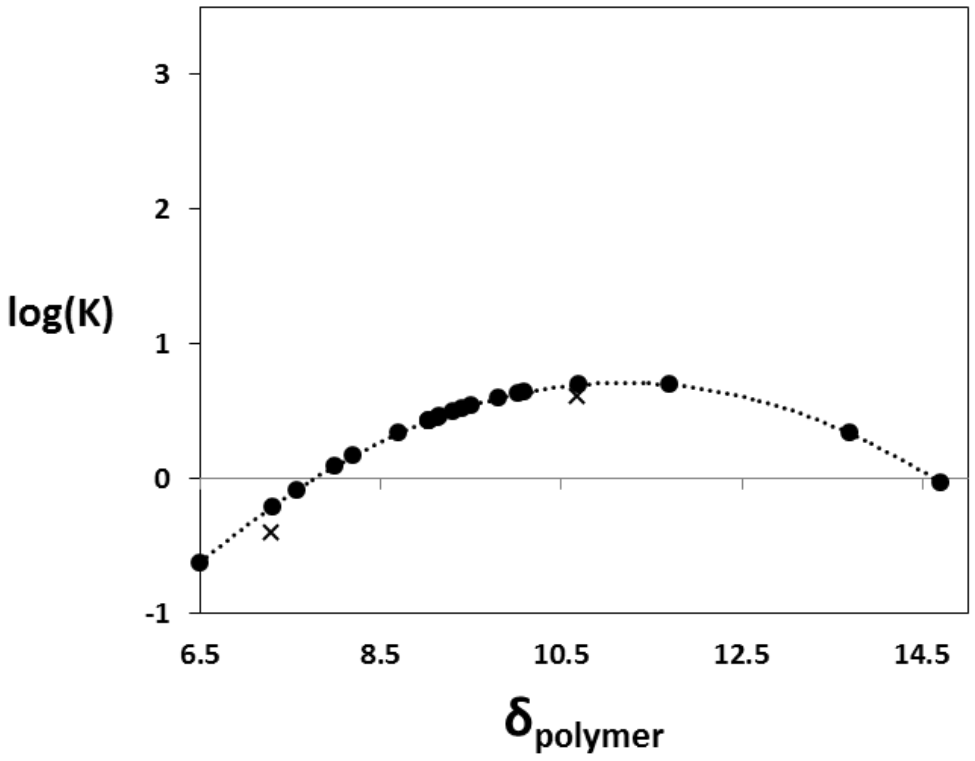

Figure 5.6: Flory-Huggins theoretical calculations of log (K) for furfural are plotted versus polymer solubility parameters. Theoretically data is plotted with filled circles. Our SPME/Raman data are plotted as (x).

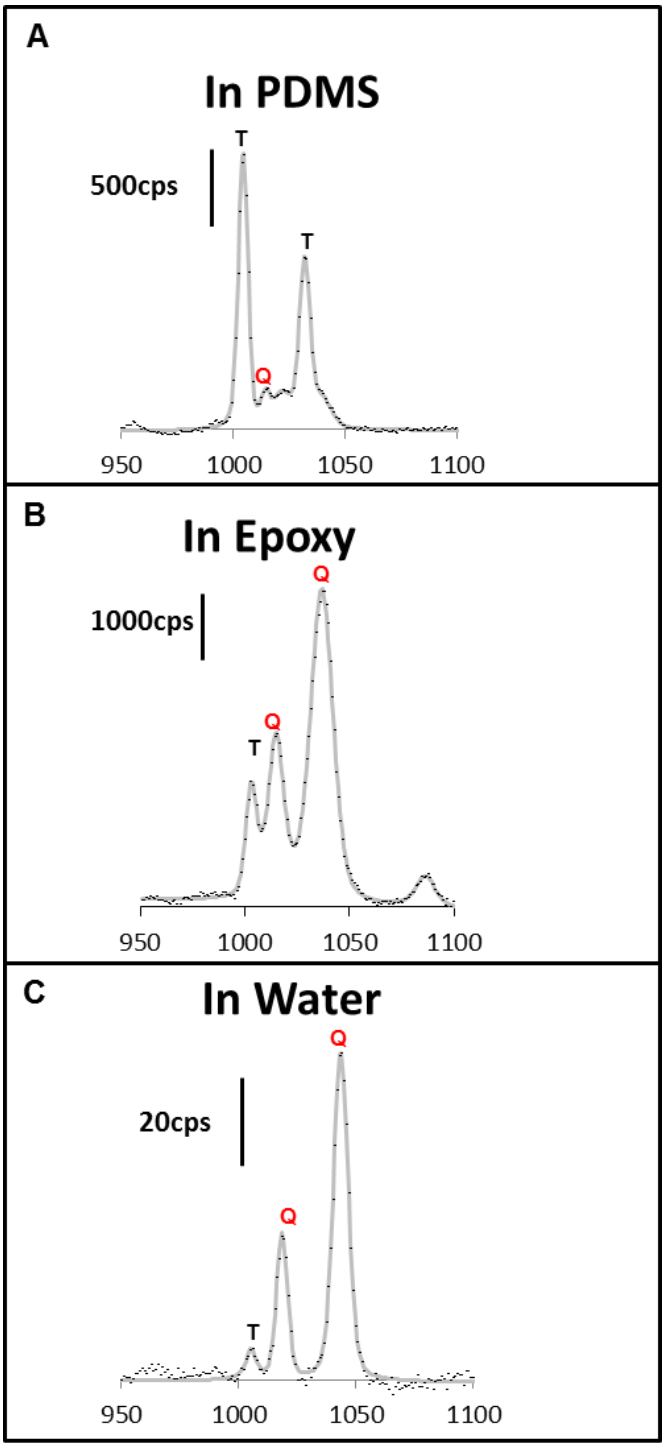

Figure 5.7: Raman spectra of a multi-component quinoline and toluene system in equilibrated PDMS and epoxy and water phases. (A) Spectrum of the PDMS phase showing prominent toluene peaks. (B) Spectrum of the epoxy phase showing enhancement of both peaks. (C) Spectrum of the aqueous solution showing prominent quinoline peaks. Q & T indicates quinoline and toluene peaks. Black dots are the raw data and the gray lines are the Vogt curve fits.

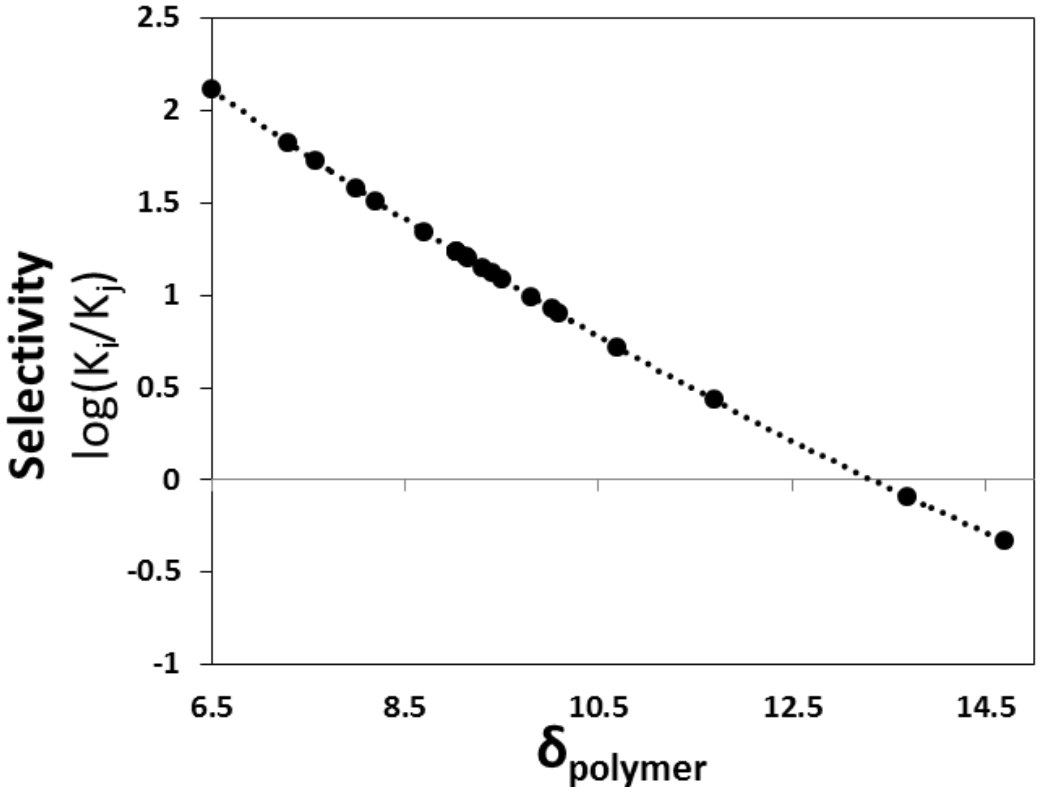

Figure 5.8: Selectivity of toluene (i) to quinoline (j) is plotted versus polymer solubility parameters using Flory-Huggins theoretical calculations of log (K).

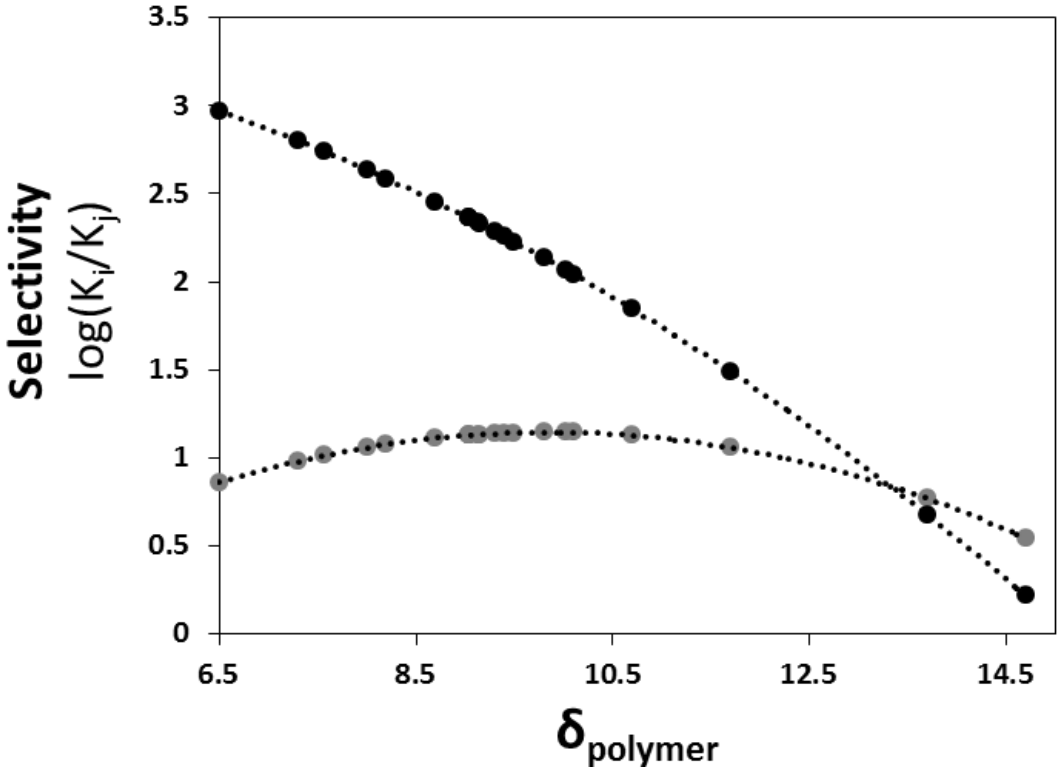

Figure 5.9: Selectivity of toluene (i) to furfural (j) is plotted versus polymer solubility parameters (black) and quinoline (i) to furfural (j) (gray). Flory-Huggins theoretical calculations of log (K) were used across the range of solubility parameters for known polymers.

Chapter 6

Conclusions and Recommendations for Future Work

6.1 Conclusions

Many research efforts look to find a universally robust detection platform which can enable detection and diagnosis complex real-world samples. Raman Spectroscopy has come a long way since its discovery in the late 1920s towards easy and affordable analysis. Today's portable Raman systems are at the threshold of fitting the role of a truly universal sampling platform. This is mainly due to its intrinsic chemical fingerprinting base on vibrational modes fundamental to the detected analyte. However, it is also this trait that limits it from detection of real world samples. There are many routes being investigated to make Raman detection more robust. It was to this end we investigated SPME/Raman.

To build the solid foundation for SPME making Raman more robust for universal detection Chapter 2 sought to make SPME/Raman more quantitative. Using PDMS, the cornerstone polymeric material for both SPME analytical and modern microfluidics, to analyze well known trace crude-oil components in water was the best launching point for our investigation into the technique and its potentials. Through this study, we show that SPME/Raman can be a reasonably quantitative while also making Raman Spectroscopy 1-2 orders more sensitive. We show that our estimated values for the partition coefficient of toluene, benzene, and quinoline in a PDMS/water system closely matched values from other quantitative techniques. In addition to being a crucial first step towards our goal, the work also hinted at the merging of SPME analytics with modern micro-fluidics to perform next generation micro-analysis.

With the quantitative SPME/Raman technique established, Chapter 3 sought to apply it to a relevant disciple that would most benefit from the technique. Anesthesiology is a medical practice that also understands and accounts the partitioning events. When anesthetic compounds are administered, partitioning of these compounds occur between various different liquid and lipids like phases of the body. Although partitioning complicates administration of anesthetics, the same partitioning process can be used via SPME to enhance detection of these analytes. Additionally, Raman systems were used in the past to detect of such compounds. Although becoming outdated as newer technologies emerged, SPME coupled to Raman detection may bring the technique back into use in healthcare as a means to generally enhance detection of these compounds. It may also drive the technique towards more direct biological sampling and detection. Ways to directly measure concentrations in relevant biological fluids may be beneficial to researchers and clinicians.

We show that SPME improves the Raman signals of all the anesthetics examined in this study. We quantify partitioning of halothane into PDMS and obtained a range of partition coefficients (log (K) = 1.93± 0.17) for the system. With halothane and propofol, which displayed the strongest Raman signals, SPME lets us easily detect clinically relevant concentration (200μM and 35μM respectively) with modest acquisition times (10 sec). This study also showed that SPME may also have the potential to enhanced detection of other analytical methods already used in hospitals today.

Chapter 4 sought to examine another family of molecules with SPME/Raman, in the hopes to introducing polymer selection for better partitioning properties. During dilute acid and steam explosion pretreatment methods, while releasing sugars from woody biomass, side reactions occur that creates a family of fermentation inhibitory compounds like furfural (being the most

prevalent in pretreatment slurries. Polymeric adsorbents are typically used to extract furfural from these batch systems. However, SPME phases may offer a means to simultaneously extract and detect at relevant concentrations. We test two polymer phases; Polydimethylsiloxane (PDMS) and Bisphenol A diglycidyl ether resin (5 Minute Epoxy) and show qualitatively that 5 minute epoxy is a better extractor of furfural than PDMS and that PDMS actually attenuates the furfural signal when compared to detection in water. As for epoxy, we saw very drastic color change before and after soaking (unlikely the PDMS polymer phase). We quantify the partitioning into both polymers and show that PDMS gives negative values for the partition coefficient while epoxy gives positives values. We calculate theoretical values using the Flory-Huggins approximation in order to assess the accuracy of our experimentally derived values. We show that our values match the predicted values. Lastly, we demonstrate the use of these polymers to extract and detect furfural in a multi-component pretreatment mixture. This work demonstrates the potential use the extractive polymers, which use partitioning to separate fermentation inhibitors from batch systems, for enhanced detection within such systems.

Solid phase micro-extraction (SPME) is emerging in many different fields including; pharmacology, food safety, and plant/environmental monitoring. Recognizing the fact that the technique will be exposed to a wider array of potential analytes, optimization for the best polymer phase is critical to the effectiveness of the technique in the future. Chapter 5 looks to exploring the Flory-Huggins theoretical approach towards selecting and tailoring polymer phase for specific target analytes. We examine 3 molecules; toluene, quinoline, and furfural and two polymer phases: PDMS and Epoxy. These analytes were examined in prior experimental efforts and cover a wide range of solubility characteristic. Combining theoretical predictions with experiments, we have demonstrated the potential for optimization of SPME polymer phase using

the Flory-Huggins theoretical approach. We also show the use of Flory-Huggins approximation to describe polymer selectivity for one analyte over another in a multi-component system, which also illustrates the potential robustness of the approach when perfected. The impacts of such an approach could be far reaching because of the many different fields that utilize SPME. As of Raman Spectroscopy, we have shown that SPME does improve the sensitivity and selectively of the technique, bringing it one step closer to being a more robust analytical platform for analyzing real world samples.

6.2 Recommendations

This body of work has examined three different families of molecules (crude oil components, anesthetics, and fermentation inhibitors) with SPME/Raman as a means to provide guidance towards directed selection of SPME polymer phases. We have shown that effective tailoring of polymer phases for particular target analytes, using theory as well as experiments, can be achieved. In light of these efforts, we present a few recommendation and guidelines for future endeavors.

1) When tailoring towards a specific family of target analytes using guide polymer selection, one must be very cognizant of the detection system being used alongside SPME. In some ways, the polymer must be compatible with the detection system so as not to interfere with the intrinsic mechanisms the technique used in detection. Basically, even though one may find a polymer with the most optimal mechanistic and solubility properties for a target analyte, the detection system may externally hinder successful enhancements of signals. In the case of Raman Spectroscopy, knowing that the polymer has key spectral windows that don't interfere with any potential peaks of the target analyte is crucially important.
2) Besides the solubility parameters discussed in depth in chapters 4 & 5, there are other polymeric traits that one should keep in minds when optimizing the polymer phase. Polymer hardness and rigidity does play a key role in SPME processes. A harder polymer tends to means slower diffusion and permeation through the polymer matrix, which translates to a longer time to reach partitioning equilibrium. Additionally, the more crystalline a polymer becomes, the more relevant the entropic interaction parameter of the polymer to analyte is.

3) In the case of optical detection techniques, polymer transparency may also be another factor to keep in mind while selection a polymer. Although the polymer phase may be compatible with the analyte, the polymer matrix itself could attenuate the signal from the detection platform. In the case of Raman Spectroscopy, if the polymer has color centers that absorb light, this could negatively effective the signals obtained in the polymer phase. Opaqueness in polymers could also affect signals acquired.

6.3 Future Directions

Future endeavors look towards combining SPME with SERS for better enhancements. Few works have yet to endeavor to undertake this due to the complexities of the proposed system. Senapik *et al* has been at the forefront of this work, emphasizing the added enhancement provided when PDMS SPME is coupled with SERS nano-structures[51-53]. The prospects of efficiently combining SPME and SERS could further enhance SERS signals as well as provide a selective/protective polymeric coating for SERS nano-structures. The polymer could also possibly act as a layer that anchors analyte unto SERS surfaces, which would widen the library of SERS active analytes.

In light of this body of work, we also see added benefits to combined SPME/SERS enhancement. Effective tailoring of SPME polymer phases could translate into the options to selectively anchoring certain analytes while attenuating others within a multi-component real-world sample. To this end we also detail efforts to create a SERS active substrate that can be removed and stamped into a polymer phase in **Appendix A**. The technique is Orchestrated Structural Evolution (OSE), which uses nano-patterning plus electrochemical deposition to create nano-sized dot arrays by seeding and overgrowing within a printed nano-hole. Although first developed for copper deposition, the technique has been proven viable for depositing silver.

The size and pitch of these structures can be finely control by the parameters of the nano-write and deposition procedures (**See Appendix – Chapter 7**). The precise control of the spacing and size of such structures enables the creation of SERS active "hot spots". **Figure 6.1** details the fabrication of these SERS hot spots and their removal from the substrate into an adhesive polymer phase. **Figure 6.1(A)** shows a schematic of the deposition and overgrowth of the silver into the nano-patterned mask, which should create the SERS hot spot. **Figure 6.1(B)** illustrates the removal of the nano-structures after the mask is dissolved. **Figure 6.1(C)** shows a SEM image of the back sides of the structures after they have been peeled of using an adhesive polymer. Interestingly enough, the adhesive polymer phase used to remove these structures was 5 minute epoxy (which was the same polymer used in the furfural and quinoline partitioning experiments).

Embedding SERS active nano-structures within these phases could, not only combine SPME and SERS enhancement, but would also enable the creation an ultra-sensitive and selective nano-composites for Raman detection. These polymer composites could be made into thin films that can be used with various kinds of Raman probes or polymer microfluidic platforms. **Figure 6.2** shows a proposed schematic of such a system; where our OSE nano-structures are embedded into polymer films. **Figure 6.2(A)** is a proposed schematic of a SPME polymer phase used to anchor the OSE nano-structures; also taking advantage of the pre-concentration from the aqueous sample phase. **Figure 6.2(B)** is a proposed schematic of the potential of selectivity of analytes for two selected polymer phases that also contain embedded nano-structures. We detail a potential system where two different polymers can be used to selectivity extract and pre-concentrate two analytes from a multi-component system. In this case, one analyte used preferentially partition into one polymer and the other would partition into the

other. **Figure 6.2(C)** is a picture of a proposed nano-composite film with embedded OSE fabricated nano-sensor patches. Effective tailoring of polymer phases will be crucial to these types of future efforts.

6.4 Figures

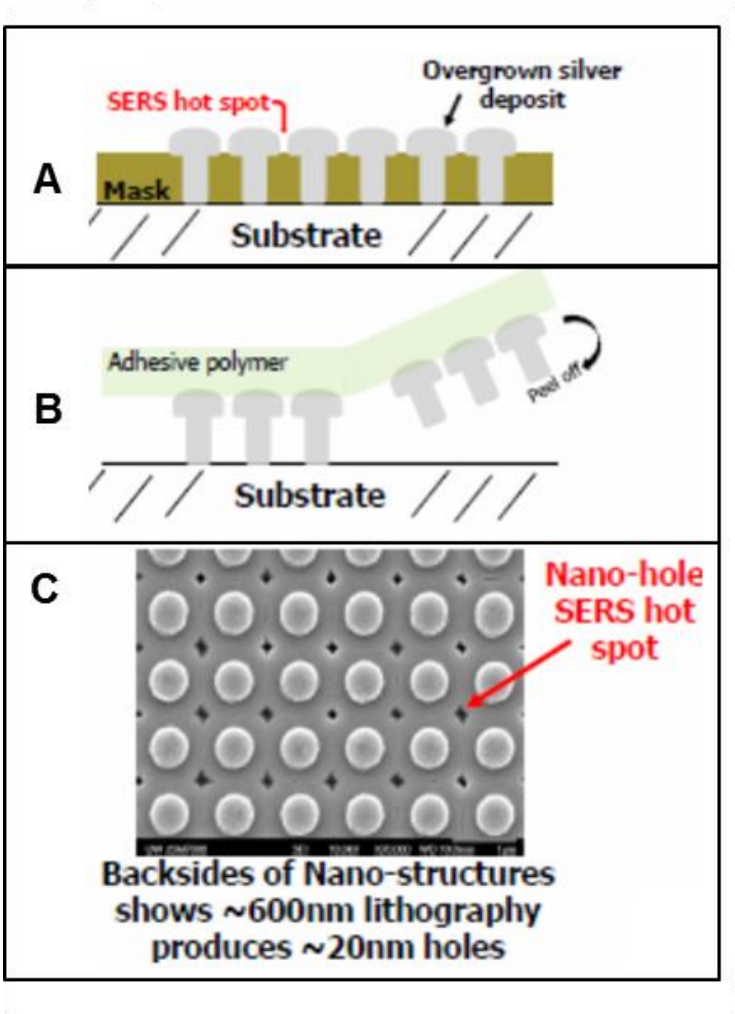

Figure 6.1: Schematic detailing the fabrication of these SERS hot spots and their removal from the substrate into an adhesive polymer phase. Schematic of the deposition and overgrowth of the silver into the nano-patterned mask creating the SERS hot spot **(A)**. Removal of the nano-structures after the mask is dissolved **(B)**. SEM image of the back sides of the structures after they have been peeled of using an adhesive polymer **(C)**.

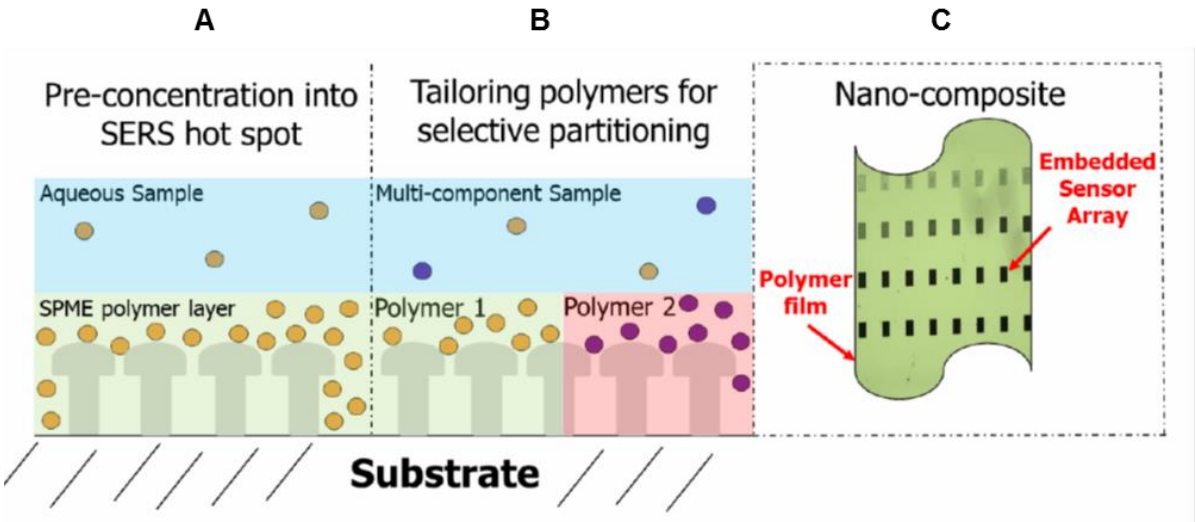

Figure 6.2: Schematic of a SPME polymer phase used to anchor the OSE nano-structures **(A)**. Schematic of selectivity of analytes for two selected polymer phases that also contain embedded nano-structures **(B)**. Proposed nano-composite film with embedded OSE fabricated nano-sensor patches **(C)**.

References

1. W. R. Browne and J. J. McGarvey, Coordination Chemistry Reviews **251**, 3-4, 454 (2007).

2. R. Singh, Physics in Perspective **4**, 4, 399 (2002).

3. S. S. Kantha, Nature **340**, 6236, 672 (1989).

4. O. S. Heavens, Nature **352**, 6338, 767 (1991).

5. R. Goodwins, Nature **397**, 6718, 401 (1999).

6. R. L. Frost, J. Cejka, G. A. Ayokol, and M. L. Weier, Journal of Raman Spectroscopy **38**, 10, 1311 (2007).

7. M. Choucair, P. Thordarson, and J. A. Stride, Nature Nanotechnology **4**, 1, 30 (2009).

8. M. Wagner, Annual Review of Microbiology **63**, 411 (2009).

9. X. M. Yang, K. Ajito, D. A. Tryk, K. Hashimoto, and A. Fujishima, Journal of Physical Chemistry **100**, 18, 7293 (1996).

10. C. Schoenherr, T. Haefele, K. Paulus, and G. Francese, European Journal of Pharmaceutical Sciences **38**, 1, 47 (2009).

11. D. Sorak, L. Herberholz, S. Iwascek, S. Altinpinar, F. Pfeifer, and H. W. Siesler, Applied Spectroscopy Reviews **47**, 2, 83 (2012).

12. E. Guzman, V. Baeten, J. A. F. Pierna, and J. A. Garcia-Mesa, Talanta **93**, 94 (2012).

13. C. Vazquez-Calvo, S. Martinez-Ramirez, M. A. de Buergo, and R. Fort, Spectroscopy Letters **45**, 2, 146 (2012).

14. M. J. Jager, D. P. McClintic, and D. C. Tilotta, Applied Spectroscopy **54**, 11, 1617 (2000).

15. J. Smulko, A. Kwiatkowski, and M. Gnyba, Bulletin of the Polish Academy of Sciences-Technical Sciences **59**, 4, 449 (2011).

16. A. Culka, J. Jehlicka, and L. Strnad, Spectrochimica Acta Part a-Molecular and Biomolecular Spectroscopy **86**, 347 (2012).

17. P. Vitek, E. M. A. Ali, H. G. M. Edwards, J. Jehlicka, R. Cox, and K. Page, Spectrochimica Acta Part a-Molecular and Biomolecular Spectroscopy **86**, 320 (2012).

18. M. D. Hargreaves, K. Page, T. Munshi, R. Tomsett, G. Lynch, and H. G. M. Edwards, Journal of Raman Spectroscopy **39**, 7, 873 (2008).

19. C. Lim, J. Hong, B. G. Chung, A. J. deMello, and J. Choo, Analyst **135**, 5, 837 (2010).

20. S. M. Angel, N. R. Gomer, S. K. Sharma, and C. McKay, Applied Spectroscopy **66**, 2, 137 (2012).

21. F. Herzog and V. P. Zakaznova-Herzog, American Mineralogist **96**, 5-6, 914 (2011).

22. B. L. Wittkamp and D. C. Tilotta, Analytical Chemistry **67**, 3, 600 (1995).

23. M. Q. Li, J. Xu, M. Romero-Gonzalez, S. A. Banwart, and W. E. Huang, Current Opinion in Biotechnology **23**, 1, 56 (2012).

24. P. Hermann, A. Hermelink, V. Lausch, G. Holland, L. Moller, N. Bannert, and D. Naumann, Analyst **136**, 6, 1148 (2011).

25. M. Q. Li, D. P. Canniffe, P. J. Jackson, P. A. Davison, S. FitzGerald, M. J. Dickman, J. G. Burgess, C. N. Hunter, and W. E. Huang, Isme Journal **6**, 4, 875 (2012).

26. Y. B. Guo, M. K. K. Oo, K. Reddy, and X. D. Fan, Acs Nano **6**, 1, 381 (2012).

27. Fleischm.M, P. J. Hendra, and McQuilla.Aj, Chemical Physics Letters **26**, 2, 163 (1974).

28. B. Sharma, R. R. Frontiera, A. I. Henry, E. Ringe, and R. P. Van Duyne, Materials Today **15**, 1-2, 16 (2012).

29. M. G. Albrecht and J. A. Creighton, Journal of the American Chemical Society **99**, 15, 5215 (1977).

30. J. M. McLellan, Y. J. Xiong, M. Hu, and Y. N. Xia, Chemical Physics Letters **417**, 1-3, 230 (2006).

31. E. C. Le Ru, E. Blackie, M. Meyer, and P. G. Etchegoin, Journal of Physical Chemistry C **111**, 37, 13794 (2007).

32. J. Xu, L. Zhang, H. Gong, J. Homola, and Q. Yu, Small **7**, 3, 371 (2011).

33. Q. Yu, S. Braswell, B. Christin, J. Xu, P. M. Wallace, H. Gong, and D. Kaminsky, Nanotechnology **21**, 35 (2010).

34. Y. Zhang, H. Hong, and W. B. Cai, Current Pharmaceutical Biotechnology **11**, 6, 654 (2010).

35. J. Kneipp, H. Kneipp, and K. Kneipp, Chemical Society Reviews **37**, 5, 1052 (2008).

36. J. Kneipp, H. Kneipp, B. Wittig, and K. Kneipp, Nanomedicine-Nanotechnology Biology and Medicine **6**, 2, 214 (2010).

37. T. Gorecki and J. Pawliszyn, Analyst **122**, 10, 1079 (1997).

38. Z. Y. Zhang and J. Pawliszyn, Analytical Chemistry **65**, 14, 1843 (1993).

39. E. Boscaini, M. L. Alexander, P. Prazeller, and T. D. Mark, International Journal of Mass Spectrometry **239**, 2-3, 179 (2004).

40. E. Boscaini, M. L. Alexander, P. Prazeller, and T. D. Mark, International Journal of Mass Spectrometry **239**, 2-3, 171 (2004).

41. E. L. Difilippo and R. P. Eganhouse, Environmental Science & Technology **44**, 18, 6917 (2010).

42. K. J. Regehr, M. Domenech, J. T. Koepsel, K. C. Carver, S. J. Ellison-Zelski, W. L. Murphy, L. A. Schuler, E. T. Alarid, and D. J. Beebe, Lab on a Chip **9**, 15, 2132 (2009).

43. B. L. Wittkamp, S. B. Hawthorne, and D. C. Tilotta, Analytical Chemistry **69**, 6, 1197 (1997).

44. B. L. Wittkamp, S. B. Hawthorne, and D. C. Tilotta, Analytical Chemistry **69**, 6, 1204 (1997).

45. D. L. Heglund and D. C. Tilotta, Environmental Science & Technology **30**, 4, 1212 (1996).

46. S. A. Merschman, S. H. Lubbad, and D. C. Tilotta, Journal of Chromatography A **829**, 1-2, 377 (1998).

47. D. C. Stahl and D. C. Tilotta, Environmental Science & Technology **33**, 5, 814 (1999).

48. D. C. Stahl and D. C. Tilotta, Environmental Science & Technology **35**, 17, 3507 (2001).

49. X. D. Fan and I. M. White, Nature Photonics **5**, 10, 591 (2011).

50. A. Y. Lau, L. P. Lee, and J. W. Chan, Lab on a Chip **8**, 7, 1116 (2008).

51. R. M. Connatser, M. Cochran, R. J. Harrison, and M. J. Sepaniak, Electrophoresis **29**, 7, 1441 (2008).

52. J. Olavarria-Fullerton, S. Wells, W. Ortiz-Rivera, M. J. Sepaniak, and M. A. De Jesus, Applied Spectroscopy **65**, 4, 423 (2011).

53. L. C. Taylor, T. B. Kirchner, N. V. Lavrik, and M. J. Sepaniak, Analyst **137**, 4, 1005 (2012).

54. S. Ulrich, Journal of Chromatography A **902**, 1, 167 (2000).

55. Y. B. Tewari, M. M. Miller, S. P. Wasik, and D. E. Martire, Journal of Chemical and Engineering Data **27**, 4, 451 (1982).

56. H. Kamaya, S. Kaneshina, and I. Ueda, Biochimica Et Biophysica Acta **646**, 1, 135 (1981).

57. A. Pohorille, M. A. Wilson, M. H. New, and C. Chipot, Toxicology Letters **101**, 421 (1998).

58. U. Norinder, P. Sjoberg, and T. Osterberg, Journal of Pharmaceutical Sciences **87**, 8, 952 (1998).

59. J. R. Weil, B. Dien, R. Bothast, R. Hendrickson, N. S. Mosier, and M. R. Ladisch, Industrial & Engineering Chemistry Research **41**, 24, 6132 (2002).

60. P. Persson, J. Andersson, L. Gorton, S. Larsson, N. O. Nilvebrant, and L. J. Jonsson, Journal of Agricultural and Food Chemistry **50**, 19, 5318 (2002).

61. H. Kataoka, Analytical Sciences **27**, 9, 893 (2011).

62. K. Flavin, H. Hughes, V. Dobbyn, P. Kirwan, K. Murphy, H. Steiner, B. Mizaikoff, and P. McLoughlin, International Journal of Environmental Analytical Chemistry **86**, 6, 401 (2006).

63. D. W. Janes, C. J. Durning, D. M. van Pel, M. S. Lynch, C. G. Gill, and E. T. Krogh, Journal of Membrane Science **325**, 1, 81 (2008).

64. W. T. Stringfellow and K. C. Oh, Ground Water Monitoring and Remediation **25**, 2, 52 (2005).

65. H. S. Dorea, J. R. L. Bispo, K. A. S. Aragao, B. B. Cunha, S. Navickiene, J. P. H. Alves, L. P. C. Romao, and C. A. B. Garcia, Microchemical Journal **85**, 2, 234 (2007).

66. C. L. Yaws and M. Rahate, Chemical Engineering **117**, 3, 44 (2010).

67. D. M. Alexander, Journal of Physical Chemistry **63**, 6, 1021 (1959).

68. S. J. Han, L. Puech, R. V. Law, J. H. G. Steinke, and A. Livingston, Journal of Membrane Science **199**, 1-2, 1 (2002).

69. X. R. Xia, R. E. Baynes, N. A. Monteiro-Riviere, and J. E. Riviere, Toxicology Mechanisms and Methods **15**, 4, 307 (2005).

70. H. Golmohammadi and Z. Dashtbozorgi, Journal of Structural Chemistry **51**, 5, 833 (2010).

71. D. H. Robinson and A. H. Toledo, Journal of Investigative Surgery **25**, 3, 141 (2012).

72. F. Kivlehan, F. Garay, J. D. Guo, E. Chaum, and E. Lindner, Analytical Chemistry **84**, 18, 7670 (2012).

73. M. S. Burch, R. K. McAllister, and T. A. Meyer, American Journal of Health-System Pharmacy **68**, 2, 125 (2011).

74. H. Lord and J. Pawliszyn, Lc Gc Europe **25**, 4, 180 (2012).

75. J. J. Langenfeld, S. B. Hawthorne, and D. J. Miller, Analytical Chemistry **68**, 1, 144 (1996).

76. I. C. Nwaneshiudu, Q. M. Yu, and D. T. Schwartz, Applied Spectroscopy **66**, 12, 1487 (2012).

77. D. Lawson, S. Samanta, P. T. Magee, and D. E. Gregonis, Journal of Clinical Monitoring **9**, 4, 241 (1993).

78. M. Weinrich, T. K. Rostovtseva, and S. M. Bezrukov, Biochemistry **48**, 24, 5501 (2009).

79. S. A. Simon, T. J. McIntosh, P. B. Bennett, and B. B. Shrivastav, Molecular Pharmacology **16**, 1, 163 (1979).

80. J. Ohmori, S. Maeda, H. Higuchi, M. Ishii, Y. Arai, Y. Tomoyasu, A. Kohjitani, M. Shimada, and T. Miyawaki, Journal of Anesthesia **25**, 4, 618 (2011).

81. R. L. Zhou, J. M. Perez-Aguilar, Q. C. Meng, J. G. Saven, and R. Y. Liu, Anesthesia and Analgesia **114**, 1, 122 (2012).

82. T. Eggeman and R. T. Elander, Bioresource Technology **96**, 18, 2019 (2005).

83. T. A. Lloyd and C. E. Wyman, Bioresource Technology **96**, 18, 1967 (2005).

84. R. R. M. Zautsen, F. Maugeri, C. E. Vaz-Rossell, A. J. J. Straathof, L. A. M. van der Wielen, and J. A. M. de Bont, Biotechnology and Bioengineering **102**, 5, 1354 (2009).

85. D. Vuckovic, X. Zhang, E. Cudjoe, and J. Pawliszyn, Journal of Chromatography A **1217**, 25, 4041 (2010).

86. J. N. Lee, C. Park, and G. M. Whitesides, Analytical Chemistry **75**, 23, 6544 (2003).

87. O. P. Togunde, H. Lord, K. D. Oakes, M. R. Servos, and J. Pawliszyn, Journal of Separation Science **36**, 1, 219 (2013).

88. F. R. Kermani, A.-M. Tugulea, J. Hnatiw, V. H. Niri, and J. Pawliszyn, Water Quality Research Journal of Canada **48**, 1, 85 (2013).

89. V. Sharma, J. Fan, A. Jerath, K. S. Pang, B. Bojko, J. Pawliszyn, J. M. Karski, T. Yau, S. McCluskey, and M. Wasowicz, Anaesthesia **67**, 11, 1242 (2012).

90. T. Gorecki, X. M. Yu, and J. Pawliszyn, Analyst **124**, 5, 643 (1999).

91. T. Gorecki, A. Khaled, and J. Pawliszyn, Analyst **123**, 12, 2819 (1998).

92. M. L. Brusseau, Environmental Toxicology and Chemistry **12**, 10, 1835 (1993).

93. S. K. Poole and C. F. Poole, Journal of Chromatography A **845**, 1-2, 381 (1999).

94. P. I. Flory, Journal of Chemical Physics **10**, 1, 51 (1942).

95. A. Georgi and F. D. Kopinke, Environmental Toxicology and Chemistry **21**, 9, 1766 (2002).

96. C. T. Chiou, D. E. Kile, T. I. Brinton, R. L. Malcolm, J. A. Leenheer, and P. Maccarthy, Environmental Science & Technology **21**, 12, 1231 (1987).

97. C. T. Chiou, Abstracts of Papers of the American Chemical Society **220**, U317 (2000).

98. J. Brandrup, E. H. Immergut, E. A. Grulke, A. Abe, and D. R. Bloch, "Polymer Handbook (4th Edition)", (John Wiley & Sons).

99. S. Abbasi, S. Kitayaporn, D. T. Schwartz, and K. F. Bohringer, Nanotechnology **22**, 16 (2011).

100. S. Kitayaporn, J. H. Hoo, K. F. Bohringer, F. Baneyx, and D. T. Schwartz, Nanotechnology **21**, 19 (2010).

101. G. Upender, R. Satyavathi, B. Raju, K. S. Alee, D. N. Rao, and C. Bansal, Chemical Physics Letters **511**, 4-6, 309 (2011).

Appendix: Characterization of SERS sensor fabricated using Orchestrated Structural Evolution (OSE)

Chapter 7

Orchestrated structure evolution (OSE) has been established as an effective on reproducible top-down, bottom-top approach to creating metal nano-structures on conductive substrates[99, 100]. OSE works by using a top-down method (Electron Beam Lithography (EBL)) to write nano-sized holes into a photoresist. After the pattern is developed, this is then followed by a bottom-up nucleation and growth of a metal (i.e. copper, nickel, or silver) into the holes using an electrochemical deposition[99]. The nanostructure growth can be controlled by the deposition time and spacing between seed holes[99]. Using OSE, SERS active silver nano-patterns (different spacing of holes) have been fabricated. Their enhancement is characterized with the Rhodamine 6G fluorescence dye.

7.0 Introduction

prior work by Kitayaporn *et al*[100] has extensively characterized nanostructures fabricated using OSE. Although this work was predominantly based on copper and nickel deposition, the rigorous characterization of nucleation and growth of these structures enabled it translation toward other metal electrolytes. Here we show the application of OSE toward the fabrication of silver nano-structures and their characterization for SERS sensing. The nano-structures created using this method have the potential to be peeled off the substrate into an adhesive polymer phase. We look towards using PDMS as the adhesive phase for potential microfluidic applications.

7.1 Methods

7.1.1 Solution Preparation

Rhodamine 6G (R6G) was purchased from Acros Organics and hexane from EMDchemical (used as purchased). 30nM R6G solutions were prepared by making a 3mM stock solution of the dye in deionized (DI) water. This was then diluted down to the desire amount. The solutions were then shaken, tightly capped, and used immediately after preparation. A 5% PDMS/catalyst (10:1 ratio) in hexane mixture was used to cast PDMS unto nano-patterns

7.1.2 Fabrication of Substrate

A 2nm/50nm Cr/Au seeding layer was thermally evaporated unto a 4" silicon wafer. A 6% polymethylmethacrylate (PMMA950A) in anisole resist (MicroChem Corp.) is spin coated unto the surface at 4000rpm for 45s and baked at 180^{o}C for 90s. The result layer has a thickness of ~300nm. Using an FEI Siron scanning electron microscope (SEM) with NPGS 9 software, 125nm disc shaped holes were patterned into the resist layer and the pattern is developed using methyl isobutyl ketone (MIBK):isopropanol (IPA) 1:3 for 70s at room temperature. This was then rinse with IPA, dried with N_2 gas, and baked again at 100^{o}C for 60s. This development exposes the gold at the bottom of the holes for the growth step using electrochemical plating.

7.1.3 Electroplating

Silver was grown at the seed holes via electrodeposition in room temperature using 0.05M $AgNO_3$, 0.2M (EDTA), and 0.3M NaOH at -250 mV versus a Ag wire reference. All experiments were done in a quiescent 40mL single compartment with a platinum wire counter electrode. **Figure 1** is a schematic already published by Abbasi *et al*[99] detailing the setup from the starting silicon substrate to the electroplating setup and finally the resulting SEM image of the structure.

7.1.4 SERS Patterning

Forty 30μm patches of the 125nm holes were developed each with different pitch distances. Distance range from 0-500nm increasing in increments of 12.5nm. The fact that these are overgrown features means that the 125nm hole could resulting in a mushroom like feature with its top being ~500nm (if nothing hindrances its growth). **Figure 2** shows SEM micrographs of the tops of these features.

7.1.5 Raman Instrumentation

Raman spectra were collected using a Renishaw inVia Raman micro-spectrometer attached to a Leica DM IRBE upright optical microscope. A 514 nm argon laser at 0.5% power was used to irradiate samples through a 50x (N.A. 0.8) objective lens. The spot area was ~3μm in diameter. Raman scattered light was acquired through the same objective lens and detected on a thermoelectrically cooled (-60 ^{o}C) CCD. All sample measurements were acquired for 10 seconds. For PDMS on sensors, a 785nm laser at 5% power was used to irradiate the samples through a 50x (N.A. 0.8) objective lens. The spot area was ~50μm^2.

7.1.6 SERS of R6G

The gold-plated silicon substrates with the deposited nano-structures were cleaved into smaller chips. Each chip had 40 silver-plated patterns. The chip was immersed in the already prepared 30nM R6G solution and let to sit for 3 hours. Afterwards, they were lightly rinsed, dried with N_2 gas and immediately analyze under the Raman spectrometer.

7.1.7 PDMS casting on substrate

A 5% PDMS/catalyst (10:1 ratio) in hexane mixture was spin coated unto the patterned chip at 2500rpm. The chip was immediately put under vacuum for 1hr to release any air bubbles. Afterwards, the resulting layer on the chip (.1-1mm) was cure at 70^{o}C overnight. Before SERS

analysis, we use optical microscopy to ensure the patterns were not compromised by the PDMS casting.

7.1.8 Data Analysis

Spectral peaks were analyzed using Wire 2.0 software. All spectra were baseline subtracted using second order polynomial or cubic spline functions producing flat baselines for subsequent analysis. Spectral peaks where fit to standard Vogt distribution profiles. Curve fit parameters were used to calculate the reported integrated peak areas. Peak areas are reported in counts per second (kcps).

7.2 Results & Discussion

7.2.1 SERS peak characterization

Figure 3 shows a typical Raman spectrum of R6G adsorbed on the OSE fabricated nano-patterns. Raman signals at 615, 770, 1188, 1312, 1362, 1503, 1572 and 1648cm^{-1} are well known characteristic Raman peaks of R6G published in prior work using Ag nano-structures with a 514nm excitation laser. For analysis we use the 1648cm^{-1} peak which corresponds to the symmetric C–C stretching vibrations modes of R6G due to the resonance enhancement effect at 514.5 nm excitation[101]. The peaks at 1312, 1362, 1503, 1572 and 1648cm^{-1} are also associated with this vibrational mode. Other peaks shown arise from C–C–C ring in-plane, C–H out of plane bending modes or C–C stretching vibrations[101].

7.2.2 Quantifying enhancement

Using the 1648cm^{-1} peak, we roughly estimate the analytical enhancement factor for one of these sensor patches by using the equation[31]:

$$AEF = \frac{I_{SERS}/C_{SERS}}{I_{RS}/C_{RS}}, \quad (1)$$

where I_{SERS} (20,000cps) is the intensity of the peak obtain using an experimental concentration C_{SERS} (3 x 10^{-8}M) and I_{RS} (19,000cps) is the intensity of the peak obtain using a reference concentration C_{RS}(3 x 10^{-4}M). We estimate an enhancement factor of AEF = 1.05 x 10^{5}.

We quantify the effect on varying the pitch distances on the peak intensities by also analyzing the 1648cm^{-1} R6G. **Figure 4** shows a bar graph of integrated peak areas as a function of pitch spacing. The inset is an optical image taken of the 30μm patches. Going from left to right (and then down the rows) the pitch distances are being increased by a factor of factor of 12.5nm. Colored boxes around specific patches in the optical image correspond to matching colored data points on the graph. SEM images of the nano-structures in these patches are shown below these points. It is evident by the shift from light blue to red to a darker blue that a change in plasmonic property is occurring. Additionally, as the distances between holes are increased, we see how the peak intensity changes yield three distinct peaks. This profile of changing peak intensities is somewhat repeatable as shown in the bottom plot.

A more quantitative equation is needed when characterizing the enhancements of multiple sensor patches relative to one another. This enhancement factor can be expressed as:

$$EF = \frac{I_{SERS}/N_{SERS}}{I_{RS}/N_{RS}}, \quad (2)$$

where is the intensity I_{SERS} and I_{RS} are intensities of SERS and Raman respectively and N_{SERS} is the number of adosrbed molecules within the collection volume on the SERS sensor and N_{RS} is the number of molecules in the regular Raman collection volume. This accounts for the fact that as the pitch distance are increased, less adsorbed R6G is present in any given collection volume (spot size) given that less of the adsorping nano-structures are in the space.

7.3 Conclusions & Implications

It is evident from **Figure 4** that pitch spacing affects multiple enhancement features such as nano-structure size/geometry, number of sensors, and amount of analytes in collection volume. This hints at a complex and dynamic system that will need to be further characterize. FDTD simulations are an efficient way to extract the parameters most critical to the SERS activity of these structures. An additionally novelity of these "mushroom-like" nano-structures is they can be spilled off the nucleation substrate into and adhesive polymer phase. Peeling off and embedding these SERS active structures into PDMS could be a significant step toward realizing SPME-SERS within a micro-fluidic device. **Figure 5** shows the enhancement of PDMS peaks signals within the range of 500-900cm^{-1} when PDMS polymer was cast unto the sensor patterns. This shows that although PDMS signals can also be enhanced by the sensors, this enhanced will not interfer with other analyte enhancements that may occur. This further exemplifies the possibilities of combining SPME with SERS.

7.4 Figures

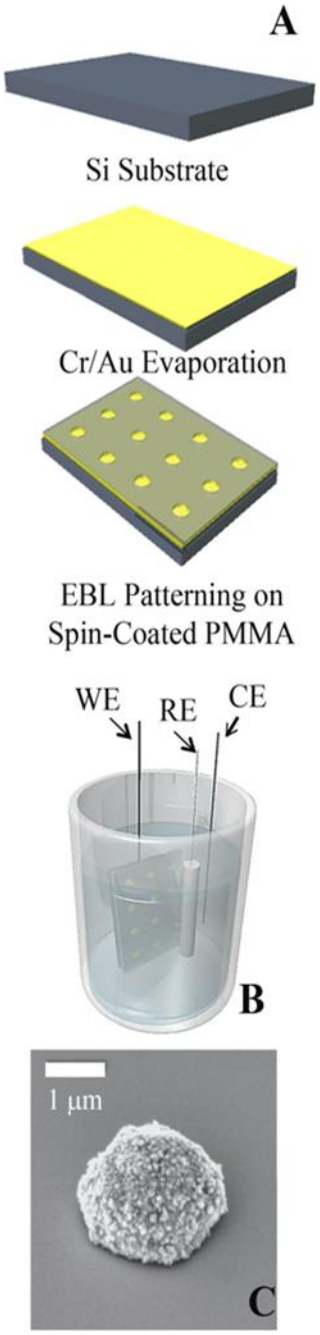

Figure 7.1: (*Kitayaporn et al)* **(A)** illustrates the gold evaporation and PMMA coating steps, **(B)** shows the plating setup and, **(C)** is an SEM image of the resulting nano-structure

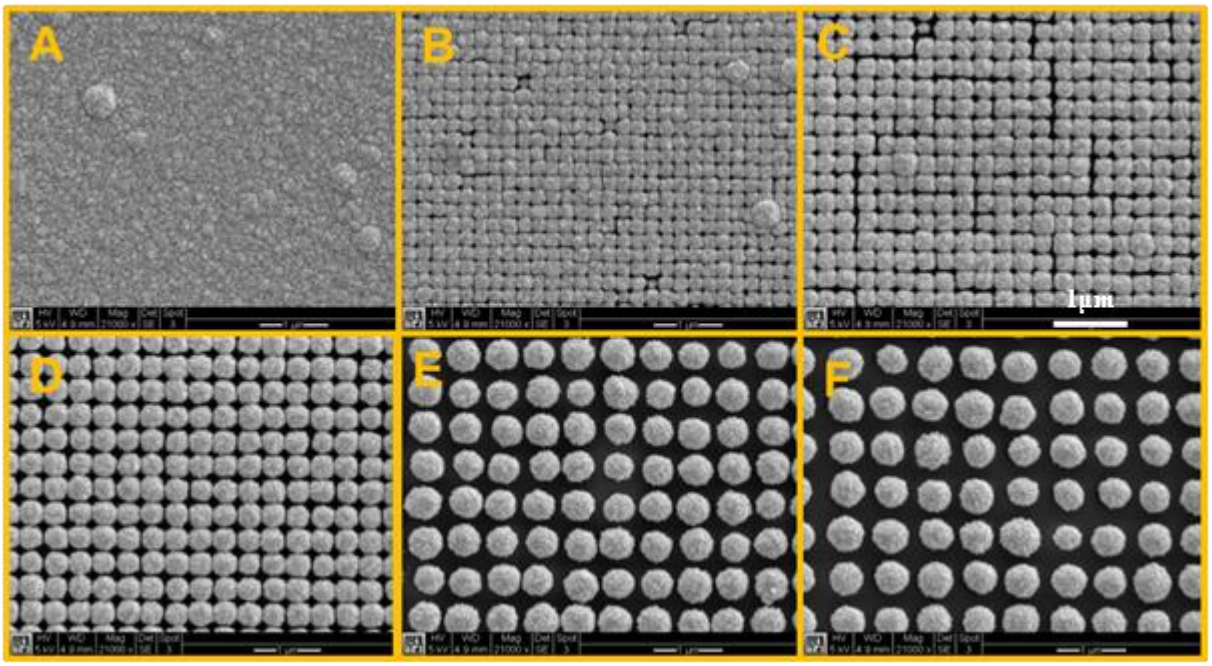

Figure 7.2: Panels **A-F** are silver nano-structures fabricated using OSE. Pitch distances are being increased going from **A-->F** with ranges from 0-500nm. Geometric and morphologic changes can be readily observed as the growth space is increased between each seed.

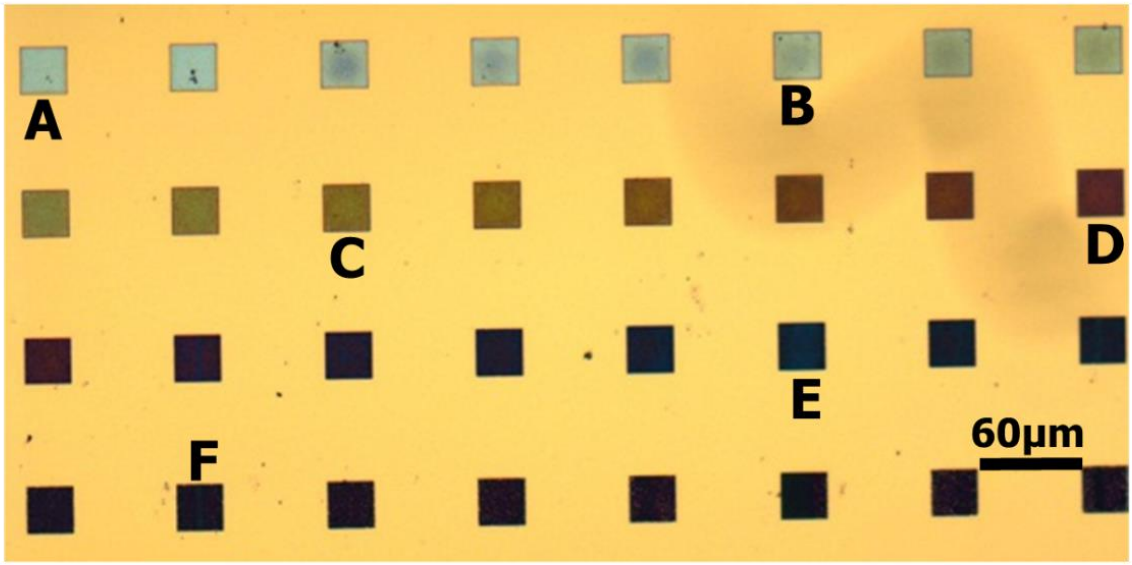

Figure 7.3: Optical image of 30µm silver patches deposited at -250 mV versus an Ag wire reference with systematically varied pitch.

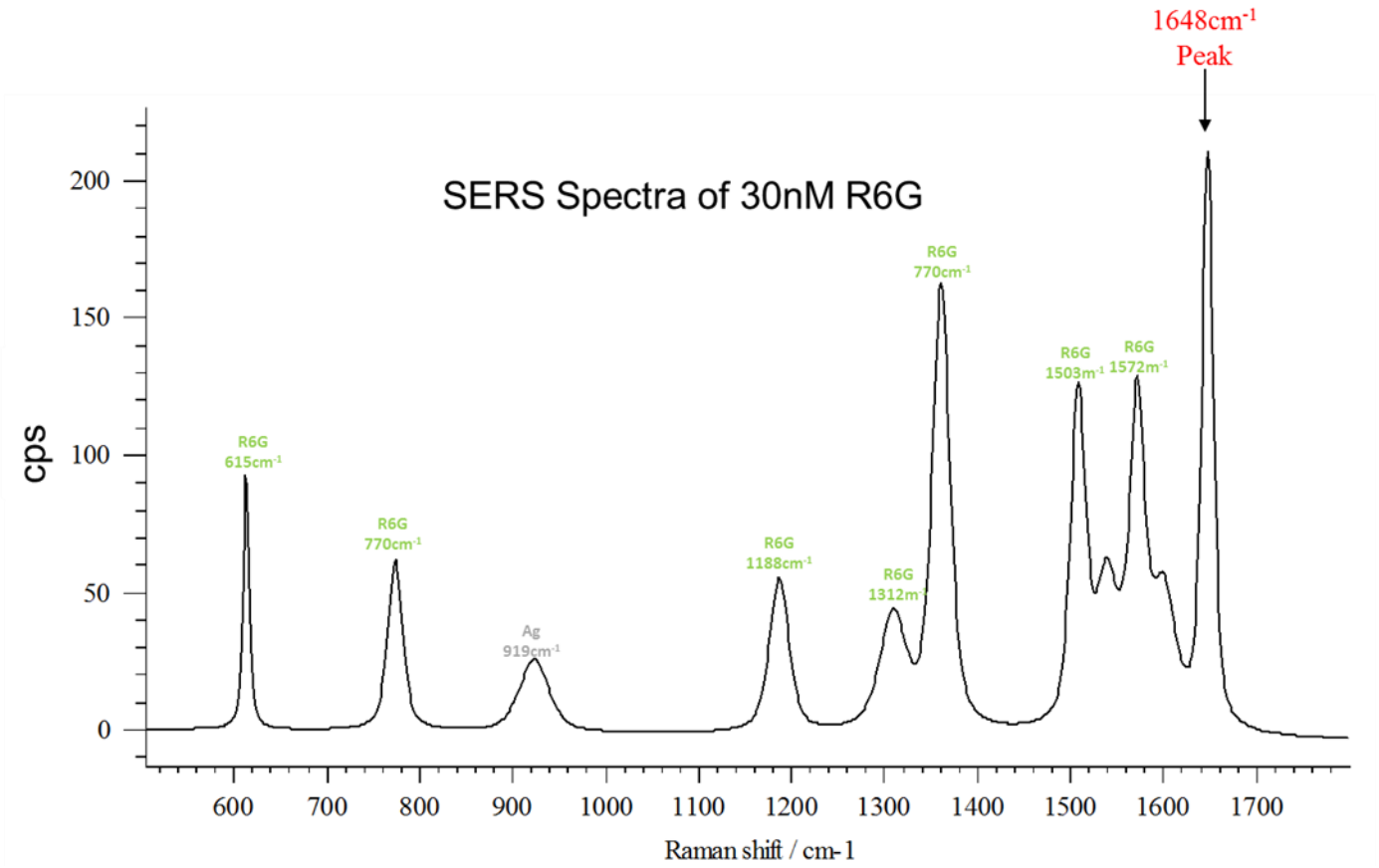

Figure 7.4: Spectral curve fit of R6G on the fabricated OSE sensor within the 500-1800cm^{-1} spectral range after baseline subtraction and exposure correction.

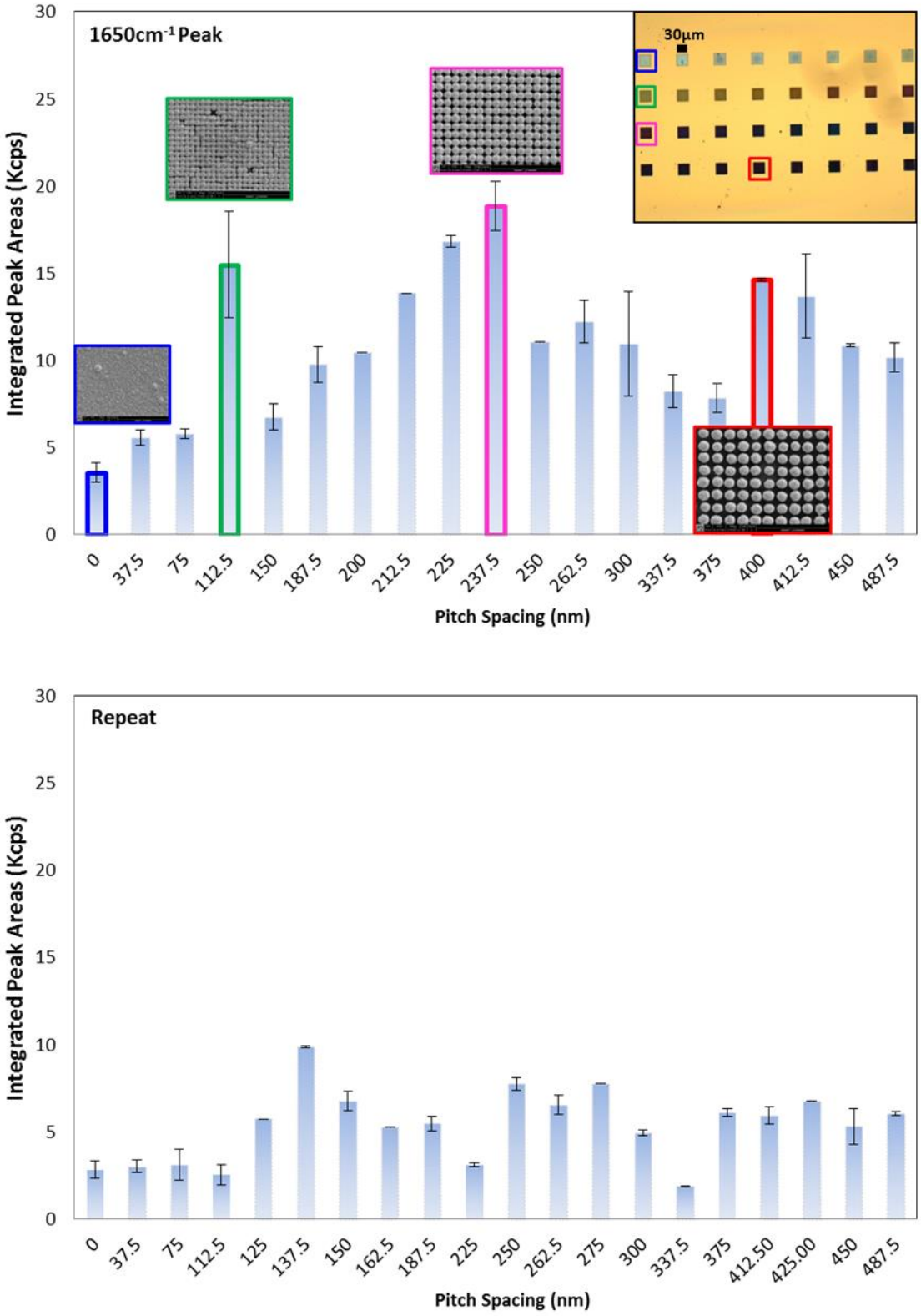

Figure 7.5: Graph of integrated peak areas as the pitch spacing is changed from 0-487.5nm. Data in top graph present 2 points on each sensor patch. The repeat experiment below represents data from four points on each patch.

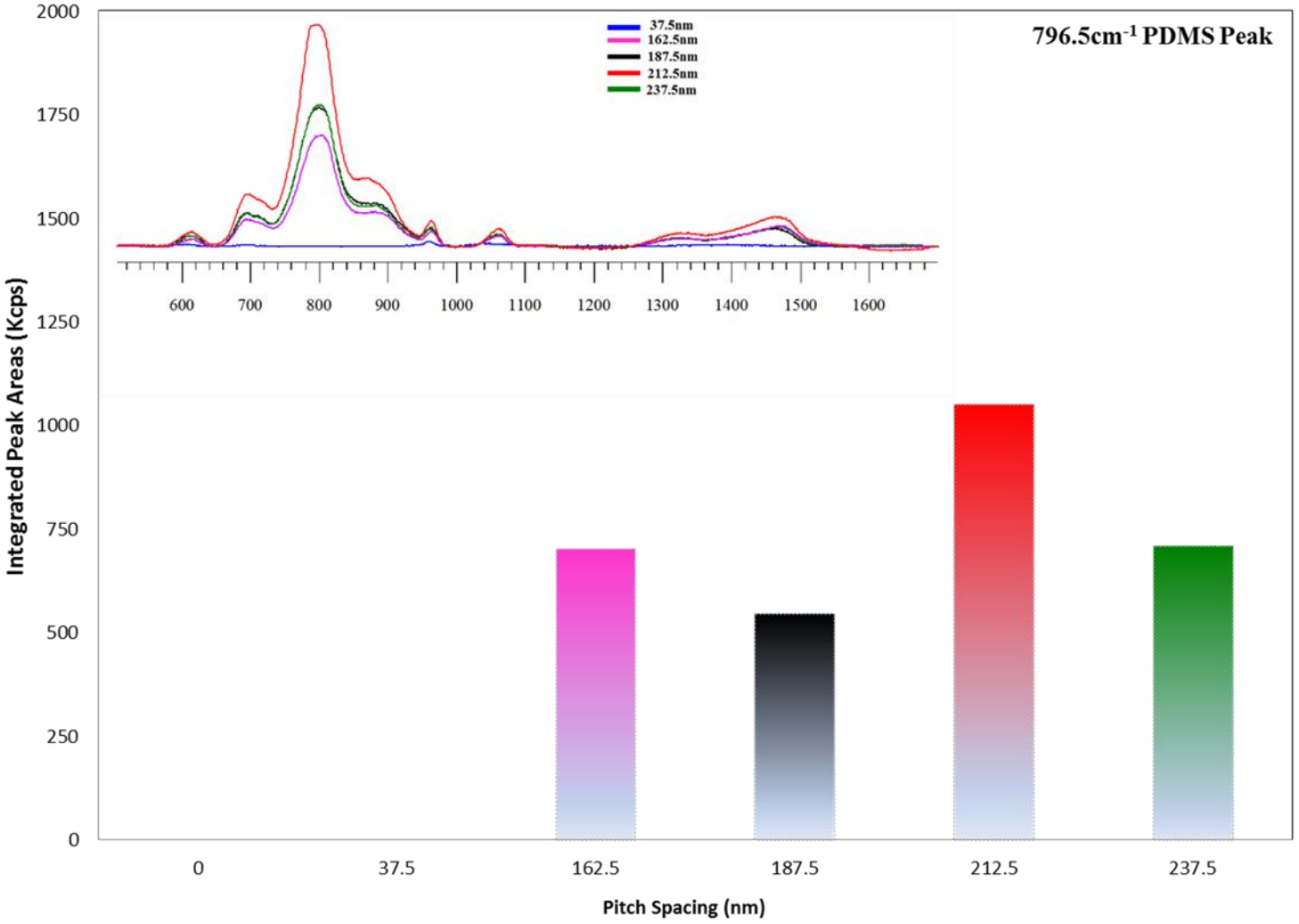

Figure 7.6: Bar graph of integrated peak areas as the pitch spacing is changed from 0-237.5nm. Data represents a single collected point on each coated sensor patch.